Thomas W. Kennedy

HIGHWAY RESEARCH **RECORD**

Number
324

Symposium on
Concrete Deformation

7 Reports

r

HIGHWAY RESEARCH **RECORD**

Thomas W. Kennedy

Number 324

Symposium on
Concrete Deformation

7 Reports

HIGHWAY RESEARCH BOARD

Characteristics of the Elastic Deformations of Concrete

SANDOR POPOVICS, Northern Arizona University

The instantaneous deformations of concrete are explained as a result of elastic deformations and internal crack propagation. Empirical formulas are presented for the numerical approximation of the stress-strain diagram. The definitions and various static and dynamic test methods are discussed for the determinations of the Young's modulus, shear modulus, and Poisson's ratio. Related formulas are also presented. Comparisons are made between static Young's moduli determined by various methods, between dynamic Young's moduli obtained by various methods, between static and related dynamic moduli, and between static and dynamic Poisson's ratios. It is shown that the constants determined by dynamic methods are greater than the corresponding static constants. Attempt is made to explain the revealed differences. Data concerning the reproducibility of the elastic constants close the paper indicating that the test methods for dynamic constants are superior in this respect. The static elastic constants of concrete are of greater significance to the design engineer than the corresponding dynamic values. On the other hand, the determination of the dynamic constants is easier.

•WHEN A LOAD is applied to a body, the body is deformed. The amount and character of deformation depend on the properties of the body, the particular environment, the magnitude of the load, the rate at which it is applied, and the elapsed time after the load application that the observation is made. Different materials vary widely in their response to load. This response is called rheological behavior. Although instantaneous response and time-depending response are not entirely separable, it is convenient to consider them separately as elastic deformations and plastic deformations respectively (1). A deformation is said to be elastic if it appears and disappears immediately on application and removal of stress.

A knowledge of the deformability of concrete is necessary to compute stresses from observed strains, to proportion sections of highway slabs and reinforced concrete members when certain design procedures are used, and to compute loss of prestress in prestressed structures. In the study of models of concrete structures, it is also necessary to know the stress-strain characteristics of the material for the model so that dimensional similarity may be obtained.

SHAPE OF THE STRESS-STRAIN DIAGRAM FOR CONCRETE

The instantaneous deformations of a specimen under load can be described conveniently by a stress-strain diagram. Figure 1 shows such a typical diagram for the axial deformation of a concrete specimen loaded with 2 different rates in uniaxial compression or tension. The stresses are averages (loads divided by cross-sectional area) and so too are the strains. The diagram is influenced considerably by the testing conditions, such as type of testing machine, rate of loading, size and shape of specimen, size and location of strain gages, and number of load repetitions (2, 3, 4, 5), as well as by the age and composition of concrete, such as type and quantity of aggregate, and especially the porosity (6), in a similar but not identical way as the concrete strength is influenced

---

by most of these factors ($\underline{7}$, $\underline{8}$). Torque-twist diagrams for concrete are similar to the stress-strain diagram ($\underline{9}$) and serve a similar purpose.

Along with the axial deformations, transverse deformations also take place under load. It is customary to characterize the lateral deformation by the Poisson's ratio, which is the absolute value of the ratio of transverse strain to the corresponding axial strain resulting from a uniformly distributed axial stress below the proportional limit of that material.

The shape of the stress-strain diagram or the torque-twist diagram or the stress-Poisson's ratio diagram for concrete can be explained in qualitative terms from the well-established fact that the fracture of concrete takes place through progressive internal cracking ($\underline{10}$). The compressive stress-strain diagram starts out with a nearly linear portion that stretches to about 30 percent of the ultimate load. Beyond this point the curve deviates gradually from the straight line. This is

Figure 1. Two typical stress-strain curves for concrete under uniaxial load. The top curve is characteristic of a loading process where the rate of stress increase is kept constant during the testing. The bottom curve is obtained by keeping the rate of strain increase constant.

attributed chiefly to the increase of cracks on the interface of coarse aggregate and mortar, that is, to the start of discontinuity in the specimen and later to extensive mortar cracking, although some creep probably also takes place ($\underline{11}$, $\underline{12}$). In accordance with this mechanism, the stress-strain diagram is usually more curved for concrete than for the comparable mortar that usually has a less flat curve than the comparable paste. This failure mechanism also implies that (a) the stress-strain diagram of concrete becomes steeper and more nearly linear with the increase of the rate of loading; (b) the curvature of the diagram increases with the amount and size of the aggregate in the concrete; (c) the shape of the diagram obtained by tensile load is similar to, although more nearly linear than, the shape of the comparable diagram obtained by compressive load; and (d) the major part of the concrete deformations that is caused by the internal cracking and creep is permanent. Experimental evidence supports these implications ($\underline{10}$). Also, when concrete and mortar specimens are subjected to increasing uniaxial compression, the Poisson's ratio for each begins to increase on attaining a certain stress level. After that the volume of the specimen also begins to increase. This can be explained again by the appearance and propagation of cracking, because hardened paste specimens continue to consolidate at an increasing rate with increased load, and stone specimens show only a slight volume expansion at stresses near failure ($\underline{13}$).

NUMERICAL APPROXIMATIONS FOR THE STRESS-STRAIN DIAGRAM OF CONCRETE

Despite the supporting experimental evidence, the best that the theory of internal cracking can do is to describe the stress-strain relationship in qualitative terms. Other theories are even less suitable for this purpose. Thus, only empirical formulas obtained from boundary conditions and by curve-fitting are available for the numerical approximation of the stress-strain diagram of concrete. Several of these formulas are compared, as shown in Figure 2, in terms of f/f_0 relative stress and ϵ/ϵ_0 relative strain. The limits of validity and degrees of approximation of these formulas are restricted. Further analysis of these formulas is presented elsewhere ($\underline{7}$).

THE STATIC ELASTIC CONSTANTS OF CONCRETE

The most common measure of elasticity is the modulus of elasticity. This term is defined, in general, by the Standard Definitions of Terms Relating to Methods of Me-

chanical Testing (ASTM Designation E 6-66) as the ratio of stress to corresponding strain below the proportional limit. Modulus of elasticity, like stress, is expressed in force per unit of area (psi or kg/cm^2). For concrete, as well as for other materials where the stress-strain relationship is curvilinear rather than linear, one of the 4 following terms may be used (Fig. 3):
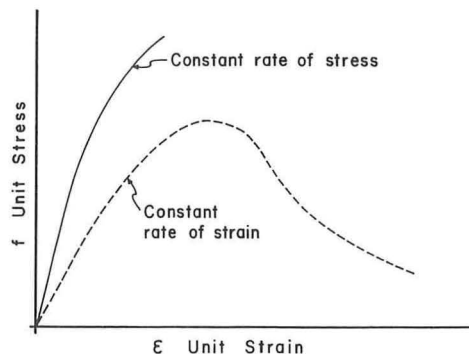
1. Initial tangent modulus—The slope of the stress-strain curve at the origin;

2. Tangent modulus—The slope of the stress-strain curve at any specified stress or strain;

3. Secant modulus—The slope of the secant drawn from the origin to any specified point on the stress-strain curve; and

4. Chord modulus—The slope of the chord drawn between any 2 specified points on the stress-strain curve.

Figure 2. Comparison of several formulas for the stress-strain diagram of concrete.

All 4 definitions refer to the static modulus of elasticity in contrast to the modulus of elasticity computed from dynamic tests.

Static modulus of elasticity may be measured in compression, tension, or shear. The modulus in tension or compression is frequently referred to as Young's modulus of elasticity and is designated by E. The shear modulus is sometimes called the modulus of rigidity or torsional modulus and is designated by G. These 2 moduli describe the elastic behavior of a homogeneous and isotropic material completely. Thus, the third usual elastic constant, the Poisson's ratio, can already be expressed in terms of E and G, as follows:

$$\mu = \frac{E}{2G} - 1 \qquad (1)$$

where μ is the Poisson's ratio.

Figure 3. Four definitions for the static Young's modulus of elasticity of concrete.

The only ASTM standard method for the determination of static elastic constants of concrete is the Standard Method of Test for Static Young's Modulus of Elasticity and Poisson's Ratio in Compression of Cylindrical Concrete Specimens (ASTM Designation C 469-65). It stipulates a chord modulus between 2 points on the stress-strain curve defined as follows: The lower point corresponds to a strain of 50 microinches/inch (μ in./in.), and the upper point corresponds to a stress equal to 40 percent of the strength of concrete at the time of loading. The lower point is near the origin but far enough removed from the origin to be free of possible irregularities in strain reading caused by seating of the testing machine platens and strain measuring devices. The upper point is taken near the upper end of the working stress range that was assumed in design. Thus, the determined modulus is approximately the average modulus of elasticity in compression throughout the working stress range (1). The specimen should be loaded at least twice without recording any data during the first loading. Calculations should be based on the average of the results of subsequent loadings. At least 2 subsequent loadings are recommended.

Usually cylinders or prisms are used for the determination of the modulus of elasticity in compression. In order to compensate for the effect of eccentric loading or non-uniform response by the specimen, strains should be measured along the axis of the specimen or along 2 or more gage lines uniformly spaced around the periphery of the cylinder. The selection of the gage length is important. It must be large in comparison with the maximum particle size of the aggregate so that local strain irregularities do not unduly influence the results. It must not, however, encroach on the ends of the specimen because strains near the ends may differ from strains elsewhere. Half the specimen height is a good gage length. Both mechanical devices and electrical gages have been used successfully for strain measurements of concrete.

The Young's modulus can also be determined, at least theoretically, on specimens loaded as beams. Deflection measurements, curvature measurements, or strain measurements in the extreme fibers can be used for this purpose. The usual approach is to measure deflections caused by known loads and to calculate the modulus of elasticity from a suitable beam-deflection formula. Unfortunately, the application of the usual simple deflection formulas provide unreliable E values for concrete for 2 reasons. First, these formulas are based on the assumption that the material follows Hooke's law, which in the case of concrete is not true. Second, the depth-to-span ratios of unreinforced concrete beams normally used for such tests are so large that shear deflection composes a significant part of the total deflection. A beam-deflection formula for center-point loading and corrected for shear ($\underline{1}$, $\underline{14}$) is as follows:

$$E_{st} = \frac{Pl^3}{48FI} \left[1 + (2.4 + 1.5\mu)(h/l)^2 - 0.84(h/l)^3 \right] \qquad (2)$$

where

E_{st} = static Young's modulus of elasticity;
F = maximum deflection,
P = applied central load,
l = distance between supports,
I = moment of inertia of the section,
μ = Poisson's ratio, and
h = depth of the beam.

When the beam has a 6- by 6-in. cross section and is loaded at the third-points of an 18-in. span, the following formula can be used ($\underline{15}$):

$$E_{st} = \frac{P}{F}(1.16 + 0.125\mu) \qquad (3)$$

where the P total load is expressed in pounds, F in inches, and E_{st} in psi. Equations 2 and 3 are not corrected for the deviation from Hooke's law. Thus, the values they provide for the E_{st} of a concrete are greater than the actual values, often to a considerable degree.

Static determination of Poisson's ratio is made by measuring both the axial strain and the corresponding transverse strain. Details are described by Yoshida ($\underline{16}$). A standard test method is given in ASTM C 469. Poisson's ratio is also commonly computed by Eq. 1 from results of Young's modulus and shear modulus. The shear modulus is most often determined dynamically or by calculation from E and μ. When a direct static determination is desired, a torsion test is the common procedure.

Static modulus of elasticity and Poisson's ratio can be calculated from splitting tensile test if principal strains are measured at the center of the concrete cylinder ($\underline{17}$). In this case, the gage length should be limited to about 0.07 of the specimen diameter because the strains encountered in this test are of rapidly changing character. Also, this method is sensitive to observational errors.

Static tests for Young's modulus and Poisson's ratio involve the application of stresses of the same order as those in practice, whereas the stresses induced in the dynamic tests are very small. Because these elastic constants are stress-dependent, the static

modulus and ratio are of greater significance to the design engineer than the corresponding dynamic values. On the other hand, the determination of the dynamic values is, in most cases, easier and more precise.

THE DYNAMIC ELASTIC CONSTANTS

The dynamic Young's modulus or the dynamic shear modulus is usually determined by the resonance frequency method. Rayleigh was the first to set forth simplified relationships among the resonant frequency of vibration of a homogeneous specimen, the velocity of a vibratory wave passing through the material, and the modulus of elasticity of the material [18]. The first application of this method on concrete was published by Powers in 1938 [19]. The ASTM standard forms of this method are based essentially on the more exact theory developed by Pickett [20] and are described in the Standard Method of Test for Fundamental Transverse, Longitudinal, and Torsional Frequencies of Concrete Specimens (ASTM Designation C 215-60). The recommended test specimens are beams that are made in accordance with the standard procedure prescribed for the flexural specimens, but other suitable specimens, such as cylinders, can also be used. The elastic constants may be calculated from the following formulas:

$$E_r = CWn^2 \qquad (4)$$

$$E_r = DW(n')^2 \qquad (5)$$

$$G_r = BW(n'')^2 \qquad (6)$$

where

E_r = dynamic Young's modulus calculated from the fundamental resonance frequency of the concrete specimen;
G_r = dynamic shear modulus calculated from the fundamental torsional frequency;
W = weight of the specimen;
n' = fundamental transverse frequency, cps; and
n'' = fundamental torsional frequency, cps.

The values of the C, D, and B factors depend on the shape and size of the specimen tested, on the units used, and on the Poisson's ratio of the concrete. Detailed instructions for the calculation of these factors may be found in ASTM Method C 215 or in the literature [21, 22, 23, 24, 25, 26]. Equation 5 can be written in the following form when E_r is in psi and when the specimen is a rectangular prism:

$$E_r = 6 \times 10^{-6} L^2 d_1 (n')^2 \qquad (7)$$

where

L = length of the prism, in.; and
d_1 = unit weight of the concrete, lb/cu ft.

Poisson's ratio does not enter heavily into the computations when Eq. 5 or Eq. 7 is used. Because the true value of Poisson's ratio is rarely known, it has become popular to use the longitudinal resonance technique for E_r so that the effect of an error in the assumed value of Poisson's ratio may be minimized. Longitudinal resonances of bars of square cross section or cylindrical rods provide particularly accurate results for Young's modulus [25]. This test method is also described in the British Standard 1881.

The application of pulse transmission, which apparently was started on concrete by Long and Kurtz [27], is not recommended for the determination of the dynamic modulus of elasticity (the pulse modulus) by the pertinent ASTM standard Tentative Method of Test for Pulse Velocity Through Concrete (ASTM Designation C 597-67 T). The reasons for this may be the marked effect of Poisson's ratio on the pulse modulus as well as the fact that the usually applied calculations do not provide proper values for the pulse modulus if the cement paste and aggregate differ greatly in elastic properties [28, 29]. If

this modulus is still to be computed from the pulse velocity, Whitehurst advises the use of the formula developed originally by Poisson for homogeneous materials as follows (21, 30):

$$E_p = \frac{V^2 d}{g} \frac{(1 + \mu)(1 - 2\mu)}{(1 - \mu)}$$ (8)

where

E_p = dynamic Young's modulus calculated from the pulse velocity,
V = longitudinal (compression) wave velocity,
d = density, and
g = gravitational acceleration.

If E_p is expressed in psi, V in ft/sec, d = d_1 in lb/cu ft, and g in ft/sec^2, the right side of Eq. 8 should also be divided by 144. Then a simplified form of this formula (μ = 0.24) is as follows:

$$E_p = 0.000183 d_1 V^2$$ (9)

The V term in Eqs. 8 and 9 is actually the velocity of the wave front and is equivalent to the wave velocity only as long as the latter does not change with frequency. Because this appears to be true for concrete, the pulse velocity can be used in Eqs. 8 and 9 with little or no error (31).

Simultaneously with the longitudinal waves, transverse (shear) and surface (Rayleigh) waves are also generated by an impulse. The 3 types of wave travel with different velocities and become separated in time as the path length increases. The S, shear, and R, Rayleigh, wave velocities and their relationship to the elastic constants of a material (16, 22, 32, 33, 34) are

$$S^2 = \frac{G}{d} = \frac{gE}{2d(1 + \mu)}$$ (10)

and

$$R = pS$$ (11)

where p = 0.911 and 0.928 when μ = 0.2 and 0.3 respectively.

It is possible, at least theoretically, to calculate the dynamic Poisson's ratio directly when, for instance, both the longitudinal frequency and the longitudinal wave velocity are available by matching Eqs. 5 and 8, or by using Eqs. 8 and 10 when both the longitudinal wave velocity and the shear wave velocity are measured, or when both the V and R velocities are available (16, 32, 35). The practical difficulty with these methods is that the S or R velocities or both cannot usually be determined accurately enough. The application of Eqs. 4 through 11 for concrete represents a more or less tolerable oversimplification because concrete is far from being a perfectly elastic, homogeneous, and isotropic material.

ESTIMATION OF THE ELASTIC CONSTANTS BY MODELS

Calculating the deformability of a composite solid material, such as concrete, given the deformabilities and amounts of the composing phases, is an important problem both from theoretical and practical standpoints. Such calculations are hindered by the fact that concrete has a complicated internal structure. Therefore, repeated attempts have been made to apply suitable simplified hypothetical structures, the so-called composite models, for such calculations.

Any model approach for composite materials involves considerable simplifying assumptions. In case of deformations, these assumptions concern stresses and strains as well as the relationship between them; for instance, elastic behavior of the model

components is usually assumed to be linear. More sophisticated models may provide more general applicability, but it is important to realize that every model contains a number of simplifying assumptions. Therefore, one should make the selection of the proper model for a given purpose by balancing the easy applicability of the model against a reasonable generality, considering that the increase of complexity of a model has usually a diminishing rate of return in reliability. It appears that the simplest models for the estimation of the modulus of elasticity, which still have an adequate reliability for considerable number of practical cases (36, 37), are represented by the following formulas:

(a) For normal-weight concrete,

$$\frac{1}{E_C} = 0.5\left(\frac{1 - g}{E_m} + \frac{G}{E_p}\right) + 0.5 \frac{1}{(1 - g)E_m + gE_p} \tag{12}$$

(b) For lightweight-aggregate concrete,

$$E_L = \frac{0.5}{(1 - g)/E_m + g/E_p} + 0.5\left[(1 - g)E_m + gE_p\right] \tag{13}$$

(c) For the effect of porosity,

$$E_p = 10^{-nv} E_0 \tag{14}$$

where

E_C, E_L, and E_p = estimated modulus of elasticity of normal-weight, lightweight, and porous concrete respectively;

E_0 = modulus of elasticity of the concrete with zero porosity;

E_m and E_p = modulus of elasticity of the cement paste and aggregate respectively;

g = fractional volume of aggregate (percent/100);

n = experimental constant; and

v = pore content.

All models are based on certain simplifying assumptions; consequently, their reliability and limits of validity are restricted. Thus, the model approach is best used for qualitative examination of material behavior.

COMPARISON OF THE VARIOUS KINDS OF YOUNG'S MODULI

The Young's moduli of a concrete obtained in various manners are usually more or less different. The size of this difference depends on several factors as described in the following sections.

Static Moduli of Elasticity

Walker (38) demonstrates that the relation of the tangent modulus to the secant modulus at the same load is 0.8 to 0.9 within practical stress limits. Davis and Troxell (39) find that the secant modulus of a granite concrete of about 2,500 psi compressive strength decreases almost linearly from 2.5×10^6 psi to 1.7×10^6 psi at the age of 28 days as the applied stress is increased from 200 to 1,000 psi. Data by Jones and Richart (40) show that the secant modulus of elasticity is about 10^6 psi less at $0.9f_c'$ than at $0.5f_c'$. Shideler (41) reports that values of the secant modulus of structural lightweight and normal concretes obtained at $0.3f_c'$ are almost identical with values obtained at $0.45f_c'$. Klieger's pertinent results as reported by Philleo (28) show a similar tendency.

Data by Klieger (15) demonstrate that the static modulus of elasticity determined by the compression of 6- by 12-in. cylinders is about three-fourths of the comparable

modulus obtained by the flexure of 6- by 6- by 30-in. beams on an 18-in. span and using Eq. 3. On the other hand, Witte and Price (42) report that the secant moduli determined by compression at the ages of 2 and 3 years are practically the same as the comparable moduli obtained by the flexure of 3- by 3- by $16\frac{1}{4}$-in. beams and using, presumably, a simple deflection formula without any correction for shear or curvilinear stress distribution. Measurements by Vile show a practical equality of elastic modulus values obtained under uniaxial compressive and tensile states of stress (43). The differences between the initial tangent and secant moduli or between secant moduli at differing stresses or between tangent and chord moduli are due to the curvilinear character of the stress-strain diagram of concrete (Fig. 3). The discrepancies between compressive and flexural moduli can be attributed to the shear and the nonlinear stress distribution in flexure.

Dynamic Moduli of Elasticity

As Figure 4 shows, the moduli of elasticity calculated from longitudinal resonance frequencies and those from transverse frequencies are practically identical (44, 45). Data by Obert and Duvall (46) support this finding. The agreement between the resonance modulus and the modulus calculated from the pulse velocity is less satisfactory. As a rule, the E_p pulse moduli are greater. This is shown in Figure 5 where pertinent values obtained on the same specimens that provided data for Figure 4 are plotted (44, 45). Data published by other investigators (32, 47) likewise show that E_p is about 10 percent greater than E_r of the same concrete. Similarly, according to Philleo (28), Whitehurst obtained pulse moduli that were up to 47 percent greater than the corresponding resonance moduli, with an average difference of 15 percent. Philleo's own data indicate a similar tendency.

Klieger (15) determined the moduli of elasticity of a series of concrete mixtures by the resonance method both on 6- by 12-in. cylinders and on comparable 6- by 6- by
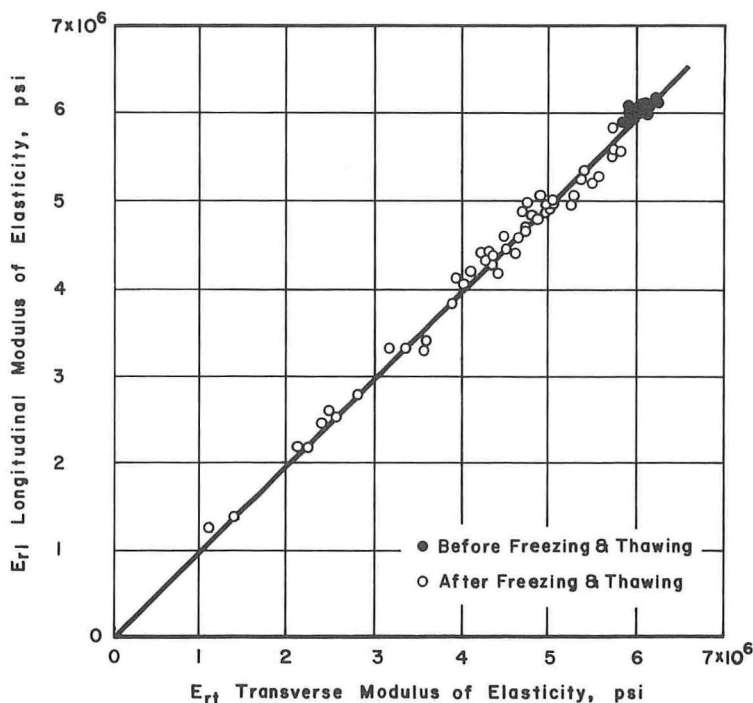
Figure 4. Comparison of moduli of elasticity from transverse resonance frequencies to moduli from longitudinal resonance frequencies (44, 45).
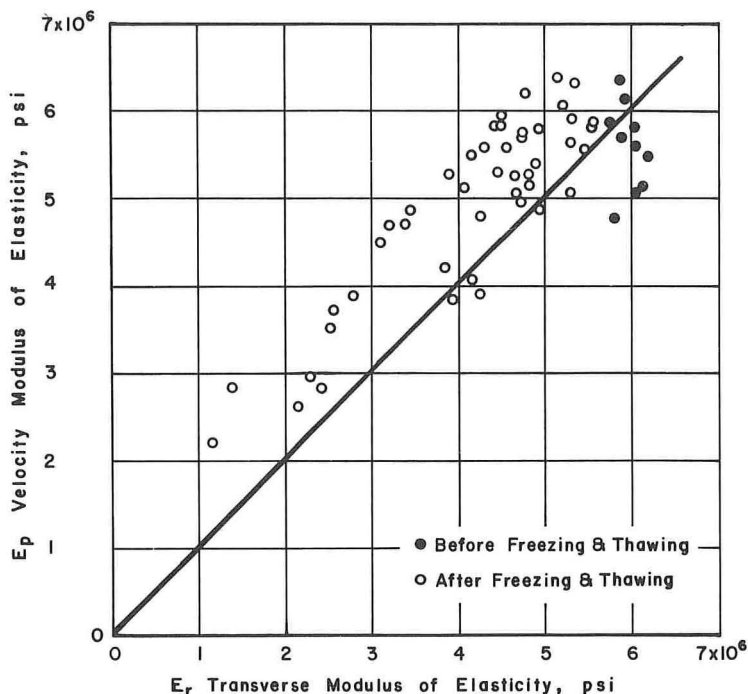
Figure 5. Comparison of moduli of elasticity from transverse resonance
frequencies to moduli from pulse velocity (44, 45).

30-in. beams, having found the latter values to be about 8 percent higher. A similar
test series by Stanton (48), however, shows close agreement between the moduli of the
2 types of specimens.

The most likely reason for the tendency of E_p to be greater than E_r is that the pulse
velocity is less affected by porosity than by the resonance frequency. This is supported
by Figure 5 that indicates the loosening of the internal structure of concrete to be caused
by repeated freezing and thawing, which reduces the value of E_p to less than that of E_r.

Static Versus Dynamic Moduli

The dynamic Young's moduli are, as a rule, higher than the corresponding static
values. Powers was the first to publish comparisons between the static and resonance
moduli of concrete (19). He found good agreement between these 2 types of moduli both
when the static values were determined by the compression of 6- by 12-in. cylinders
and, in another series, when static secant moduli, at about one-third the ultimate
strength, were calculated from central deflections of plain concrete beams. (No cor-
rections were applied for shear or stress distribution.) In calculating the resonance
modulus, however, he used an oversimplified formula. Had he used the formula cor-
rected by Pickett (20), he would have obtained 7 to 10 percent higher values for E_r. In
accordance with this, later investigators find that, by using Pickett's equations, the res-
onance moduli are regularly higher than the comparable static secant moduli. This dif-
ference is influenced by numerous factors, such as the composition and age of concrete
and the curing and testing conditions.

Stanton (48) reports that the secant modulus of 6- by 12-in. cylinders at 1,000 psi
was found to range from 62 percent of the resonance modulus at 28 days to approximately
75 percent at later periods. Data by Shideler (41) show that values of the resonance

moduli of his moist-cured structural lightweight concretes are about 350,000 psi greater than the secant moduli, whereas this difference for sand-and-gravel concretes is about 1,500,000 psi. He also demonstrates that, as the concretes dry, the difference between the secant modulus and resonance modulus is reduced. Similarly, Reichard (49) finds that the average ratios of the resonance to the secant modulus at the ages of 1 day, 28 days, and 1 year are 1.13, 1.11, and 1.10 respectively for lightweight concretes and 1.37, 1.32, and 1.16 respectively for normal-weight concretes. Data by Hirsch (50) demonstrate that the secant moduli are approximately 10 percent less than the resonance moduli. Chefdeville (51) suggests that the E_{st}/E_r ratio increases to unity as the stress related to the E_{st} decreases. Klieger's pertinent comparison (15) shows that for 6- by 12-in. cylinders made of a wide range of concrete composition, the static moduli are, in all cases, lower than the related resonance moduli, the differences being smaller at 1 and 3 years than at 28 days. Other experimental evidence also indicates (52, 53, 54) that the higher the modulus of elasticity is the closer the agreement between resonance and static moduli will be.

A few comparisons are also available between values of static secant modulus computed by Eq. 2 or 3 from deflection measurements to the related resonance modulus. Philleo noticed a tendency for such E_r/E_{st} ratios to decrease as the modulus of elasticity increased (28). Klieger reports (15) that such static moduli are slightly lower at 28 days than the resonance moduli, but at 1 and 3 years these differences are small and irregular. Thus, it seems that on the average the static secant moduli from deflection formulas, corrected for shear, agree fairly well with the resonance moduli.

Some experimental evidence seems to indicate that the ratio of the pulse modulus to the static modulus is close to the unity when the static modulus is about 6×10^6 psi and increases rapidly with the decrease of the static modulus (28). A group of aerated concrete in the range of 450 to 1,000 psi compressive strength also provided practically the unity for the E_p/E_{st} ratio (55).

There is nothing surprising in the fact that the static and dynamic moduli of elasticity, as a rule, differ. In the static test, there is always an inelastic portion of the measured strain at a particular stress that reduces the calculated value of the modulus. The magnitude of this inelastic portion varies with age and composition of concrete, curing, testing conditions, and other variables. In the dynamic tests, the fundamental resonance frequency or the pulse velocity is determined at a very low stress level of 1 psi. Consequently, the inelastic deformations are almost completely eliminated. For this reason, several investigators consider the dynamic modulus as equivalent to the static initial tangent modulus. Also, the static modulus and the dynamic modulus are affected by the composite character of concrete in different ways. Experimental evidence seems to indicate, for instance, that the value of Young's modulus determined statically is more dependent on the elastic properties of the paste and less on the properties of aggregate than the modulus determined dynamically (28).

Poisson's Ratios

Several investigators have reached the conclusion that dynamic Poisson's ratios are consistently higher than the corresponding static values. Also, there seems to be a difference between dynamic Poisson's ratios obtained by different methods.

Anson and Newman (31) are of the opinion that dynamic Poisson's ratios calculated by Eq. 1 from E_r and G_r flexural and torsional resonance moduli may be 0.03 to 0.05 higher than the corresponding dynamic ratios calculated from pulse velocity and longitudinal resonance frequency tests. Simmons (57) as well as Elvery (53) report that ratios calculated by Eq. 1 from longitudinal and torsional resonance frequencies are consistently about 0.04 lower than the corresponding values from pulse velocity and longitudinal resonance frequency measurements, which, in turn, are about 0.08 higher than the corresponding static ratios. Data by Shideler (41) show that the dynamic Poisson's ratio calculated again by Eq. 1 from flexural and torsional resonance frequencies is, on the average, 0.02 higher for structural lightweight concretes, and 0.03 higher for sand-and-gravel concretes than the static ratio in the case of wet concretes. In the case of dry concretes this difference is practically negligible.

The source of the differences between various Poisson's ratios is similar to that for the various Young's moduli. A significant portion of the difference between static and dynamic ratios is probably due to the inelastic deformations that occur when loads are applied in the static test. Thus, the dynamic Poisson's ratio might be considered as equivalent to the tangent static ratio at zero stress. Also, the static Poisson's ratio and the dynamic ratio are affected by the composite character of concrete in different ways. The dynamic ratio appears to decrease with an increase in aggregate content and age of concrete but increases as the water-cement ratio is increased, whereas the static ratio is hardly affected by the water-cement ratio and increases toward the dynamic value with the age of concrete (56).

A possible reason for the differences between various dynamic Poisson's ratios is that the application of Eq. 1, as well as Eqs. 4 through 11, to concrete is an oversimplification because concrete is not an elastic, homogeneous, and isotropic material.

REPRODUCIBILITY OF THE MEASUREMENTS OF ELASTIC CONSTANTS

The few available experimental data appear to indicate that the reproducibility of the static elastic constants is poorer than that of the dynamic constants. In a comparative test series Mather (58) finds that pulse velocity determinations in uncracked concrete could generally be reproduced within 2 percent by various instruments and operators for mass structures. Wider variation may be expected for short path lengths of the order of 1 ft or less. Witte and Price (42) report average coefficients of variation of 2.3, 7.4, and 10.3 percent for the resonance Young's modulus, compressive secant, and flexural secant moduli respectively.

Simmons (57) shows that the standard deviations of static Poisson's ratio measurements, of dynamic ratios calculated by Eq. 1, and of dynamic ratios calculated from pulse velocity and resonance frequency measurements are 0.014, 0.007, and 0.009 respectively. These values correspond to coefficients of variation of 8.9, 3.6, and 3.8 percent respectively. McCoy and Mather (59) report that the coefficients of variation of dynamic Poisson's ratios calculated by Eq. 1 are 11 percent at the age of 14 days and 9 percent at 180 days. Their specimens all contained the same aggregate, but the types of the applied cements varied within wide limits.

The variation in the elastic constants of concrete in situ can be, of course, much higher. Neville (60) reports cases after Elvery where the ratio of maximum to minimum value of the modulus of elasticity is as high as two.

CONCLUSIONS

1. The shape of the stress-strain diagram for concrete can be derived only qualitatively from the available theories. Empirical formulas can be used for numerical approximation.

2. There are several methods for the determination of each of the elastic constants, and the results are more or less different. As a rule, the constants determined by dynamic methods are greater than the corresponding static constants.

3. A part of these differences is due to the fact that the stresses induced in the dynamic testing are much smaller than those in the static testing. Another reason is that the concrete is not an elastic, homogeneous, or isotropic material.

4. Static tests for the elastic constants involve the application of stresses of the same order as those in practice. Thus, the static constants are of greater significance to the design engineer than the corresponding dynamic values. On the other hand, the determination of the dynamic values is easier and more precise.

5. The reproducibility of the dynamic elastic constants is better than that of the static constants.

REFERENCES

1. Philleo, R. E. Elastic Properties and Creep. In Significance of Tests and Properties of Concrete and Concrete Making Materials, ASTM, Philadelphia, STP 169-A, 1966, pp. 160-175.

12

2. Clark, L. E., Gerstle, K. H., and Tulin, L. G. Effect of Strain Gradient on the Stress-Strain Curve of Mortar and Concrete. ACI Jour., Proc. Vol. 64, No. 9, Sept. 1967, pp. 580-586.

3. Halász, I. Deformations in Concrete. Proc. Technical Univ. of Building and Transport Engineering, Budapest, Vol. 12, No. 6, 1967, pp. 125-154.

4. Rüsch, H. Influence of the Deformation Characteristics of Concrete on the Stress Distribution. Schweizerische Bauzeitung, Vol. 77, No. 9, Feb. 1959, pp. 119-126.

5. Rasch, C. Stress-Strain Curves of Concrete and Stress Distribution in the Compressed Zone at Constant Strain Velocity. Deutscher Ausschuss für Stahlbeton, Wilhelm Ernst und Sohn, Berlin, Vol. 154, 1962.

6. Helmuth, R. A., and Turk, D. H. Elastic Moduli of Hardened Portland Cement and Tricalcium Silicate Pastes: Effect of Porosity. HRB Spec. Rept. 90, 1966, pp. 135-144.

7. Popovics, S. A Review of Stress-Strain Relationships for Concrete. ACI Jour., Proc. Vol. 67, No. 3, March 1970, pp. 243-248.

8. Popovics, S. Effect of Porosity on the Strength of Concrete. Jour. of Materials, Vol. 4, No. 2, June 1969, pp. 356-371.

9. Hughes, B. P., and Ash, J. F. Short-Term Loading and Deformation of Concrete in Uniaxial Tension and Pure Torsion. Magazine of Concrete Research, Vol. 20, No. 64, Sept. 1968, pp. 145-154.

10. Popovics, S. Fracture Mechanism in Concrete: How Much Do We Know? Jour. Engineering Mech. Div., Proc. ASCE, Vol. 95, No. EM3, Proc. Paper 6604, June 1969, pp. 531-544.

11. Ross, A. D., Illston, J. M., and England, G. L. Short-and-Long-Term Deformations of Concrete as Influenced by Its Physical Structure and State. In The Structure of Concrete, Cement and Concrete Assn., London, 1968, pp. 407-422.

12. L'Hermite, R. Volume Changes of Concrete. In Chemistry of Cement, Proc. Fourth Internat. Symposium, National Bureau of Standards, Monograph 43, Vol. 2, 1962, pp. 659-694.

13. Shah, S. P., and Chandra, S. Critical Stress, Volume Change, and Microcracking of Concrete. ACI Jour., Proc. Vol. 65, No. 9, Sept. 1968, pp. 770-781.

14. Seewald, F. Stresses and Deformations of Beams of Rectangular Cross Section. Abhandlungen aus dem Aerodynamischen Institut an der Technischen Hochschule Aachen, Springer-Verlag, Berlin, No. 7, 1927, pp. 11-33.

15. Klieger, P. Long-Time Study of Cement Performance in Concrete. ACI Jour., Proc. Vol. 54, Dec. 1957, pp. 481-504.

16. Yoshida, H. Elastic Properties of Concrete. Verlag Julius Springer, Berlin, 1930.

17. Hondros, G. The Evaluation of Poisson's Ratio and the Modulus of Materials of a Low Tensile Resistance by the Brizilian (Indirect Tensile) Test With Particular Reference to Concrete. Australian Jour. of Applied Science, Vol. 10, No. 3, Sept. 1959, pp. 243-268.

18. Rayleigh, Lord. The Theory of Sound, Volumes 1 and 2. Dover Publications, New York, 1945 (original edition 1877).

19. Powers, T. C. Measuring Young's Modulus of Elasticity by Means of Sonic Vibrations. Proc. ASTM, Vol. 38, Pt. 2, 1938, pp. 460-467.

20. Pickett, G. Equations for Computing Elastic Constants From Flexural and Torsional Resonant Frequencies of Vibration of Prisms and Cylinders. Proc. ASTM, Vol. 45, 1945, pp. 846-863.

21. Whitehurst, E. A. Evaluation of Concrete Properties From Sonic Tests. American Concrete Institute, Monograph 2, 1966.

22. Jones, R. Non-Destructive Testing of Concrete. Cambridge Univ. Press, 1962.

23. Malhotra, V. M. Non-Destructive Methods for Testing Concrete. Department of Energy, Mines and Resources, Ottawa, Mines Branch Monograph 875, 1968.

24. Spinner, S., and Valore, R. C., Jr. Comparison of Theoretical and Empirical Relations Between the Shear Modulus and Torsional Resonance Frequencies of

Bars of Rectangular Cross Section. Jour. of Research, National Bureau of Standards, Vol. 60, No. 5, May 1958, pp. 459-464.

25. Spinner, S., and Tefft, W. E. A Method for Determining Mechanical Resonance Frequencies and for Calculating Elastic Moduli From These Frequencies. Proc. ASTM, Vol. 61, 1961, pp. 1221-1238.

26. Krautkrämer, J., and Krautkrämer, H. Ultrasonic Testing of Materials. Springer-Verlag, New York, 1969.

27. Long, B. G., and Kurtz, H. H. Effect of Curing Methods Upon the Durability of Concrete as Measured by Changes in the Dynamic Modulus of Elasticity. Proc. ASTM, Vol. 43, 1943, pp. 1051-1065.

28. Philleo, R. E. Comparison of Results of Three Methods for Determining Young's Modulus of Elasticity of Concrete. ACI Jour., Proc. Vol. 51, Jan. 1955, pp. 461-469.

29. Beauzee, M. C. Errors of Measurement in the Determination of the Modulus of Elasticity by the Sonic Method. Internat. Symposium on Nondestructive Testing of Materials and Structures, RILEM, Paris, Vol. 1, 1954, pp. 120-136.

30. Whitehurst, E. A. Dynamic Tests. In Significance of Tests and Properties of Concrete and Concrete Making Materials, ASTM, Philadelphia, STP 169-A, 1966, pp. 176-188.

31. Anson, M., and Newman, K. The Effect of Mix Proportions and Method of Testing on Poisson's Ratio for Mortars and Concretes. Magazine of Concrete Research, Vol. 18, No. 56, Sept. 1966, pp. 115-130.

32. Leslie, R., Jr., and Cheesman, W. J. An Ultrasonic Method of Studying Deterioration and Cracking in Concrete Structures. ACI Jour., Proc. Vol. 46, No. 9, Sept. 1949, pp. 17-36.

33. Habrecht, L. Testing Concrete Slabs by Measuring the Phase Velocity of Mechanical Waves. Zerstörungsfreie Prüf-und Messtechnik für Beton und Stahlbeton, Proc. Internat. Conf., Leipzig, April 1969, pp. 53-56.

34. Schwaderer, W. Ultrasonic Measurements on Highways. Zerstörungsfreie Prüf-und Messtechnik für Beton und Stahlbeton, Proc. Internat. Conf., Leipzig, April 1969, pp. 67-70.

35. Hanke, I. Methods for the Determination of Transverse Waves Generated by Vertical Sonic Vibration of Concrete. Zerstörungsfreie Prüf-und Messtechnik für Beton und Stahlbeton, Proc. Internat. Conf., Leipzig, April 1969, pp. 57-60.

36. Popovics, S. Structural Model Approach to Two-Phase Composite Materials: State of the Art. American Ceramic Society Bull., Vol. 48, No. 11, Nov. 1969, pp. 1060-1064.

37. Popovics, S., and Erdey, M. R. A. Estimation of the Modulus of Elasticity of Concrete-Like Materials. Materials and Structures—Research and Testing, Vol. 3, No. 17, Sept.-Oct. 1970.

38. Walker, S. Modulus of Elasticity of Concrete. Proc. ASTM, Vol. 19, Pt. 2, 1919, pp. 510-585.

39. Davis, R. E., and Troxell, G. E. Modulus of Elasticity and Poisson's Ratio for Concrete, and the Influence of Age and Other Factors Upon These Values. Proc. ASTM, Vol. 29, Pt. 2, 1929, pp. 678-701.

40. Jones, P. G., and Richart, F. E. The Effect of Testing Speed on Strength and Elastic Properties of Concrete. Proc. ASTM, Vol. 36, Pt. 2, 1936, pp. 380-391.

41. Shideler, J. J. Lightweight Aggregate Concrete for Structural Use. ACI Jour., Proc. Vol. 54, Oct. 1957, pp. 299-328.

42. Witte, L. P., and Price, W. H. Discussion of Reference (48), ASTM Bull. 131, Dec. 1944, pp. 20-22.

43. Vile, G. W. D. The Strength of Concrete Under Short-Term Static Biaxial Stress. In The Structure of Concrete, Cement and Concrete Assn., London, 1968, pp. 275-288.

44. Batchelder, G. M., and Lewis, D. W. Comparison of Dynamic Methods of Testing Concretes Subjected to Freezing and Thawing. Proc. ASTM, Vol. 53, 1953, pp. 1053-1068.

14

45. Woods, K. B., and McLaughlin, J. F. Application of Pulse Velocity Tests to Several Laboratory Studies of Materials. HRB Bull. 206, 1959, pp. 14-27.

46. Obert, L., and Duvall, W. Discussion of Dynamic Methods of Testing Concrete With Suggestions For Standardization. Proc. ASTM, Vol. 41, 1941, pp. 1053-1070.

47. Cheesman, W. J. Dynamic Testing of Concrete With the Soniscope Apparatus. HRB Proc., Vol. 29, 1949, pp. 176-183.

48. Stanton, T. E. Tests Comparing the Modulus of Elasticity of Portland Cement Concrete as Determined by the Dynamic (Sonic) and Compression (Secant at 1000 psi) Methods. ASTM Bull. 131, Dec. 1944, pp. 17-20.

49. Reichard, T. W. Creep and Drying Shrinkage of Lightweight and Normalweight Concretes. National Bureau of Standards, Monograph 74, March 1964.

50. Hirsh, T. J. Modulus of Elasticity of Concrete Affected by Elastic Moduli of Cement Paste Matrix and Aggregate. ACI Jour., Proc. Vol. 59, No. 3, March 1962, pp. 427-451.

51. Chefdeville, J. Application of the Method for Estimating the Quality of Concrete. RILEM, Paris, Bull. No. 15, Aug. 1953, pp. 59-78.

52. Takabayashi, T. Comparison of Dynamic Young's Modulus and Static Young's Modulus for Concrete. Internat. Symposium on Nondestructive Testing of Materials and Structures, RILEM, Paris, Vol. 1, 1954, pp. 34-44.

53. Elvery, R. H. Symposium on the Non-Destructive Testing of Concrete. Internat. Symposium on Nondestructive Testing of Materials and Structures, RILEM, Paris, Vol. 1, 1954, pp. 111-119.

54. Sharma, M. R., and Gupta, B. L. Sonic Modulus as Related to Strength and Static Modulus of High Strength Concrete. Indian Concrete Jour., Vol. 34, No. 4, April 1960, pp. 139-141.

55. Morschtschichin, W. N. Determination of the Modulus of Elasticity of Concrete by Sonic Impulse Methods. Zerstörungsfreie Prüf-und Messtechnik für Beton und Stahlbeton, Proc. Internat. Conf., Leipzig, April 1969, pp. 45-48.

56. Anson, M. An Investigation Into a Hypothetical Deformation and Failure Mechanism for Concrete. Magazine of Concrete Research, Vol. 16, No. 47, June 1964, pp. 73-82.

57. Simmons, J. C. Poisson's Ratio of Concrete: A Comparison of Dynamic and Static Measurements. Magazine of Concrete Research, Vol. 7, No. 20, July 1955, pp. 61-68.

58. Mather, B. Comparative Tests of Soniscopes. HRB Proc., Vol. 33, 1954, pp. 217-226.

59. McCoy, E. E., and Mather, B. Discussion of paper Dynamic Testing of Materials (Mitchell, L. J.), HRB Proc., Vol. 33, 1954, pp. 256-258.

60. Neville, A. M. Concrete—A Non-Elastic Material in the Laboratory and in Structures. Stanton Walker Lecture Series on the Materials Sciences, Univ. of Maryland, Lecture 6, Nov. 1968.

Time-Dependent Deformation of Noncomposite and Composite Prestressed Concrete Structures

D. E. BRANSON, B. L. MEYERS, and K. M. KRIPANARAYANAN,
Department of Civil Engineering, University of Iowa

This paper reports the results of an investigation of the use of sand-lightweight concrete in prestressed laboratory beams and bridge girders. The study is divided into 3 parts: a materials study of the concrete behavior itself, a laboratory study of the behavior of both noncomposite (5 beams) and composite (4 beams) prestressed beams, and the field measurement of camber of prestressed girders (5 girders) used in the fabrication of a composite bridge in Iowa. In addition, systematic design procedures are presented and verified by the experimental results. The methods described for predicting material behavior and structural response are generalized to apply to prestressed concrete structures of different weight concretes. Continuous time functions are provided for all needed parameters so that the general solutions readily lend themselves to computer solutions. Approximate equations are also included. Design procedures are presented for calculation of strength and elastic properties, and creep and shrinkage of the sand-lightweight concrete of this project at any time, including ultimate values. An indication is given of the calculation of these properties for normal-weight, sand-lightweight, and all-lightweight concrete in general. Design procedures are also given for calculation of loss of prestress and camber at any time, including ultimate values, of noncomposite and composite prestressed structures. Results computed by these methods are shown to be in agreement with the control specimen data, the laboratory beam data, and the bridge girder data.

•ALTHOUGH the behavior of noncomposite and composite prestressed beams of normal-weight concrete has been studied extensively, with most of these referring to noncomposite beams only (1, 2, 3, 4, 5, 6, 7, 8), it appears that no such investigation has been made of composite prestressed members of lightweight concrete.

Sinno (9), in his study of lightweight noncomposite prestressed bridge girders, concluded that hyperbolic functions (used in modified form in this paper) can be used to predict loss of prestress and camber. Branson and Ozell (5) and Sinno (9) observed that camber tends to reach its ultimate value relatively early compared to creep and shrinkage, because of the offsetting effects of loss of prestress on the one hand and camber growth due to creep on the other.

Methods used in this study for predicting loss of prestress and camber are based in part on papers by Branson and Ozell (5), Branson (10), and ACI Committee 435 (11).

DESCRIPTION OF EXPERIMENTAL INVESTIGATION

Materials and Test Specimens

The details of the laboratory beams and bridge girders are shown in Figure 1 and are given in Appendix B. The laboratory beams were designed as follows:

16

Group A—three noncomposite beams with different prestress moments.
Group B—three beams, two of which are composite beams. The slabs were cast
    at 4 weeks and 10 weeks after the prestressed beams were cast. The
    same prestress moment was used for the 3 beams.
Group C—same as Group B but with a different prestress moment.

The laboratory beams (moist-cured for 3 days and prestressed at age 7 days) and
bridge girders (steam-cured until prestressed at age 2 or 3 days) are sand-lightweight
aggregate concrete (100 percent sand substitution for fines along with lightweight coarse
aggregate), while the slabs are normal-weight concrete. The composite bridge deck
was cast 9 weeks after the bridge girders were cast.

The mix ingredients per cubic yard of sand-lightweight concrete were cement (Type
1), 705 lb; sand, 1,395 lb; idealite aggregate (60 percent of $\frac{3}{4}$ to $\frac{5}{16}$ in. and 40 per-
cent of $\frac{5}{16}$ in. to No. 8), 822 lb; water, 35.0 gal; Darex at $\frac{7}{8}$ oz per sack, 6.5 oz; and
WRDA (used instead of 21.0 oz of pozzolith for lab beams), 50 oz. Two shrinkage
specimens and 3 creep specimens (6 by 12 in. cylinders placed under a sustained uni-
form stress of about 30 percent of the ultimate concrete strength) were cast for each
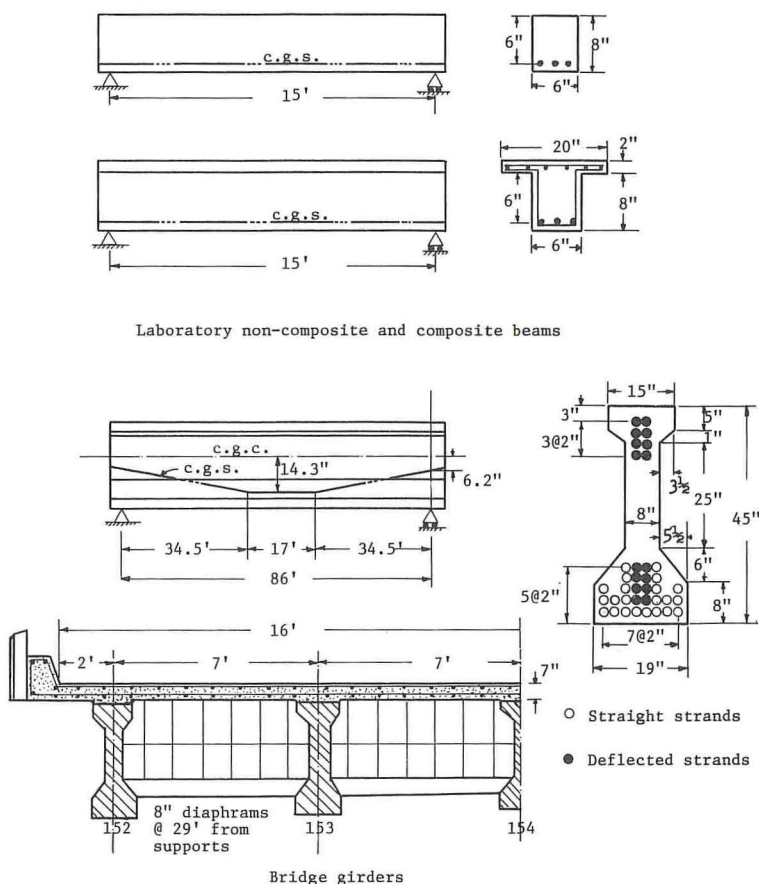sand-lightweight concrete.

Laboratory non-composite and composite beams

Bridge girders

Figure 1. Laboratory beams and bridge girders.

Instrumentation and Test Data

The principal instrumentation for the laboratory beams included load cells for each strand to measure the prestressing force, dial gages for camber, and a Whittemore strain gage for concrete strains. A level rod and precise level were used to obtain the camber measurements for the bridge girders.

The laboratory specimen experimental data consist of the following:

1. Concrete strength properties, elastic properties, creep and shrinkage data from control specimens, and steel properties;
2. Temperature and humidity data;
3. Steel relaxation data;
4. Initial and time-dependent concrete beam strains (these are used in determining experimental loss of prestress); and
5. Initial and time-dependent camber.

Camber data for the bridge girders were obtained in cooperation with Young's study (12). Material properties of the bridge girder concrete were measured in the laboratory. The concrete and steel properties, and other data, are given in Appendix B.

STRENGTH AND ELASTIC PROPERTIES

A study of concrete strength versus time in this project and elsewhere (13) indicates an appropriate general equation in the form of Eq. 1 for predicting compressive strength at any time.

$$(f'_c)_t = \frac{t}{a + bt} (f'_c)_{28d} \tag{1}$$

where a and b are constants, $(f'_c)_{28d}$ = 28-day strength, and t is time.

The following equations were developed in this study and by Branson and Christiason (13) and were used by ACI Committee 209 (14) for normal-weight, sand-lightweight, and all-lightweight concrete (using both moist- and steam-cured concrete and Types 1 and 3 cement). Equations 2 and 4 refer to the concrete (Type 1 cement) of this project.

For moist-cured concrete, Type 1 cement,

$$(f'_c)_t = \frac{t}{4.00 + 0.85t} (f'_c)_{28d}; \text{ or } (f'_c)_{7d} = 0.70(f'_c)_{28d}, (f'_c)_u = 1.18(f'_c)_{28d} \tag{2}$$

For moist-cured concrete, Type 3 cement,

$$(f'_c)_t = \frac{t}{2.30 + 0.92t} (f'_c)_{28d}; \text{ or } (f'_c)_{7d} = 0.80(f'_c)_{28d}, (f'_c)_u = 1.09(f'_c)_{28d} \tag{3}$$

For steam-cured concrete, Type 1 cement,

$$(f'_c)_t = \frac{t}{1.00 + 0.95t} (f'_c)_{28d}; \text{ or } (f'_c)_{2.0d} = 0.69(f'_c)_{28d}, (f'_c)_u = 1.05(f'_c)_{28d} \tag{4}$$

For steam-cured concrete, Type 3 cement,

$$(f'_c)_t = \frac{t}{0.70 + 0.98t} (f'_c)_{28d}; \text{ or } (f'_c)_{2.0d} = 0.75(f'_c)_{28d}, (f'_c)_u = 1.02(f'_c)_{28d} \tag{5}$$

where t is age of concrete in days, and $(f'_c)_u$ refers to an ultimate (in time) value. The results of Eqs. 2 and 4 agree with the experimental data of this project, as shown in Figure 2. As shown elsewhere (13, 14), Eqs. 2, 3, 4, and 5 refer to average values only (the references give ranges of variation).

The secant, initial tangent, and computed moduli of elasticity (using Eq. 6) for the laboratory beam and bridge girder concrete are given in Appendix B.
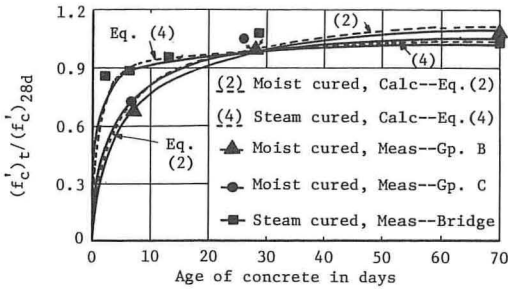
Figure 2. Measured and computed compressive strength versus time curves for the moist-cured laboratory beam concrete and steam-cured bridge girder concrete.

$$E_c = 33\,w^{1.5}\sqrt{f_c'},\ \text{psi};$$

$$w \text{ in pcf and } f_c' \text{ in psi} \qquad (6)$$

The computed values for the limited number of tests made were from 6 to 15 percent higher than the initial tangent values. However, the computed initial camber of the laboratory beams and bridge girders was in aggrement with the measured results (Table 2). Equation 6 (15) is considered satisfactory for normal-weight, sand-lightweight, and all-lightweight concrete.

CREEP AND SHRINKAGE

The principal variables that affect creep and shrinkage are outlined and discussed in Appendix C. The design approach presented here for predicting creep and shrinkage refers to "standard conditions" and correction factors for other than standard conditions.

Based largely on the data and information from several sources (16, 17, 19, 20, 21, 22, 23, 24, 25, 26) and from this project, the following design procedure, which was developed in this project and by Branson and Christiason (13) and used by ACI Committee 209 (14), is recommended for predicting a creep coefficient and unrestrained shrinkage at any time, including ultimate values. The general values suggested for C_u and $(\epsilon_{sh})_u$ should be used only in the absence of specific creep and shrinkage data for local aggregates and conditions. However, the time-ratio part on the right side, except for C_u and $(\epsilon_{sh})_u$, of Eqs. 7 through 9 have been found (13) to apply quite generally. Branson and Christiason (13) and ACI Committee 209 (14) show that these general values of C_u and $(\epsilon_{sh})_u$ refer to average values only and give ranges of variation.

1. Standard creep equation—4 in. or less slump, 40 percent ambient relative humidity, minimum thickness of member 6 in. or less, loading age 7 days for moist-cured and 1 to 3 days for steam-cured concrete.

$$C_t = \frac{t^{0.60}}{10 + t^{0.60}}\,C_u \qquad (7)$$

For the laboratory beam sand-lightweight concrete (moist-cured) of this project, $C_u = 1.75$. The average relative humidity, H, was 40 percent.

For the bridge girder sand-lightweight concrete (steam-cured) of this project, $C_u = 2.15$ for H = 40 percent. H was 70 percent. From Eq. 12 for H = 70 percent, $C_u = 0.80(2.15) = 1.72$.

General value suggested for all weights of structural concrete (both moist- and steam-cured concrete, Types 1 and 3 cement), $C_u = 2.35$ for H = 40 percent. From Eq. 12 for H = 70 percent, $C_u = 0.80(2.35) = 1.88$.

2. Standard shrinkage equations—4 in. or less slump, 40 percent ambient relative humidity, minimum thickness of member 6 in. or less.

a. Shrinkage at any time after age 7 days for moist-cured concrete,

$$(\epsilon_{sh})_t = \frac{t}{35 + t}\,(\epsilon_{sh})_u \qquad (8)$$

For the laboratory beam sand-lightweight concrete of this project, $(\epsilon_{sh})_u = 650 \times 10^{-6}$ in./in. The average relative humidity, H, was 40 percent.

General value suggested for all weights of structural concrete (both Types 1 and 3 cement), $(\epsilon_{sh})_u = 0.70(800 \times 10^{-6}) = 560 \times 10^{-6}$ in./in.

b. Shrinkage at any time after age 1 to 3 days for steam-cured concrete,

$$(\epsilon_{sh})_t = \frac{t}{55 + t} (\epsilon_{sh})_u \tag{9}$$

For the bridge girder sand-lightweight concrete of this project, $(\epsilon_{sh})_u = 560 \times 10^{-6}$ in./in. for H = 40 percent. H was 70 percent. From Eq. 13 for H = 70 percent, $(\epsilon_{sh})_u = 0.70(560 \times 10^{-6}) = 392 \times 10^{-6}$ in./in.

General value suggested for all weights of structural concrete (both Types 1 and 3 cement), $(\epsilon_{sh})_u = 730 \times 10^{-6}$ in./in. for H = 40 percent. From Eq. 13 for H = 70 percent, $(\epsilon_{sh})_u = 0.70(730 \times 10^{-6}) = 510 \times 10^{-6}$ in./in.

In Eqs. 7, 8, and 9, t is time in days after loading for creep and time after initial shrinkage is considered. Values from the standard Eqs. 7, 8, and 9 of C_t/C_u and $(\epsilon_{sh})_t/(\epsilon_{sh})_u$ are given in the following:

Item	1 Month	3 Months	6 Months	1 Year	5 Years
C_t/C_u, Eq. 7	0.44	0.60	0.69	0.78	0.90
$(\epsilon_{sh})_t/(\epsilon_{sh})_u$, Eq. 8	0.46	0.72	0.84	0.91	0.98
$(\epsilon_{sh})_t/(\epsilon_{sh})_u$, Eq. 9	0.35	0.62	0.77	0.87	0.97

The lower creep and shrinkage for the concrete of this project, as compared with the average or general values, was probably due to the high concrete strengths attained. The computed (Eqs. 7 and 8) and measured creep and shrinkage for the moist-cured concrete of this project are shown in Figures 3 and 4.
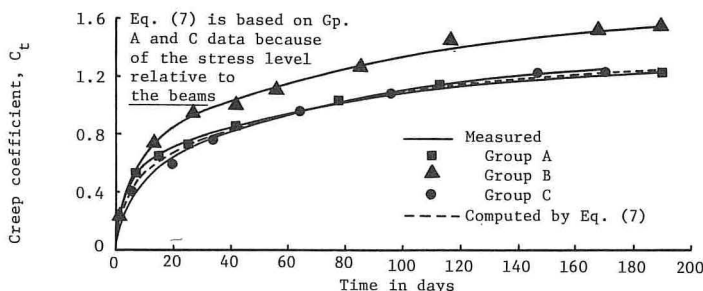
Figure 3. Measured and computed creep coefficient for the sand-lightweight concrete of Groups A, B, and C—slump less than 3 in., loaded at age 7 days, average relative humidity 40 percent, and thickness of specimens 6 in.
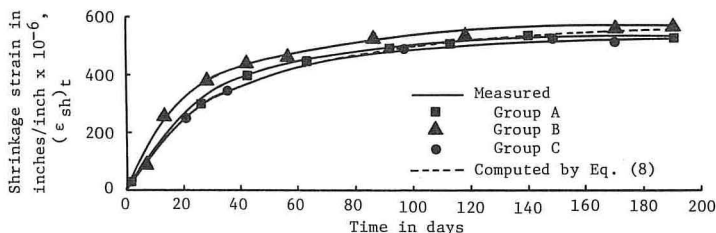

Figure 4. Measured and computed shrinkage strains for the sand-lightweight concrete of Groups A, B, and C—slump less than 3 in., shrinkage from age 7 days, average relative humidity 40 percent, and thickness of specimens 6 in.

3. Correction factors—All correction factors are applied to ultimate values. However, because creep and shrinkage for any period in Eqs. 7, 8, and 9 are linear functions of the ultimate values, the correction factors in this procedure may be applied to short-term creep and shrinkage as well.

For slumps greater than 4 in., see Figure 11.

For loading ages later than 7 days for moist-cured concrete and later than 1 to 3 days for steam-cured concrete, use Eqs. 10 and 11 for the creep correction factors (13). These results are also shown in Figure 5.

$$\text{Creep (C.F.)}_{LA} = 1.25\ t_{LA}^{-0.118}\ \text{for moist-cured concrete} \tag{10}$$

$$\text{Creep (C.F.)}_{LA} = 1.13\ t_{LA}^{-0.095}\ \text{for steam-cured concrete} \tag{11}$$

where t_{LA} is the loading age in days. Examples are as follows:

t_{LA}	Moist-Cured (C.F.)$_{LA}$	Steam-Cured (C.F.)$_{LA}$
10	0.95	0.90
20	0.87	0.85
30	0.83	0.82
60	0.77	0.76
90	0.74	0.74

For shrinkage considered from other than 7 days for moist-cured concrete and other than 1 to 3 days for steam-cured concrete, determine the differential in Eqs. 8 and 9 for any period starting after this time. For shrinkage of moist-cured concrete from 1 day (used to estimate differential shrinkage in composite beams, for example), use Shrinkage C.F. = 1.20.

For greater than 40 percent ambient relative humidity, use Eqs. 12 and 13 for the creep and shrinkage correction factors (13, 25, 27).

$$\text{Creep (C.F.)}_H = 1.27 - 0.0067\ H,\ H \geq 40\ \text{percent} \tag{12}$$

$$\text{Shrinkage (C.F.)}_H = \begin{array}{l} 1.40 - 0.010\ H,\ 40 \leq H \leq 80\ \text{percent} \\ 3.00 - 0.030\ H,\ 80 \leq H \leq 100\ \text{percent} \end{array} \tag{13}$$

where H is relative humidity in percent. Examples are as follows:

H	Creep (C.F.)$_H$	Shrinkage (C.F.)$_H$
40 or less	1.00	1.00
50	0.94	0.90
60	0.87	0.80
70	0.80	0.70
80	0.73	0.60
90	0.67	0.30
100	0.60	0.00

For minimum thickness of members greater than 6 in., see Figure 11 for the creep and shrinkage correction factors as a function of length of drying and loading periods. For most design purposes, this effect (as shown in Appendix C) can be neglected for creep of members up to about 10 to 12 in. minimum thickness, and for shrinkage of members up to about 8 to 9 in. minimum thickness.

This method of treating the effect of member size was based on information from other sources (13, 16, 28) and this project. For large-thickness members, refer to the method of Hansen and Mattock (28) and others for relating size and shape effects for creep and shrinkage to the volume-surface ratio of the members.
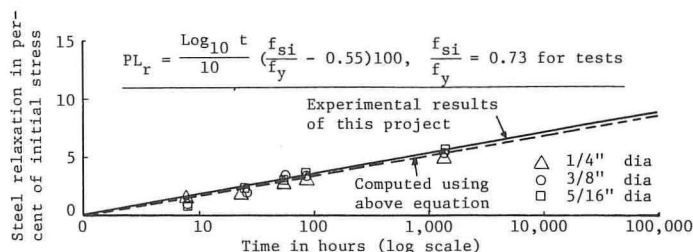
Figure 5. Measured and computed steel relaxation for relaxation tests.

Other correction factors for creep and shrinkage, which are usually not excessive and tend to offset each other, are described in Appendix C. For design purposes, these may normally be neglected.

LOSS OF PRESTRESS AND CAMBER

Relaxation Tests

Relaxation measurements were made for 3 different diameter 7-wire prestressing strands. The results agreed well with the equation suggested by Magura et al. (29) as shown in Figure 5.

It should be noted, however, that the relaxation of steel stress in a prestressed member takes place under decreasing steel strain (due to creep and shrinkage), rather than at constant length as in a relaxation test. The loss of prestress due to steel relaxation is also affected by slab-casting (level of stress in steel is raised) in the case of composite beams. Because of these effects and the practice of overtensioning to counteract the relaxation that takes place between the time of tensioning and release (this practice was assimilated in the laboratory beam tests, where it is shown in Figure 5 that about 2 percent relaxation takes place in 24 hours, for example), it is felt that about 75 percent of the steel relaxation in a constant-length relaxation test should be used in prestressed concrete loss calculations.

Antill concluded (30) that steel relaxation is probably insignificant beyond 100,000 hours (11.4 years), and that this ultimate value might be taken as twice the value at 1,000 hours (1.4 months). The relaxation equation recommended in this paper is the same time-function (log t) as that of Magura et al. (29) except that it is reduced by 25 percent in magnitude and has incorporated Antill's idea (30) that the ultimate value be taken as twice the value at 1,000 hours. This results in an ultimate steel relaxation for prestressed concrete of 7.5 percent, as shown in Term 4 of Eq. 14 and in the other equations.

Computed Loss of Prestress and Camber

The discussion in this section is based on or related to previous studies by the authors and others (5, 6, 7, 10, 11, 29, 30, 31, 32).

Noncomposite Beams at Any Time, Including Ultimate Values—The loss of prestress, in percentage of initial tensioning stress, is given by Eq. 14.

$$PL_t = \left[\overbrace{(n\,f_c)}^{1} + \overbrace{(n\,f_c)C_t\left(1 - \frac{\Delta F_t}{2\,F_0}\right)}^{2} \right.$$

$$\left. + \underbrace{(\epsilon_{sh})_t\,E_s/(1 + npk_s)}_{3} + \underbrace{\frac{f_{si}}{100}\,1.5\log_{10}t}_{4} \right] \frac{100}{f_{si}} \qquad (14)$$

Term 1 is the prestress loss due to elastic shortening $= PL_{el}$; $f_c = \dfrac{F_i}{A_t} + \dfrac{F_i\, e^2}{I_t} - \dfrac{M_D\, e}{I_t}$; and n is the modular ratio at the time of prestressing. Frequently F_o, A_g, and I_g are used instead of F_i, A_t, and I_t, where $F_o = F_i\,(1 - n\,p)$. Only the first 2 terms for f_c apply at the ends of simple beams. For continuous members, the effect of secondary moments due to prestressing should also be included.

Term 2 is the prestress loss due to concrete creep. The expression, $C_t\!\left(1 - \dfrac{\Delta F_t}{2\,F_o}\right)$, was used by Branson and Ozell (5) and by ACI Committee 435 (11) to approximate the creep effect resulting from the variable stress history. A later section on required calculations and summary of general parameters gives approximate values of $\Delta F_t/F_o$ (in form of $\Delta F_s/F_o$ and $\Delta F_u/F_o$) for this secondary effect (expression in parentheses) at 3 weeks to 1 month, 2 to 3 months, and ultimate values.

Term 3 is the prestress loss due to shrinkage (32). The expression, $(\epsilon_{sh})_t\, E_s$, somewhat (approximately 1 percent loss differential for the bridge girder ultimate value in the example here) overestimates on the safe side Term 3. The denominator represents the stiffening effect of the steel.

Term 4 is the prestress loss due to steel relaxation and assumes maximum value = 7.5 percent (at or above 10^5 hours = 11.4 years). In this term, t is time after initial stressing in hours. This expression applies only when f_{si}/f_y is greater than or equal to 0.55, in which f_y is the 0.1 percent offset yield strength.

The camber is given by Eq. 15. It is suggested that an average of the end and mid-span loss be used for straight tendons (laboratory beams here) and 1-point harping, and the midspan loss for 2-point harping (bridge girders here).

$$\underbrace{\Delta_t}_{} = \underbrace{(\Delta_i)_{F_o}}_{1} - \underbrace{(\Delta_i)_D}_{2} + \underbrace{\left[-\frac{\Delta F_t}{F_o} + \left(1 - \frac{\Delta F_t}{2\,F_o}\right) C_t \right] (\Delta_i)_{F_o}}_{3} - \underbrace{C_t (\Delta_i)_D}_{4} - \underbrace{\Delta_L}_{5} \quad (15)$$

Term 1 is the initial camber due to the initial prestress force after elastic loss, F_o. Appendix D gives common cases of prestress moment diagrams with formulas for computing camber, $(\Delta_i)_{F_o}$. Here $F_o = F_i(1 - n\, f_c/f_{si})$, where f_c is determined as in Term 1 of Eq. 14. For continuous members, the effect of secondary moments due to prestressing should also be included.

Term 2 is the initial dead load deflection of the beam; $(\Delta_i)_D = K\,M\,L^2/E_{ci}\,I_g$. Appendix A gives the K and M formulas. I_g is suggested instead of I_t for practical reasons.

Term 3 is the creep (time-dependent) camber of the beam due to the prestress force. This expression includes the effects of creep and loss of prestress, that is, the creep effect under variable stress. ΔF_t refers to the total loss at any time minus the elastic loss. It is noted that the term, $\Delta F_t/F_o$, refers to the steel stress or force after elastic loss, and the prestress loss in percent, PL (as used here), refers to the initial tensioning stress or force. The two are related as

$$\frac{\Delta F_t}{F_o} = \frac{1}{100}(PL_t - PL_{el})\frac{f_{si}}{f_o}$$

and can be closely approximated by

$$\frac{\Delta F_t}{F_o} = \frac{1}{100}(PL_t - PL_{el})\frac{1}{1 - n\,p}$$

Term 4 is the dead load creep deflection of the beam.

Term 5 is the live load deflection of the beam.

Unshored and Shored Composite Beams at Any Time, Including Ultimate Values—
Subscripts 1 and 2 are used to refer to the slab (or effect of the slab such as under

slab dead load) and precast beam respectively. The loss of prestress, in percentage of initial tensioning stress, for unshored and shored composite beams is given by Eq. 16:

$$PL_t = \left[\overbrace{(n \; f_c)}^{1} + \overbrace{(n \; f_c)C_{S_2}\left(1 - \frac{\Delta F_s}{2 \, F_o}\right)}^{2} + \overbrace{(n \; f_c)(C_{t_2} - C_{S_2})\left(1 - \frac{\Delta F_s + \Delta F_t}{2 \, F_o}\right)\frac{I_2}{I_c}}^{3} \right.$$

$$\left. + \overbrace{(\epsilon_{sh})_t \; E_s/(1 + npk_s)}^{4} + \overbrace{\frac{f_{si}}{100}1.5\log_{10}t}^{5} - \overbrace{(m \; f_{cs})}^{6} - \overbrace{(m \; f_{cs})C_{t_1}\frac{I_2}{I_c}}^{7} - \overbrace{PG_{DS}}^{8} \right]\frac{100}{f_{si}}$$

(16)

Term 1 is the prestress loss due to elastic shortening. Term 1 of Eq. 14 gives the calculation of f_c.

Term 2 is the prestress loss due to concrete creep up to the time of slab-casting. C_{S_2} is the creep coefficient of the precast beam concrete at the time of slab-casting. Term 2 of Eq. 14 has comments concerning the reduction factor $\left(1 - \dfrac{\Delta F_s}{2 \, F_o}\right)$.

Term 3 is the prestress loss due to concrete creep for any period following slab-casting. C_{t_2} is the creep coefficient of the precast beam concrete at any time after slab-casting. The reduction factor, $1 - [(\Delta F_s + \Delta F_t)/2 \, F_o]$, with the incremental creep coefficient, $(C_{t_2} - C_{S_2})$, estimates the effect of creep under the variable pre-stress force that occurs after slab-casting. The reduction factor term was modified from previous references. The expression, I_2/I_c, modifies the initial value and accounts for the effect of the composite section in restraining additional creep curvature (strain) after slab-casting.

Term 4 is the prestress loss due to shrinkage. Term 3 of Eq. 14 has comments.

Term 5 is the prestress loss due to steel relaxation. In this term, t is time after initial stressing in hours. Term 4 of Eq. 14 gives the maximum value and limitations.

Term 6 is the elastic prestress gain due to slab dead load, and m is the modular ratio at the time of slab-casting.

$$f_{cs} = \frac{M_{s,Di} \; e}{I_g}, \quad M_{s,Di}$$

refers to slab or slab plus diaphragm dead load, and e and I_g refer to the precast beam section properties for unshored construction and the composite beam section properties for shored construction.

Term 7 is the prestress gain due to creep under slab dead load. C_{t_1} is the creep coefficient for the slab loading, where the age of the precast beam concrete at the time of slab-casting is considered. For shored construction, the term, I_2/I_c, is dropped.

Term 8 is the prestress gain due to differential shrinkage. $PG_{DS} = m \; f_{cd}$, where $f_{cd} = \dfrac{Q \; y_{cs} \; e_c}{I_c}$, and f_{cd} is the concrete stress at the steel cgs. The nomenclature in Appendix A gives additional descriptions of terms. Because this effect results in a prestress gain, not loss, and is normally small (Table 3), it may usually be neglected.

The camber of unshored and shored composite beams is given by Eqs. 17 and 18 respectively.

Unshored Construction—

$$\Delta_t = \overbrace{(\Delta_i)_{F_o}}^{1} - \overbrace{(\Delta_i)_2}^{2} + \overbrace{\left[-\frac{\Delta F_s}{F_o} + \left(1 - \frac{\Delta F_s}{2 \, F_o}\right)C_{S_2}\right](\Delta_i)_{F_o}}^{3}$$

$$+ \left[-\frac{\Delta F_t - \Delta F_s}{F_o} + \left(1 - \frac{\Delta F_s + \Delta F_t}{2 F_o}\right)(C_{t_2} - C_{s_2})\right]^{\overbrace{4}} (\Delta_i) F_o \frac{I_2}{I_c} \overset{5}{- C_{s_2}(\Delta_i)_2}$$

$$\overset{6}{- (C_{t_2} - C_{s_2})(\Delta_i)_2 \frac{I_2}{I_c}} \overset{7}{- (\Delta_i)_1} \overset{8}{- C_{t_1}(\Delta_i)_1 \frac{I_2}{I_c}} \overset{9}{- \Delta_{DS}} \overset{10}{- \Delta_L} \tag{17}$$

Term 1 is the initial camber due to the initial prestress force after elastic loss, F_o. Term 1 of Eq. 15 gives a further explanation.

Term 2 is the initial dead load deflection of the precast beam. $(\Delta_i)_2 = K M_2 L^2 / E_{ci} I_g$. Term 2 of Eq. 15 has a further explanation.

Term 3 is the creep (time-dependent) camber of the beam due to the prestress force up to the time of slab-casting. Term 3 of Eq. 15 and Terms 2 and 3 of Eq. 16 give further explanations.

Term 4 is the creep camber of the composite beam due to the prestress force for any period following slab-casting. Term 3 of Eq. 15 and Terms 2 and 3 of Eq. 16 give further explanations.

Term 5 is the creep deflection of the precast beam up to the time of slab-casting due to the precast beam dead load. C_{s_2} is the creep coefficient of the precast beam concrete at the time of slab-casting.

Term 6 is the creep deflection of the composite beam for any period following slab-casting due to the precast beam dead load. Term 3 of Eq. 16 has a further explanation.

Term 7 is the initial deflection of the precast beam under slab dead load. $(\Delta_i)_1 = K M_1 L^2 / E_{cs} I_g$. The nomenclature in Appendix A contains K and M formulas. When diaphragms are used, additions to $(\Delta_i)_1$ are required:

$$(\Delta_i)_{1D} = \frac{M_{1D}}{E_{cs} I_g}\left(\frac{L^2}{8} - \frac{a^2}{6}\right)$$

where M_{1D} is the moment between diaphragms, and a is $L/4$, $L/3$, and so on for 2 symmetrical diaphragms at the quarter points, third points, and so on respectively.

Term 8 is the creep deflection of the composite beam due to slab dead load. C_{t_1} is the creep coefficient for the slab loading, where the age of the precast beam concrete at the time of slab-casting is considered. Term 3 of Eq. 16 gives comments concerning I_2/I_c.

Term 9 is the deflection due to differential shrinkage. For simple spans, $\Delta_{DS} = Q y_{cs} L^2 / 8 E_{cs} I_c$, where $Q = D A_1 E_1 / 3$. The nomenclature in Appendix A has additional descriptions of terms. The factor 3 provides for the gradual increase in the shrinkage force from day 1, and also approximates the creep and varying stiffness effects (7). This factor 3 is also consistent with the data here and elsewhere. Table 4 gives numerical values used here. In the case of continuous members, differential shrinkage produces secondary moments (similar to the effect of prestressing but opposite in sign, normally) that should be included (35).

Term 10 is the live-load deflection of the composite beam, in which the gross-section flexural rigidity, $E_c I_c$, is normally used.

Shored Construction—

$$\Delta_t = \text{Eq. } 17 \tag{18}$$

with Terms 7 and 8 modified as follows:

Term 7 is the initial deflection of the composite beam under slab dead load. $(\Delta_i)_1 = K M_1 L^2 / E_{cs} I_c$. Appendix A gives K and M formulas.

Term 8 is the creep deflection of the composite beam under slab dead load $= C_{t_1}(\Delta_i)_1$. The composite-section effect is already included in Term 7.

It is suggested that the 28-day moduli of elasticity for both slab and precast beam concretes, and the gross 1 (neglecting the steel), be used in computing the composite moment of inertia, I_c, in Eqs. 16, 17, and 18.

Special Case of "Ultimate" Loss of Prestress and Camber—For computing ultimate values of loss of prestress and camber, Eqs. 19, 20, 21, 22, and 23 correspond term-by-term to Eqs. 14, 15, 16, 17, and 18 respectively.

Loss of prestress for noncomposite beams, as per Eq. 14:

$$PL_u = \left[\overbrace{(n\,f_c)}^{1} + \overbrace{(n\,f_c)C_u\left(1 - \frac{\Delta F_u}{2\,F_o}\right)}^{2} + \overbrace{(\epsilon_{sh})_u E_s/(1 + npk_s)}^{3} + \overbrace{0.075\,f_{si}}^{4} \right] \frac{100}{f_{si}} \quad (19)$$

Camber of noncomposite beams, as per Eq. 15:

$$\Delta_u = \overbrace{(\Delta_i)_{F_o}}^{1} - \overbrace{(\Delta_i)_D}^{2} + \overbrace{\left[-\frac{\Delta F_u}{F_o} + \left(1 - \frac{\Delta F_u}{2\,F_o}\right)C_u \right](\Delta_i)_{F_o}}^{3} - \overbrace{C_u(\Delta_i)_D}^{4} - \overbrace{\Delta_L}^{5} \quad (20)$$

Loss of prestress for unshored and shored composite beams, as per Eq. 16:

$$PL_u = \left[\overbrace{(n\,f_c)}^{1} + \overbrace{(n\,f_c)(\alpha_s C_u)\left(1 - \frac{\Delta F_s}{2\,F_o}\right)}^{2} + \overbrace{(n\,f_c)(1 - \alpha_s)C_u\left(1 - \frac{\Delta F_s + \Delta F_u}{2\,F_o}\right)\frac{I_2}{I_c}}^{3} \right.$$

$$\left. + \overbrace{(\epsilon_{sh})_u E_s/(1 + npk_s)}^{4} + \overbrace{0.075\,f_{si}}^{5} - \overbrace{(m\,f_{cs})}^{6} - \overbrace{(m\,f_{cs})(\beta_s C_u)\frac{I_2}{I_c}}^{7} \right.$$

$$\left. - \overbrace{PG_{DS}}^{8} \right] \frac{100}{f_{si}} \quad (21)$$

Camber of unshored composite beams, as per Eq. 17:

$$\Delta_u = \overbrace{(\Delta_i)_{F_o}}^{1} - \overbrace{(\Delta_i)_2}^{2} + \overbrace{\left[-\frac{\Delta F_s}{F_o} + \left(1 - \frac{\Delta F_s}{2\,F_o}\right)\alpha_s\,C_u \right](\Delta_i)_{F_o}}^{3}$$

$$+ \overbrace{\left[-\frac{\Delta F_u - \Delta F_s}{F_o} + \left(1 - \frac{\Delta F_s + \Delta F_u}{2\,F_o}\right)(1 - \alpha_s)C_u \right](\Delta_i)_{F_o}\frac{I_2}{I_c}}^{4} - \overbrace{\alpha_s C_u(\Delta_i)_2}^{5}$$

$$- \overbrace{(1 - \alpha_s)C_u(\Delta_i)_2\frac{I_2}{I_c}}^{6} - \overbrace{(\Delta_i)_1}^{7} - \overbrace{\beta_s C_u(\Delta_i)_1\frac{I_2}{I_c}}^{8} - \overbrace{\Delta_{DS}}^{9} - \overbrace{\Delta_L}^{10} \quad (22)$$

Camber of shored composite beams, as per Eq. 18:

$$\Delta_u = \text{Eq. 22} \quad (23)$$

except that the composite moment of inertia is used in Term 7 to compute $(\Delta_i)_1$, and the ratio, I_2/I_c, is eliminated in Term 8.

It is noted that Eqs. 14 through 23 could be greatly shortened by combining terms and substituting the approximate parameters given in Eqs. 24, 25, and 26. They are presented in the form of separate terms, however, in order to show the separate effects or contributions to the behavior (such as the prestress force, dead load, creep, and shrinkage that occur both before and after slab-casting). The grossly approximate equations are as follows:

For noncomposite beams,

$$\Delta_u = \Delta_i + \Delta_i C_u \left(1 - \frac{\Delta F_u}{2 F_o} \right), \quad \Delta_i = (\Delta_i)_{F_o} - (\Delta_i)_D \tag{24}$$

For composite beams,

$$PL_u = \left[n f_c \left(1 + \frac{C_u}{2} \right) - n f_{cs} + (\epsilon_{sh})_u E_s + 0.075 f_{si} \right] \frac{100}{f_{si}} \tag{25}$$

$$\Delta_u = \Delta_i + \Delta_i C_u (I_2/I_c), \quad \Delta_i = (\Delta_i)_{F_o} - (\Delta_i)_2 - (\Delta_i)_1 \tag{26}$$

Required Calculations and Summary of General Parameters

Continuous time functions are provided for all needed material parameters (and for different weight concretes, moist- and steam-cured), so that the equations here readily lend themsleves to computer solutions. Certain other read-in data (such as the effect of behavior before and after slab-casting—α_s, β_s, m, and $\Delta F_s/F_o$) are also included. The parameters related to material properties are summarized later so that, for composite beam hand calculations, for example (in addition to the section properties, prestress force, F_o, and concrete stresses, f_c, f_{cs}), the only calculations needed for computing prestress loss and camber are the initial camber, $(\Delta_i)_{F_o}$, $(\Delta_i)_2$, and $(\Delta_i)_1$; Δ_{DS}; and Δ_L.

The following loss of prestress ratios at the time of slab-casting and ultimate are suggested for most calculations:

1. $\Delta F_s/F_o$ for 3 weeks to 1 month between prestressing and slab-casting = 0.11 for normal-weight, 0.13 for sand-lightweight, and 0.15 for all-lightweight;

2. $\Delta F_s/F_o$ for 2 to 3 months between prestressing and slab-casting = 0.15 for normal-weight, 0.18 for sand-lightweight, and 0.21 for all-lightweight; and

3. $\Delta F_u/F_o = 0.22$ for normal-weight, 0.25 for sand-lightweight, and 0.29 for all-lightweight.

Note that these are defined as the total loss (at slab-casting and ultimate) minus the initial elastic loss divided by the prestress force after elastic loss. The different

TABLE 1
AVERAGE MODULAR RATIOS

Modular Ratio	Normal-Weight (w = 145)		Sand-Lightweight (w = 120)		All-Lightweight (w = 100)	
	MC	SC	MC	SC	MC	SC
At release of prestress, n =	7.3	7.3	9.8	9.8	12.9	12.9
3 weeks between prestressing and slab-casting, m =	6.1	6.2	8.1	8.3	10.7	10.9
1 month between prestressing and slab-casting, m =	6.0	6.2	8.0	8.2	10.5	10.7
2 months between prestressing and slab-casting, m =	5.9	6.1	7.9	8.2	10.2	10.6
3 months between prestressing and slab-casting, m =	5.8	6.0	7.7	8.0	10.2	10.5

values for the different weight concretes are due primarily to different initial strains (because of different E's) for normal stress levels.

Table 1 gives average modular ratios based on f'_{ci} = 4,000 to 4,500 psi for both moist-cured (MC) and steam-cured (SC) concrete and Type 1 cement for both 250 and 270 K prestressing strands. Up to 3 months, f'_c = 6,360 to 7,150 psi (using Eq. 2) for MC; and at 3 months, f'_c = 6,050 to 6,800 psi (using Eq. 4) for SC.

E_s = 27 × 10⁶ psi for 250 K strands, E_s = 28 × 10⁶ psi for 270 K strands, α_s refers to the part of the total creep that takes place before slab-casting ($\alpha_s = \dfrac{t^{0.60}}{10 + t^{0.60}}$, as per Eq. 7), and β_s [equal to the average Creep (C.F.)$_{LA}$ from Eqs. 10 and 11] is the creep correction factor for the precast beam concrete age when the slab is cast (under slab dead load). Equations 7, 8, and 9 and the correction factors here give suggested values of C_u and $(\epsilon_{sh})_u$.

The following may be substituted for normal-weight, sand-lightweight, and all-lightweight concrete (moist- and steam-cured, and Types 1 and 3 cement):

Time Between Prestressing and Slab-Casting	α_s	β_s
3 weeks	0.38	0.85
1 month	0.44	0.83
2 months	0.54	0.78
3 months	0.60	0.75

Sample Calculations

The following numerical substitutions for ultimate loss of prestress at midspan, using Eqs. 21 and 25, and ultimate midspan camber, using Eqs. 22 and 26, with the general parameters given here, are made for the sand-lightweight, steam-cured composite bridge girders (with slab moist-cured) of this project.

Parameters and Terms for Interior Girders—Span = 86 ft; girder spacing = 7 ft; 2-point harping at 0.4 L pt. from end, 3 (midspan) = 14.3 in.; e (end) = 6.2 in.; f_{si} = 190,000 psi; F_i = 867 k; A_s = 4.56 in.²; A_g = 520 in.²; p = 0.00883; I_g = 108,500 in.⁴; M_D (precast beam) = 410 ft-k; I_c = 334,100 in.⁴ (using slab width divided by a factor of E_{stem}/E_{slab} = 3.42/3.41 = 1.00); and $M_{S,Di}$ (slab plus diaphragm moment at midspan span) = 630 ft-k.

Moduli of elasticity (using Eqs. 2, 4, and 6 for concrete): E_s = 28 × 10⁶ psi, as suggested for 270 K grade strands here. Slab E_c = 3.41 × 10⁶ psi, for f'_c = 3,500 psi, w = 145 pcf (Table 7). Precast beam (description of m and n is given in general parameters section for concrete properties): E_{ci} = E_s/n = 28 × 10⁶/9.8 = 2.86 × 10⁶ psi; and E_{cs} = E_s/m = 28 × 10⁶/8.2 = 3.42 × 10⁶ psi.

Using F_i, A_t, and I_t, as per Term 1 of Eq. 14 or 16 or 21, f_c = 2,467 psi; as per Term 6 of Eq. 16 or 21, f_{cs} = 1,006 psi. These concrete stresses refer to the midspan section. As per Term 1 of Eq. 15 or 17 or 22, for camber, F_o = $F_i(1 - n\, f_c/f_{si})$ = 758 k, using f_c = 2,467 psi.

From the general parameters section, n = E_s/E_{ci} = 9.8; for 2-month period between prestressing and slab-casting, m = E_s/E_{cs} = 8.2; α_s = 0.54; β_s = 0.78; and $\Delta F_s/F_o$ = 0.18. $\Delta F_u/F_o$ = 0.25.

From Eqs. 7 and 9, for H = 70 percent, C_u = 1.88 and $(\epsilon_{sh})_u$ = 510 × 10⁻⁶ in./in. From Eq. 8, for differential shrinkage, $(\epsilon_{sh})_u$ = 1.2(560) = 670 × 10⁻⁶ in./in.

Initial camber and deflection, and differential shrinkage deflection: $(\Delta_i)_{F_o}$ = 4.09 in., as per Term 1 of Eq. 15 or 17 or 22; $(\Delta_i)_2$ = 1.74 in., as per Term 2 of Eq. 15 or 17 or 22; and $(\Delta_i)_1$ = 2.26 in., as per Term 7 of Eq. 17 or 22. This deflection is due to the slab and diaphragm dead load. Δ_{DS} = 0.49 in., as per Term 9 of Eq. 17 or 22.

Solutions for Interior Girders—Ultimate loss of prestress at midspan using Eq. 21 is

$$
\begin{array}{ccccccccc}
(1) & (2) & (3) & (4) & (5) & (6) & (7) & (8) \\
\end{array}
$$

$$
PL_u = 12.7 + 11.7 + 2.8 + 6.5 + 7.5 - 4.3 - 2.0 - 1.6 = 33.3 \text{ percent}
$$

Ultimate midspan camber using Eq. 22 minus Δ_L is

$$
\begin{array}{ccccccccc}
(1) & (2) & (3) & (4) & (5) & (6) & (7) & (8) & (9) \\
\end{array}
$$

$$
\Delta_u = 4.09 - 1.74 + 3.05 + 0.80 - 1.77 - 0.48 - 2.26 - 1.06 - 0.49 = 0.14 \text{ in.}
$$

Ultimate loss of prestress at midspan using the approximate Eq. 25 is

$$
PL_u = 24.6 - 5.2 + 7.5 + 7.5 = 34.4 \text{ percent}
$$

Ultimate midspan camber using the approximate Eq. 26 is

$$
\Delta_u = 0.09 + 0.05 = 0.14 \text{ in.}
$$

where $\Delta_i = 4.09 - 1.74 - 2.26 = 0.09$ in.

Also given in Tables 2 and 3 are the prestress loss and camber results by the more reliable Eqs. 14 through 17 and 19 through 22, and the approximate Eqs. 24 through 26, for the laboratory beams and bridge girders. Although the agreement is good (note the camber is near zero due to the slab effect) by these methods, the approximate method may be suitable in many cases (Tables 2 and 3) for rough calculations only. Also, the calculations needed by the approximate methods are not significantly fewer than those by the other methods. The more reliable equations should be preferable for computer use.

Experimental Loss of Prestress and Camber Results

The loss of prestress at the end and midspan for the laboratory beams was determined from the measured concrete strains. However, this measured loss does not include the steel relaxation loss, because steel relaxation is a "stress relaxation at constant length—or nearly so in the case of a prestressed concrete beam" phenomenon.

Initial plus time-dependent strain distribution diagrams
from concrete strains measured on the sides of the beams
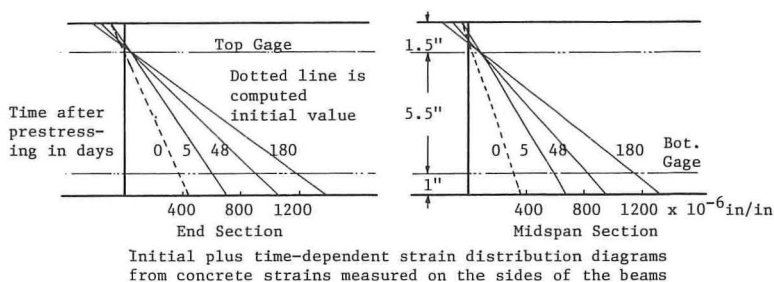
Typical experimental prestress loss determined for end section at 180 days, where f_{si} = 172 ksi, E_s = 27 x 10³ ksi, and observed concrete strain at cgs = 1,001 x 10⁻⁶ in./in.

Item	Percent
Loss from measured strains $(1,001 \times 10^{-6})(27 \times 10^3)(100)/172$	15.7
Increase in measured loss due to lateral distribution (determined as 2.5 percent of 15.7)	0.4
Measured loss due to steel relaxation (75 percent of value shown in Fig. 5)	5.5
Total experimental loss of prestress	21.6

Figure 6. Typical measured strain distribution diagrams for the end and midspan sections of Beam B1, and example of experimental prestress loss determined for the end section at 180 days after prestressing.

Separate relaxation tests were made, and the results are shown in Figure 5. From these and other tests, the relaxation equation given in Term 4 of Eq. 14 was determined. An example of the experimental determination of prestress loss for a typical laboratory beam is shown in Figure 6.

Experimental and computed loss of prestress versus time curves for the laboratory beams are shown in Figure 7, and the computed curves for the bridge girders are shown in Figure 8. Measured and computed midspan camber versus time curves for the beams and girders are shown in Figures 9 and 10. The general Eqs. 14 through 17 with experimental parameters were used in all comparisons with test results in Figures 7, 9, and 10. These results are given in Tables 2 and 3 at release of prestress (camber only), just before slab-casting (3 and 9 weeks for the beams and 9 weeks for the girders, after prestressing), and at 180 days for the beams and 560 days for the
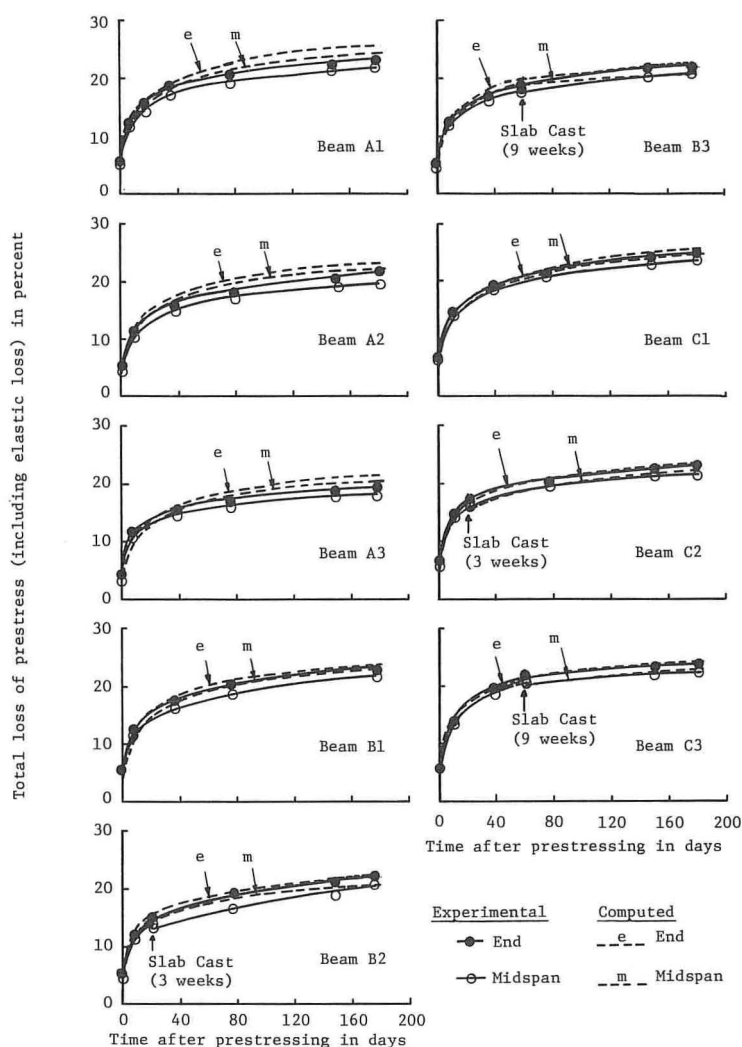

Figure 7. Experimental and computed loss of prestress (using general Eqs. 14 and 16 with experimental parameters) for the laboratory beams.
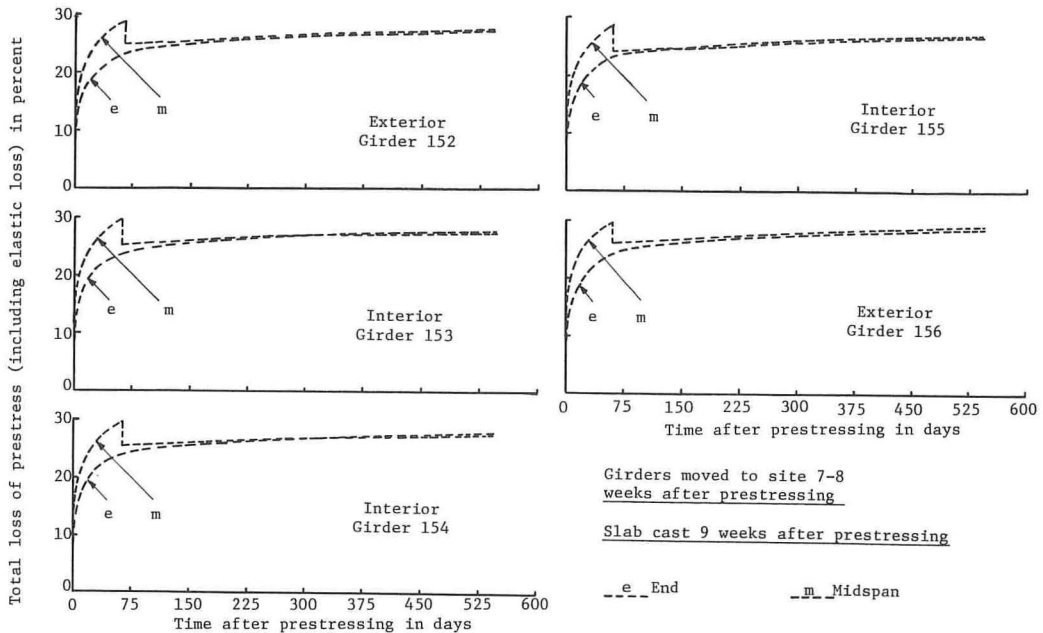
Figure 8. Computed loss of prestress (using general Eq. 16 with experimental parameters) for the bridge girders.

TABLE 2

EXPERIMENTAL AND COMPUTED LOSS OF PRESTRESS FOR LABORATORY BEAMS AND COMPUTED LOSS OF PRESTRESS FOR BRIDGE GIRDERS

No.	Time Between Prestress and Slab-Cast[a] (days)	Computed Loss Just Before Slab-Cast		Experimental Loss at 180 Days[b]		Computed Loss by General Eqs. 14 and 16 With Exp. Parameters[c]				Computed Ultimate Loss[d]					
										Gen. Eqs. 14 and 16 With Exp. Parameters		Ult. Eqs. 19 and 21 With Gen. Parameters		Approx. Eq. 25 With Gen. Parameters	
		Mid	Ratio	End	Mid	End	Ratio	Mid	Ratio	End	Mid	End	Mid	End	Mid
Laboratory Beams															
A1	—	—	—	23.5	22.0	25.5	1.09	24.6	1.12	31.7	30.5	36.9	35.4	—[e]	—
A2	—	—	—	21.0	19.5	23.2	1.10	22.3	1.14	28.9	27.8	33.5	32.1	—	—
A3	—	—	—	19.0	18.5	21.4	1.13	20.4	1.10	26.7	25.5	32.0	30.6	—	—
B1	—	—	—	21.6	21.0	24.0	1.11	22.9	1.09	29.8	28.6	34.6	33.1	—	—
B2	21	15.0	1.07	21.9	20.5	22.2	1.02	20.7	1.01	26.5	25.0	28.9	27.2	31.0	29.4
B3	63	19.4	1.10	21.4	20.0	22.6	1.06	21.1	1.05	26.8	25.2	29.4	27.6	31.0	29.4
C1	—	—	—	25.0	24.0	25.7	1.03	24.7	1.03	31.9	30.8	37.2	35.7	—	—
C2	21	16.4	0.97	23.0	21.4	23.7	1.03	22.4	1.05	28.2	26.7	30.9	29.3	33.1	31.6
C3	63	21.1	1.01	23.6	22.3	24.4	1.03	23.0	1.03	28.7	27.2	31.7	30.0	33.1	31.6
Bridge Girders															
152	65	28.4	—	—	—	27.3	—	28.2	—	29.4	29.6	30.4	34.0	30.5	35.0
153	65	29.4	—	—	—	28.0	—	28.6	—	30.2	30.0	30.3	33.3	30.5	34.4
154	65	29.4	—	—	—	28.0	—	28.6	—	30.2	30.0	30.3	33.3	30.5	34.4
155	60	28.4	—	—	—	27.2	—	27.0	—	29.3	28.7	30.3	33.3	30.5	34.4
156	60	29.8	—	—	—	28.4	—	29.2	—	30.5	31.0	30.4	34.0	30.5	35.0

Note: All losses are expressed in percentage of initial stress. The ratios in the table are computed-experimental. The note to Table 4 gives a description of the experimental parameters. The section on sample calculations gives a description of the general parameters.

[a]The laboratory beams and bridge girders were prestressed at age 7 days and 2 to 3 days respectively.

[b]Figure 6 shows an example of the experimental prestress loss determination. The 180 days and 560 days in footnote c refer to days after prestressing.

[c]180 days for laboratory beams and 560 days for bridge girders.

[d]Because the laboratory beam concrete strengths at release were well beyond the range specified for the general parameters, the n and m values in the general parameter columns were computed separately for the laboratory beams. Where general parameters are used, a correction factor is applied for relative humidity only.

[e]No approximate equation was given in the paper for noncomposite beam loss of prestress. Equation 25 refers to composite beams only.
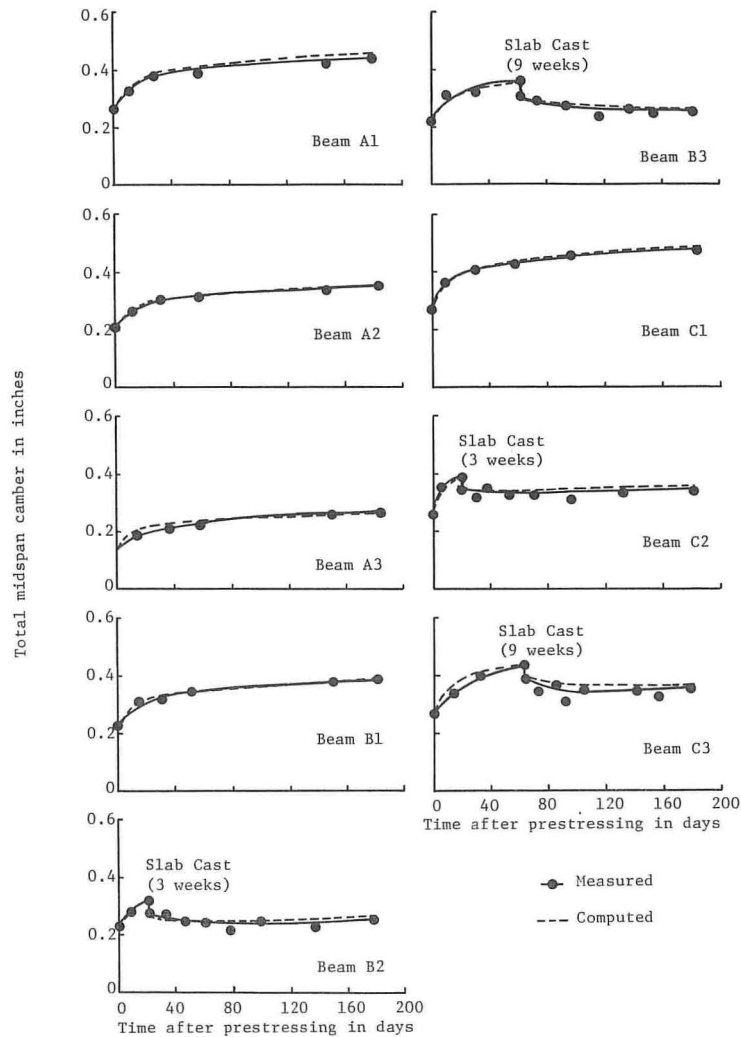
Figure 9. Measured and computed camber (using general Eqs. 15 and 17
with experimental parameters) for the laboratory beams.

32

высокий

TABLE 3

MEASURED AND COMPUTED MIDSPAN CAMBER FOR LABORATORY BEAMS AND BRIDGE GIRDERS

No.	Initial Camber			Time Between Prestress and Slab-Cast[a] (days)	Camber Just Before Slab-Cast			Computed Camber by General Eqs. 15 and 17 With Exp. Parameters[b]			Computed Ultimate Camber[c]		
											Gen. Eqs. 15 and 17 With Exp. Parameters	Ult. Eqs. 20 and 22 With Gen. Parameters	Approx. Eqs. 24 and 26 With Gen. Parameters
	Meas	Comp	Ratio		Meas	Comp	Ratio	Meas	Comp	Ratio			
Laboratory Beams													
A1	0.27	0.25	0.93	—	—	—	—	0.44	0.46	1.04	0.54	0.68	0.77
A2	0.20	0.19	0.95	—	—	—	—	0.35	0.35	1.00	0.42	0.52	0.59
A3	Bad D.	0.15	—	—	—	—	—	0.27	0.26	0.96	0.31	0.38	0.44
B1	0.22	0.22	1.00	—	—	—	—	0.39	0.39	1.00	0.46	0.58	0.66
B2	0.23	0.22	0.96	21	0.32	0.32	1.00	0.25	0.27	1.08	0.28	0.26	0.29
B3	0.23	0.22	0.96	63	0.36	0.35	0.97	0.26	0.27	1.04	0.28	0.28	0.30
C1	0.27	0.27	1.00	—	—	—	—	0.47	0.49	1.04	0.57	0.73	0.75
C2	0.27	0.27	1.00	21	0.39	0.39	1.00	0.34	0.36	1.06	0.38	0.37	0.39
C3	0.27	0.27	1.00	63	0.44	0.44	1.00	0.35	0.37	1.06	0.39	0.39	0.39
Bridge Girders													
152	2.05	2.14	1.04	65	3.10	3.06	0.98	0.50	0.45	0.90	0.43	0.51	0.53
153	2.05	2.22	1.08	65	3.10	3.13	1.02	0.25	0.19	0.76	0.16	0.14	0.14
154	2.10	2.22	1.06	65	3.05	3.13	1.03	0.20	0.19	0.95	0.16	0.14	0.14
155	1.90	2.14	1.13	60	2.95	3.04	1.03	-0.02	0.04	—	—	0.01	0.14	0.14
156	1.85	2.27	1.23	60	2.92	3.16	1.08	0.30	0.52	1.74[d]	0.50	0.51	0.53

Note: All camber values are in inches. The ratios in the table are computed-measured. The note to Table 4 gives a description of the experimental parameters. The section on sample calculations gives a description of the general parameters.

[a]The laboratory beams and bridge girders were prestressed at age 7 days and 2 to 3 days respectively. The 180 days and 560 days in footnote b refer to days after prestressing.
[b]180 days for laboratory beams and 560 days for bridge girders.
[c]Because the laboratory beam concrete strengths at release were well beyond the range specified for the general parameters, the n and m values in the general parameter columns were computed separately for the laboratory beams.
[d]Camber has been reduced from about 3 in. before slab-casting to less than ½ in. after 1 year (Fig. 10). This ratio is large for the near-zero camber even though the difference in camber is 0.22 in.
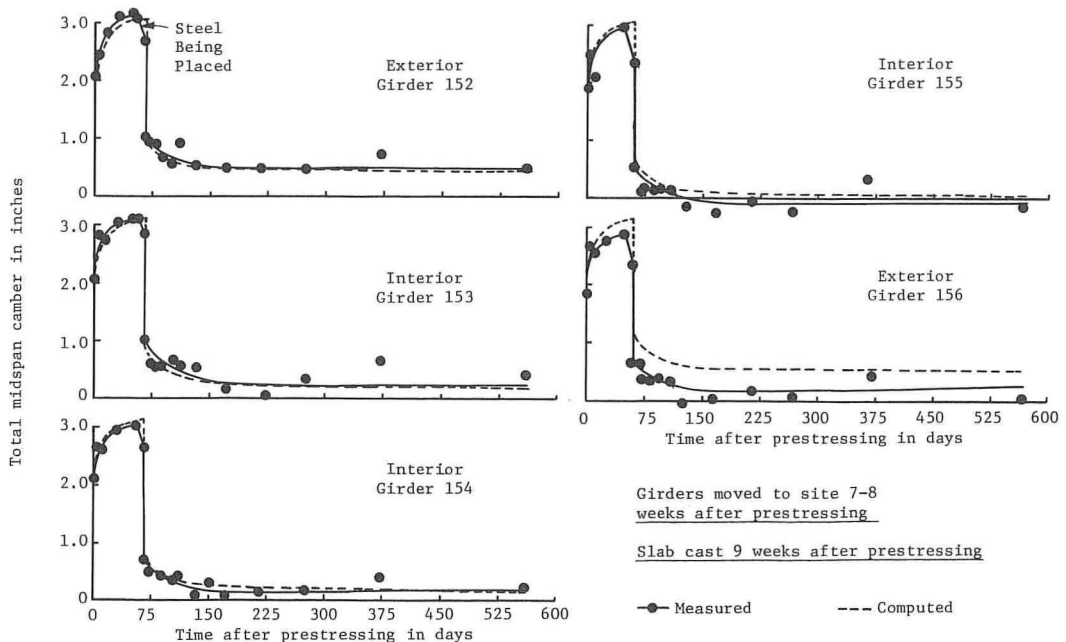

Figure 10. Measured and computed camber (using general Eq. 17 with experimental parameters) for the bridge girders.

TABLE 4

COMPUTED ULTIMATE LOSS OF PRESTRESS AT MIDSPAN, BY TERMS, FOR LABORATORY
BEAMS AND BRIDGE GIRDERS, USING GENERAL EQS. 14 AND 16 WITH EXPERIMENTAL PARAMETERS

No.	Elastic Loss	Creep Loss Before Slab-Cast	Creep Loss After Slab-Cast	Shrink Loss	Relax Loss	Elastic Gain Due to Slab	Creep Gain Due to Slab	Gain Due to Differential Shrink	Total Loss, Eqs. 14 and 16
				Laboratory Beams					
A1	5.2	8.0	—	9.8	7.5	—	—	—	30.5
A2	4.1	6.3	—	9.9	7.5	—	—	—	27.8
A3	3.2	4.8	—	10.0	7.5	—	—	—	25.5
B1	4.5	6.9	—	9.7	7.5	—	—	—	28.6
B2	4.5	2.9	1.2	9.7	7.5	-0.4	-0.2	-0.2	25.0
B3	4.5	4.0	0.9	9.7	7.5	-0.4	-0.2	-0.8	25.2
C1	5.4	8.3	—	9.6	7.5	—	—	—	30.8
C2	5.4	3.5	1.5	9.6	7.5	-0.4	-0.2	-0.2	26.7
C3	5.4	4.8	1.1	9.6	7.5	-0.4	-0.2	-0.6	27.2
				Bridge Girders					
152	11.5	9.8	2.1	4.5	7.5	-3.7	-1.5	-0.6	29.6
153	12.0	10.3	2.2	4.5	7.5	-4.2	-1.7	-0.6	30.0
154	12.0	10.3	2.2	4.5	7.5	-4.2	-1.7	-0.6	30.0
155	11.5	9.6	2.2	4.5	7.5	-4.3	-1.7	-0.6	28.7
156	12.3	10.3	2.3	4.5	7.5	-3.8	-1.5	-0.6	31.0

Note: The table is arranged in the order of terms in Eq. 16. All losses are expressed in percentage of initial stress. The experimental parameters used in the calculations for this table are shown in Table 7 (strength and elastic properties) and elsewhere in this paper for the sand-lightweight concrete of this project. The slab shrinkage is shown here only. The correction factors given here for age of loading, humidity, and member thickness (8 in. for bridge girders) are used where appropriate with experimental parameters. The resulting creep and shrinkage factors used are as follows:

Item	Laboratory Beams (40 percent relative humidity)	Bridge Girders (70 percent relative humidity)
Precast beam creep	$C_u = 1.75$	$C_u = 1.62$
Precast beam shrinkage (x 10^{-6} in./in.)	$(\epsilon_{sh})_u = 650$	$(\epsilon_{sh})_u = 352$
Slab shrinkage (from day 1), used in computing differential shrinkage (x 10^{-6} in./in.)	$(\epsilon_{sh})_u = 470$	$(\epsilon_{sh})_u = 330$

The section on sample calculations gives a comparison with the general parameter results.

TABLE 5

COMPUTED ULTIMATE MIDSPAN CAMBER, BY TERMS, FOR LABORATORY BEAMS AND BRIDGE GIRDERS,
USING GENERAL EQS. 15 AND 17 WITH EXPERIMENTAL PARAMETERS

No.	Initial Camber Due to Prestress	Initial Deflection Due to Beam Dead Load	Creep Camber up to Slab-Cast	Creep Camber After Slab-Cast	Dead Load Creep Deflection up to Slab-Cast	Beam Dead Load Deflection After Slab-Cast	Elastic Deflection Due to Slab Dead Load	Creep Deflection Due to Slab Dead Load	Deflection Due to Differential Shrink	Total Camber, Eqs. 15 and 17
					Laboratory Beams					
A1	0.30	-0.05	0.37	—	-0.09	—	—	—	—	0.53
A2	0.24	-0.05	0.31	—	-0.09	—	—	—	—	0.41
A3	0.19	-0.05	0.25	—	-0.09	—	—	—	—	0.30
B1	0.27	-0.05	0.34	—	-0.10	—	—	—	—	0.46
B2	0.27	-0.05	0.14	0.07	-0.04	-0.02	-0.05	-0.02	-0.01	0.29
B3	0.27	-0.05	0.19	0.05	-0.05	-0.01	-0.04	-0.02	-0.04	0.30
C1	0.32	-0.05	0.40	—	-0.09	—	—	—	—	0.58
C2	0.32	-0.05	0.16	0.08	-0.03	-0.02	-0.04	-0.02	-0.01	0.39
C3	0.32	-0.05	0.22	0.06	-0.05	-0.01	-0.04	-0.02	-0.04	0.39
					Bridge Girders					
152	3.71	-1.56	2.33	0.65	-1.42	-0.36	-1.96	-0.78	-0.18	0.43
153	3.87	-1.64	2.39	0.68	-1.49	-0.38	-2.21	-0.87	-0.19	0.16
154	3.87	-1.64	2.39	0.68	-1.49	-0.38	-2.21	-0.87	-0.19	0.16
155	3.72	-1.57	2.28	0.71	-1.40	-0.37	-2.26	-0.91	-0.19	0.01
156	3.96	-1.68	2.38	0.73	-1.50	-0.39	-2.01	-0.81	-0.18	0.50

Note: The table is arranged in the order of terms in Eq. 17. All values are in inches. The note to Table 4 gives a description of the experimental parameters. The section on sample calculations gives a comparison with the general parameter results.

girders. The test period for the laboratory beams was terminated after 6 months in order to conduct load-deflection tests.

The computed ultimate values are also given in Tables 2 and 3 using the general Eqs. 14 through 17 with experimental parameters determined for the sand-lightweight concrete of this project, and using the ultimate-value Eqs. 19 through 26 with general parameters given for normal-weight, sand-lightweight, and all-lightweight concrete. For the general parameters, the same creep and shrinkage factors are suggested for all 3 concretes, with different modular ratios and prestress loss ratios ($\Delta F_s/F_0$ and $\Delta F_u/F_0$) for each. The computed ultimate values for loss of prestress and camber are given term-by-term in Tables 4 and 5 using the general Eqs. 14 through 17 with experimental parameters.

DISCUSSION AND CONCLUSIONS

The experimental and computed loss of prestress and camber for the sand-lightweight concrete structures of this project are shown in Figures 5 through 10 and Tables 2 through 5. Results both by general Eqs. 14 through 17 (for values at any time, including ultimate) with experimental parameters and by Eqs. 19 through 22 and 24 through 26 (for ultimate values) with general parameters (given here) are included. These results serve to substantiate the generalized procedure presented for predicting loss of prestress and camber of noncomposite and composite prestressed structures. The approximate Eqs. 24 through 26 may be suitable for rough calculations only in some cases.

Results computed by the material parameter, Eqs. 2, 4, 7, 8, and 9, are compared with the data of this project in Figures 2 through 4. Equations 2 through 9 are generalized for different weight concretes. The procedure for predicting creep and shrinkage is one of providing standard functions, with suggested ultimate values for different weight concretes, and correction factors for pertinent conditions other than "standard" (13). These conditions are briefly described in the text and in Appendix C. The ultimate values suggested should be used only in the absence of specific information pertaining to local aggregates and conditions.

Continuous time functions are provided for all needed material parameters (and for different weight concretes, moist- and steam-cured), so that the prestress loss and camber equations readily lend themselves to computer solutions. Certain other read-in data (such as for the effect of behavior before and after slab casting—α_s, β_s, m, and $\Delta F_s/F_0$) are also included, along with a summary of parameters convenient for hand calculations. By using these parameters, the calculations needed in the approximate Eqs. 24 through 26 are not significantly fewer than those needed in the more reliable Eqs. 14 through 23.

It is noted that Eqs. 14 through 23 could be greatly shortened by combining terms, but they are presented in the form of separate terms (results are given in Tables 4 and 5 and in the section on sample calculations) in order to show the separate effects or contributions to the behavior (such as prestress force, dead load, creep, and shrinkage that occur both before and after slab-casting).

The following specific observations and conclusions are made relative to the results shown in Figures 5 and 7 through 12 and given in Tables 1 through 4 and other parts of the paper.

1. The ultimate steel relaxation percentage recommended for regular 7-wire strand to be used in prestressed concrete structures is 7.5 [Fig. 5 and its results and discussion, Term 4 of Eq. 14, and other research (29, 30)].

2. The computed initial camber agreed well in most cases with the measured initial camber, as given in Table 2.

3. The computed prestress loss for the laboratory noncomposite beams was slightly higher (from 0.3 to 2.8 percent prestress loss differential after 6 months) than the experimental results (Fig. 7 and Table 2). The direct application of laboratory creep data for uniformly loaded specimens to beams with nonuniform stress distribution appears to slightly overestimate the creep effect relative to loss of prestress of noncomposite beams. The same overprediction was not found in the case of camber,

apparently because the F/A stress component, which is a dominant factor in loss of prestress results, does not contribute directly to camber. The camber results and other prestress loss results (for composite beams) shown in Figures 7, 9, and 10 and given in Tables 2 and 3 are considered to be in very good agreement. For these cases (noncomposite beam camber and composite beam loss and camber), offsetting creep (and shrinkage in the case of composite beams) effects occur.

4. As shown in Figures 7 and 8 and as given in Table 2, the difference in the end and midspan prestress loss was quite small for the laboratory beams, and relatively large for the bridge girders before slab-casting. After slab-casting, the prestress loss in the bridge girders was only slightly different at end and midspan.

5. The loss of prestress for the sand-lightweight concrete bridge girders was of the order of 27 to 29 percent at 560 days after prestressing and 29 to 31 percent ultimately (Fig. 8 and Table 2). It was determined that loss percentages for bridges under similar conditions using normal-weight concrete will normally be somewhat lower than these (of the order of 25 percent), and those for bridges using all-lightweight concrete will normally be somewhat higher than these (of the order of 35 percent or higher). Higher losses for the lighter concretes, for example, are due primarily to the lower modulus of elasticity (higher elastic strains for a given stress level) and not necessarily to greater creep and shrinkage behavior.

6. Slab-casting causes an elastic deflection (downward) and prestress gain and a time-dependent deflection and prestress gain due to creep and differential shrinkage. Loss of prestress due to creep and camber growth under the prestress force and precast beam dead load is also reduced by the effect of the hardened slab (as opposed to the case of no composite slab). These results are given in Tables 4 and 5 and in the section on sample calculations. The composite slab reduces the ultimate loss of prestress at midspan of the bridge girders about 11 percent (41 - 30 = 11 percent). The camber curves nearly level off at about 3.0 in. just before slab-casting (Fig. 10 and Table 3). After slab-casting and up to ultimate, the camber is reduced to near zero.

7. The effect of the 3-week and 9-week slab-casting schedules for the laboratory beams had only a small effect on loss of prestress (Fig. 7) and a more noticeable effect on camber (Fig. 9). When considering a 3-week slab (slab cast 3 weeks after prestressing) for the bridge girders, as compared with the actual 9-week slab, the ultimate loss of prestress at midspan was about 2 percent less and the ultimate midspan camber about 0.10 in. less for the 3-week slab. These results serve to point out the relatively small beneficial effect of casting the deck slab as early as possible [also indicated by Corley et al. (6)]. It is noted that there are also offsetting effects in the case of the effect of slab-casting schedules. An earlier slab tends to reduce total creep deformation (causing upward camber) by forming an earlier composite section, but it also reduces differential shrinkage deformation (causing downward deflection).

8. The different individual contributions to prestress loss and camber, as illustrated by the different terms in Eqs. 14 through 23, are sensitive to the stiffness, creep, and shrinkage concrete properties. However, the net results of these equations tend toward more correct solutions than the individual terms because of offsetting effects. This is especially true in the case of composite beams and is less the case for noncomposite beams (Tables 2 and 3, and also the comparison of ultimate-value results with experimental parameters and general parameters).

9. The inclusion of all terms in Eqs. 14 through 23 appears to incorporate all significant effects in the reliable prediction of prestress loss and camber. These effects can be seen in the term-by-term data given in Tables 4 and 5 and in the section on sample calculations. In the sample calculations for the bridge girders using the general parameters, for example, the 7 terms (omitting Term 8, differential shrinkage) for loss of prestress varied from 1.6 to 12.7 percent, and the 9 terms for camber varied from 0.48 to 4.09 in. The results by the approximate Eqs. 24 through 26 and the more reliable equations were in reasonably good agreement (Tables 2 and 3 and the section on sample calculations) for the structures of this project.

10. All of the bridge girder data shown in Figure 10 indicated an increase in camber of about 0.4 in. between 300 to 370 days (starting in April). This appears to be due to higher temperatures and is consistent with the observations of Delarue (33).

36

11. The systematic procedures described in this paper for predicting time-dependent behavior are deterministic in nature. Probabilistic methods are also needed for estimating variability of behavior.

ACKNOWLEDGMENTS

REFERENCES

1. Finsterwalder, Ulrick. Ergenbnisse von Kriech und Schwindmessungen an Spannbetonbauwerken. Beton und Stahlbetonbau, Vol. 53, No. 5, May 1958, pp. 136-144.
2. Lofroos, W. N., and Ozell, A. M. The Apparent Modulus of Elasticity of Prestressed Concrete Beams Under Different Stress Levels. Prestressed Concrete Institute Jour., Vol. 4, No. 2, Sept. 1959, pp. 23-47.
3. Pauw, Adrian, and Breen, J. E. Field Testing of Two Prestressed Concrete Girders. HRB Bull. 307, 1961, pp. 42-63.
4. Mattock, A. H. Precast-Prestressed Concrete Bridges; 5. Creep and Shrinkage Studies. Jour., Research and Development Laboratories, Portland Cement Assn., Vol. 3, No. 2, May 1961, pp. 32-66.
5. Branson, D. E., and Ozell, A. M. Camber in Prestressed Concrete Beams. ACI Jour., Proc. Vol. 57, No. 12, June 1961, pp. 1549-1574.
6. Corley, W. G., Sozen, M. A., and Siess, C. P. Time-Dependent Deflections of Prestressed Concrete Beams. HRB Bull. 307, 1961, pp. 1-25.
7. Branson, D. E. Time-Dependent Effects in Composite Concrete Beams. ACI Jour., Proc. Vol. 61, No. 2, Feb. 1964, pp. 213-230.
8. Zia, P., and Stevenson, J. F. Creep of Concrete Under Non-Uniform Stress Distribution and Its Effect on Camber of Prestressed Concrete Beams. Highway Research Program, Rept. ERD-110-R, June 1964, pp. 1-110.
9. Sinno, R. The Time-Dependent Deflections of Prestressed Concrete Bridge Girders. Texas A&M Univ., PhD dissertation, 1968.
10. Branson, D. E. Design Procedures for Computing Deflections. ACI Jour., Proc. Vol. 65, No. 9, Sept. 1968, pp. 730-742.
11. ACI Committee 435. Deflections of Prestressed Concrete Members. ACI Jour., Proc. Vol. 60, No. 12, Dec. 1963, pp. 1697-1728; ACI Manual of Concrete Practice, Part 2, 1967.
12. Young, J. A. Field Observation of Five Lightweight Aggregate Pretensioned Prestressed Concrete Bridge Beams, Final Report. Iowa Highway Research Board, 1969, pp. 1-39.
13. Branson, D. E., and Christiason, M. L. Time-Dependent Concrete Properties Related to Design—Strength and Elastic Properties, Creep and Shrinkage. ACI Jour. in press. Based on MS thesis, Univ. of Iowa, Feb. 1970, pp. 1-21.
14. ACI Committee 209. Prediction of Creep, Shrinkage, and Temperature Effects in Concrete Structures. Symposium paper presented by D. E. Branson, Chairman of Subcommittee II, at 1970 ACI Convention, New York, April 1970.
15. Pauw, Adrian. Static Modulus of Elasticity of Concrete as Affected by Density. ACI Jour., Proc. Vol. 57, No. 6, Dec. 1960, pp. 679-687.
16. Jones, R. R., Hirsch, T. J., and Stephenson, H. K. The Physical Properties of Structural Quality Lightweight Aggregate Concrete. Texas Transportation Institute, Texas A&M Univ., College Station, Aug. 1959, pp. 1-46.
17. Neville, A. M., and Meyers, B. L. Creep of Concrete: Influencing Factors and Prediction. ACI Spec. Publ. 9, 1964, pp. 1-33.
18. Pauw, A., and Chai, J. W. Creep and Creep Recovery for Plain Concrete. Missouri Cooperative Highway Research Program, Rept. 67-8.

19. Ross, A. M. Concrete Creep Data. The Structural Engineer, Vol. 15, No. 8, Aug. 1937, pp. 314-326.
20. Lorman, W. R. The Theory of Concrete Creep. Proc. ASTM, Vol. 40, 1940, pp. 1082-1102.
21. Hanson, J. A. Prestress Loss as Affected by Type of Curing. Jour., Prestressed Concrete Institute, Vol. 9, No. 2, April 1964, pp. 69-93.
22. Pfeifer, D. W. Sand Replacement in Structural Lightweight Concrete—Creep and Shrinkage Studies. ACI Jour., Proc. Vol. 65, No. 2, Feb. 1968, pp. 131-142.
23. Troxell, G. E., Raphael, J. M., and Davis, R. E. Long Time Creep and Shrinkage Tests of Plain and Reinforced Concrete. Proc. ASTM, Vol. 58, 1958, pp. 1-20.
24. Richart, T. W. Creep and Drying Shrinkage of Lightweight and Normal-Weight Concretes. National Bureau of Standards, Monograph 74, March 1964.
25. Keeton, J. R. Study of Creep in Concrete, Phases 1-5. U. S. Naval Civil Eng. Laboratories, Port Hueneme, Calif., Tech. Repts. R333-I, R333-II, and R333-III, 1965.
26. Meyers, B. L., Branson, D. E., and Anderson, G. H. Creep and Shrinkage Properties of Lightweight Concrete Used in the State of Iowa. Iowa State Highway Commission, Phase I Progress Rept. of Proj. HR-136, Oct. 1968, pp. 1-62.
27. Drying Shrinkage of Concrete. The California Producers Committee on Volume Change and Affiliated Technical Organizations, March 1966, pp. 1-40.
28. Hansen, T. C., and Mattock, A. H. Influence of Size and Shape of Member on Shrinkage and Creep of Concrete. ACI Jour., Proc. Vol. 63, No. 2, Feb. 1966, pp. 267-290.
29. Magura, D. D., Sozen, M. A., and Siess, C. P. A Study of Relaxation in Prestressing Reinforcement. Jour. Prestressed Concrete Institute, Vol. 9, No. 2, April 1964, pp. 13-58.
30. Antill, J. M. Relaxation Characteristics of Prestressing Tendons. Civil Engineering Transactions, Inst. of Engr., Australia, Vol. CE 7, No. 2, 1965.
31. Branson, D. E., Meyers, B. L., and Kripanarayanan, K. M. Time-Dependent Deformation of Non-Composite and Composite Sand-Lightweight Prestressed Concrete Structures. Iowa State Highway Commission, Research Rept. 69-1, Feb. 1969, 80 pp.; also Univ. of Iowa, Rept. 70-3, June 1970, 28 pp.
32. Evans, R. H., and Bennett, E. W. Pre-Stressed Concrete. John Wiley and Sons, New York, 1958.
33. Delarue, J. Fluage et Beton Précontraint. RILEM, Paris, Nov. 1958.
34. Shideler, J. J. Lightweight Aggregate Concrete for Structural Use. ACI Jour., Proc. Vol. 54, No. 4, Oct. 1957, pp. 299-328.
35. Design of Continuous Highway Bridges With Precast, Prestressed Concrete Girders. Portland Cement Assn., EB014.01E, Aug. 1969, pp. 1-18.

Appendix A

NOTATION

1 = subscript denoting cast-in-place slab of a composite beam or the effect of the slab as due to slab dead load.

2 = subscript denoting precast beam.

A = area of section.

A_g = area of gross section, neglecting the steel.

A_s = area of prestressed steel.

A_t = area of transformed section.

a = empirical constant in Eq. 1 (also used in Term 7 of Eq. 17 as the distance from end of beam to the nearest of 2 symmetrical diaphragms, and in Appendix D from end to harped point in 2-point harping).

b = empirical constant in Eq. 1.

C = creep coefficient defined as ratio of creep strain to initial strain.

C.F. = correction factor.

C_s = creep coefficient at time of slab-casting.

C_t = creep coefficient at any time.

C_{t_1} = creep coefficient of the composite beam under slab dead load.

C_{t_2} = creep coefficient due to precast beam dead load.

C_u = ultimate creep coefficient.

c = subscript denoting composite section (also used to denote concrete, as E_c).

cp = subscript denoting creep.

D = differential shrinkage strain (also used to denote dead load).

DS = subscript denoting differential shrinkage.

d = effective depth of section.

E_c = modulus of elasticity of concrete such as at 28 days.

E_{ci} = modulus of elasticity of concrete at the time of transfer of prestress.

E_{cs} = modulus of elasticity of concrete at the time of slab-casting.

E_s = modulus of elasticity of prestressing steel.

e = eccentricity of steel cgs.

e_c = eccentricity of steel at center of beam (see Appendix D; also used in Eq. 16 to denote eccentricity of steel in composite section).

e_o = eccentricity of prestressed steel at end of beam (see Appendix D).

F = prestress force after losses.

F_i = initial tensioning force.

F_o = prestress force at transfer (after elastic losses).

ΔF = loss of prestress due to time-dependent effects only, such as creep, shrinkage, steel relaxation (the elastic loss is deducted from the tensioning force, F_i, to obtain F_o).

ΔF_s = total loss of prestress at slab-casting minus the initial elastic loss that occurred at the time of prestressing.

ΔF_t = total loss of prestress at any time minus the initial elastic loss.

ΔF_u = total ultimate loss of prestress minus the initial elastic loss.

f_c = concrete stress such as at steel cgs due to prestress and precast beam dead load in the prestress loss equations.

f_{cd} = concrete stress at steel cgs due to differential shrinkage.

f_{ci} = concrete stress at the time of transfer of prestress.

f_{cs} = concrete stress at steel cgs due to slab dead load (plus diaphragm and dead load when applicable).

f_o = stress in prestressing steel at transfer (after elastic loss).

f_{si} = initial or tensioning stress in prestressing steel.

f_y = yield strength of steel (defined here as 0.1 percent offset).

f'_c = compressive strength of concrete.

$(f'_c)_t$ = compressive strength of concrete at any time.

$(f'_c)_{7d}$ = compressive strength of concrete at 7 days (similarly for 2.0 days, or 1 to 3 days, and 28 days).

$(f'_c)_u$ = ultimate (in time) compressive strength of concrete.

H = relative humidity in percent.

I = moment of inertia (second moment of area).

I_1 = moment of inertia of slab.

I_2 = moment of inertia of precast beam.

I_c = moment of inertia of composite section with transformed slab (slab is transformed into equivalent precast beam concrete by dividing the slab width by E_{c_2}/E_{c_1}).

I_g = moment of inertia of gross section, neglecting the steel.

I_t = moment of inertia of transformed section.

i = subscript denoting initial value.

K = deflection coefficient. For example, for beams of uniform section and uniform load,

K = $\frac{1}{4}$, for cantilever beam,

K = $\frac{5}{48}$, for simple beam,

K = $\frac{8}{185}$, for hinged-fixed beam (one end continuous), and

K = $\frac{1}{32}$, for fixed-fixed beam (both ends continuous).

k_S = $1 + e^2/r^2$, where $r^2 = I_g/A_g$.

L = span length (also used as a subscript to denote live load).

LA = subscript denoting loading age.

M = bending moment. When used as the numerical maximum bending moment for beams of uniform section and uniform load,

$(-)\ M = q\ L^2/2$, for cantilever beam,

$(+)\ M = q\ L^2/8$, for simple beam,

$(-)\ M = qL^2/8$, for hinged-fixed beam (one end continuous), and

$(-)\ M = q\ L^2/12$, for fixed-fixed beam (both ends continuous).

M_1 = maximum bending moment under slab dead load.

M_2 = maximum bending moment under precast beam dead load.

M_{1D} = bending moment between symmetrically placed diaphragms.

$M_{S,Di}$ = bending moment due to slab or slab plus diaphragm dead load.

m = modular ratio of the precast beam concrete, E_s/E_{cs}, at the time of slab-casting.

n = modular ratio, E_s/E_{ci}, at release of prestress.

PG = prestress gain in percentage of initial tensioning stress or force.

PG_{DS} = prestress gain due to differential shrinkage.

PL = total prestress loss in percentage of initial tensioning stress or force.

PL_{el} = prestress loss due to elastic shortening.

PL_r = prestress loss due to steel relaxation.

PL_t = total prestress loss in percent at any time.

PL_u = ultimate prestress loss in percent.

p = steel percentage, A_s/A_g.

Q = differential shrinkage force = $D\ A_1\ E_1/3$. The factor 3 provides for the gradual increase in the shrinkage force from day 1, and also approximates the creep and varying stiffness effects (7, 30).

q = uniformly distributed load.

r = radius of gyration, $r^2 = I_g/A_g$.

s = subscript denoting time of slab-casting (also used to denote steel).

sh = subscript denoting shrinkage.

t = time in general, time in hours in the steel relaxation equation, and time in days in other equations here.

t_{LA} = age of concrete when loaded, in days.

u = subscript denoting ultimate value.

w = unit weight of concrete in pcf.

y_{cs} = distance from centroid of composite section to centroid of slab.

α = ratio of creep coefficient at any time to ultimate creep coefficient.

α_s = ratio of creep coefficient at the time of slab-casting to C_u.

β = creep correction factor for the precast beam concrete age when loaded.

β_s = creep correction factor for the precast beam concrete age when slab cast.

Δ = maximum camber (positive) or deflection (negative).

Δ_i = initial camber, deflection.

$(\Delta_i)_1$ = initial deflection under slab dead load.

$(\Delta_i)_{1D}$ = initial deflection due to diaphragm dead load.

$(\Delta_i)_2$ = initial deflection under precast beam dead load.

$(\Delta_i)_D$ = initial dead load deflection.

$(\Delta_i)_{F_o}$ = initial camber due to the initial prestress force, F_o.

Δ_{DS} = differential shrinkage deflection.

Δ_L = live load deflection.

Δ_t = total camber, deflection, at any time.

Δ_u = ultimate camber, deflection.

$(\epsilon_{sh})_t$ = shrinkage strain in microinches per inch at any time.

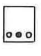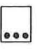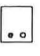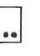$(\epsilon_{sh})_u$ = ultimate shrinkage strain in microinches per inch.
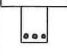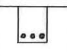
Appendix B

DETAILS OF DESIGN AND TESTS OF BEAMS AND GIRDERS

The details of the laboratory beams and bridge girders are given in Table 6, and the concrete properties, temperature, and humidity data are given in Table 7.

TABLE 6

[e]DETAILS OF LABORATORY BEAMS AND BRIDGE GIRDERS

Beam Group	[a]All Beams are 6" x 8", d=6", Span=15', [b]Slabs are 20" x 2"									L=86', 7"slab
	Group A			Group B			Group C			Bridge Girder
Beam No.	A1	A2	A3	B1	B2	B3	C1	C2	C3	152–156
Beam			[c]							end mid
Prestressing $_{in}$ Strand dia	2-3/8 1-5/16	3-5/16	1-3/8 1-5/16	3-5/16	3-5/16	3-5/16	2-3/8 1-5/16	2-3/8 1-5/16	2-3/8 1-5/16	30-1/2
A_s in^2	0.2176	0.1734	0.1377	0.1734	0.1734	0.1734	0.2176	0.2176	0.2176	4.56
$p = A_s/A_g$	0.00453	0.00361	0.00287	0.00361	0.00361	0.00361	0.00453	0.00453	0.00453	0.00883
Des.Pre.For.F_i,k	38.0	30.0	24.0	30.0	30.0	30.0	38.0	38.0	38.0	867.0
Meas.Pre. F_i,kip	37.0	29.6	23.4	30.0	29.9	29.9	38.0	37.9	37.9	867.0
[d]Concrete Stresses at release of prestress,psi	t=+388 b=-1932	t=+311 b=-1541	t=+244 b=-1224	t=+313 b=-1563	t=+312 b=-1555	t=+312 b=-1555	t=+395 b=-1975	t=+394 b=-1970	t=+394 b=-1970	t=-429 b=-2633 t=-107 b=-2955

[a] ○3/8" Strand, ●5/16" Strand, Measured stress in all strands of lab. beams = (172 ± 4) ksi. Measured stress in all strands of bridge girders = 190 ksi.

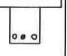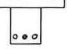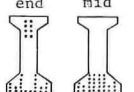[b] Six gage WWF, 6" by 6" (A_s=0.058 in^2 per ft width), slab steel placed in center of slab. No. 3 U-Stirrups in form of ties for composite slab are spaced at 6" cc. in end quarter span and at 22 1/2" cc. in middle half of beam.

[c] Strands placed so that lateral eccentricity is eliminated.

[d] These stresses are computed using the Measured F_i: t = top fiber stress, b = bottom fiber stress. These initial stresses refer to the prestressed section in all cases. The stresses in the case of laboratory beams refer to the end section only. The rectangular (6" by 8") beam dead load, extreme fiber stress at midspan = 218 psi.

[e] The ultimate strength and yield strength (0.1% offset) were: for the laboratory beam steel 250 ksi and and 235 ksi, respectively, and for the bridge girder steel 270 ksi and 250 ksi respectively.

TABLE 7

[a-g]CONCRETE PROPERTIES, TEMPERATURE AND HUMIDITY DATA

Property	Gp.A Lt.Wt	Gp.B Lt.Wt	Gp.C Lt.Wt	Slab B2 N.Wt	Slab C2 N.Wt	Slab B3 N.Wt	Slab C3 N.Wt	[f]Bridge Lt.Wt	Bridge [g]Slab N.Wt
f_c' (7 days) psi	6700	5500	6150	--	--	--	--	5600	
f_c' (28 days) psi	9350	8150	8750	4800	4140	5100	4300	6100	3500
Unit Wt (Wet) pcf	124.0	124.0	125.0	--	--	--	--	--	--
U. Wt (Dry-7d)pcf	123.0	123.5	123.5	153	152	152	153	122.0	145
Meas. Air Ent. %	4.0	6.0	6.0	--	--	--	--	--	--
Slump in	2.0	2.5	2.5	2.5	2.5	3.0	2.5	--	--
[c]Modulus of psi Elasticity at 7 Days x 10^6	-- 3.68	-- 3.35	a. 3.20 b. 3.33 c. 3.55	-- --	-- --	-- --	-- --	a. 3.04 b. 3.10 c. 3.32	-- --
[c]Modulus of psi Elasticity at 28 Days x 10^6	-- 4.35	-- 4.09	a. 3.28 b. 3.58 c. 4.23	-- 4.33	-- 3.97	-- 4.41	-- 4.05	-- 3.47	-- 3.41

[a]Lab. temp: 61-85 deg. F., avg. temp. 78 deg. F. Lab. relative humidity:
25-61%, avg. rel. hum. 40%. Avg. rel. hum. for central Iowa (from U.S.
Weather Bur.): Jan.-79%, July-66%, Mean Annual 71%. For Spr-Sum-Fall, use 70%.

[b]Stress levels for creep tests were approx. design stresses for lab. beams:

Mix	Strength, f_c', at 7 days	Stress Level for Creep Tests	% of 7d-f_c'
Gp. A	6700 psi	2010 psi	30%
Gp. B	5500	1375	25
Gp. C	6150	1845	30

[c]The modulus of elasticity values are as follows: a. Measured secant (to
0.5 f_c') mod. of el., b. Measured initial tangent mod. of el., c. All
values underlined are computed using $E_c = 33 \sqrt{w^3} \, f_c'$, psi.

[d]Computed values of modulus of elasticity at release for bridge girders:

Girder No.	Age at Release	Strength at Rel.	[c]Mod. of El. at Rel.
152	2 days	5160 psi	3.19 x 10^6 psi
153	2	4670	3.04
154	2	4685	3.05
155	3	5130	3.19
156	3	4440	2.96

[e]Computed mod. of el. of pres. units at time of slab casting, [c]E_c x 10^6psi: Gp.B
--4.09, 4.30; Gp.C--4.23, 4.44; Girders 152,153,154--3.50; Girders 155,156--3.40.

[f]Concrete specimens for data in this column obtained from casting yard for
Bridge Girders 155 and 156. Measurements made in laboratory.

[g]"Design" values were used for bridge slab concrete.

Appendix C

PRINCIPAL VARIABLES AFFECTING CREEP AND SHRINKAGE

Presented here is a summary of the principal variables that affect creep and shrink-
age (15, 16, 17, 18, 19) in most cases. The corresponding nominal correction factors,
based on the standard conditions herein, are given earlier and shown in Figure 11 (13,
14, 16, 31). The results shown in Figure 11 and equations for these curves were de-
veloped by Branson and Christiason (13). The variables considered are minimum
thickness of member, water-cement ratio in the form of slump and cement content,
mix proportions in the form of percentage of fines and air content, environmental
humidity, and time of initial loading and time of initial shrinkage.

The following comments refer to the nominal correction factors for creep and shrink-
age (Fig. 11), which are normally not excessive and tend to offset each other. For de-
sign purposes, in most cases, these (except possibly the effect of member size and
slump, as discussed in the text and in the following) may normally be neglected.

42
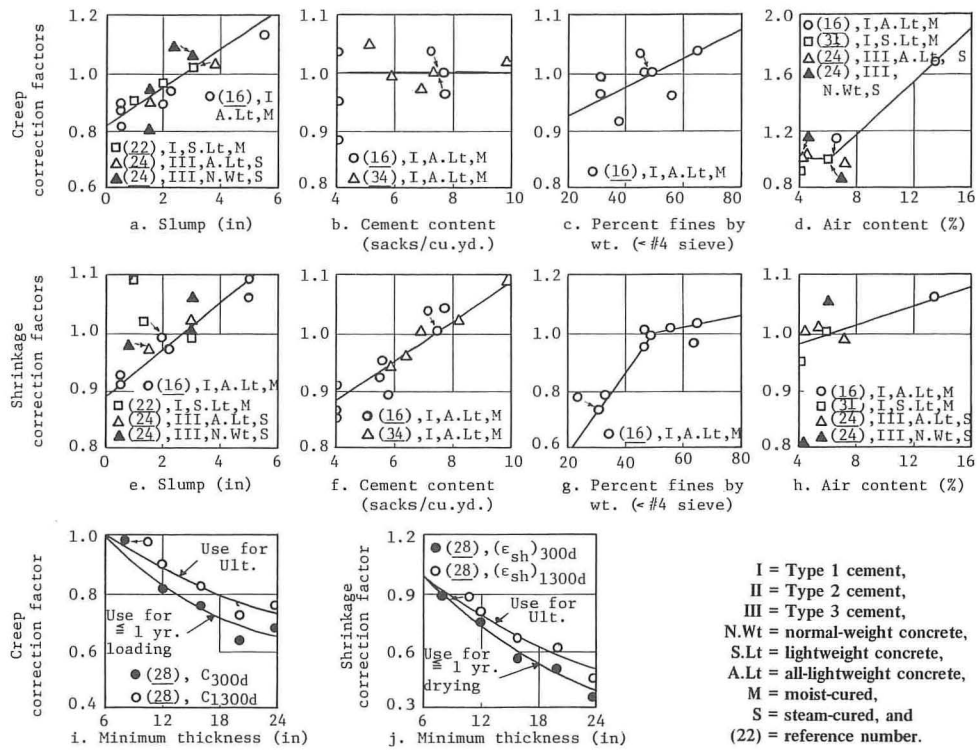
Figure 11. Nominal creep and shrinkage correction factors for the parameters shown (13).

Creep Correction Factors

Slump: C.F. = 0.95 for 2 in., 1.00 for 2.7 in., 1.02 for 3 in., 1.09 for 4 in., and 1.16 for 5 in. Tends to be offset by effect of member thickness. May be marginal but normally can be neglected.

Cement content (sacks/cu yd): C.F. = 1.00. No correction factor required for concrete of, say, 5 to 8 sacks per cu yd at least.

Percent fines (by wt): C.F. = 0.95 for 30 percent, 1.00 for 50 percent, and 1.05 for 70 percent. Normally negligible.

Air content (percent): C.F. = 1.00 for 6 percent or less, 1.09 for 7 percent, and 1.17 for 8 percent. Tends to be offset by effect of member thickness. May be neglected for, say, up to 7 percent air.

Minimum thickness of member: C.F. = 1.00 for 6 in. or less and 0.82 for 12 in. Tends to be offset by effect of slumps greater than 3 in. and air contents greater than 6 percent. Can normally be neglected for members up to about 10 to 12 in.

Shrinkage Correction Factors

Slump: C.F. = 0.97 for 2 in., 1.00 for 2.7 in., 1.01 for 3 in., 1.05 for 4 in., and 1.09 for 5 in. Tends to be offset by effect of member thickness. Normally can be neglected.

Cement content (sacks/cu yd): C.F. = 0.87 for 4 sacks, 0.95 for 6 sacks, 1.00 for 7.5 sacks, and 1.09 for 10 sacks. Normally negligible for, say, 5 to 8 sacks per cu yd at least.

Percent fines (by wt): C.F. = 0.86 for 40 percent, 1.00 for 50 percent, and 1.04 for 70 percent. May be marginal but normally can be neglected.

Air content (percent): C.F. = 0.98 for 4 percent, 1.00 for 6 percent, and 1.03 for 10 percent. Normally negligible.

Minimum thickness of member: C.F. = 1.00 for 6 in. or less and 0.84 for 9 in. Tends to be offset by effect of slumps greater than 3 in. Can normally be neglected for members up to about 8 to 9 in. minimum thickness.

Appendix D

PRESTRESS MOMENT DIAGRAMS AND CAMBER FORMULAS

The following are common cases of prestress moment diagrams with formulas for computing camber.

Prestressed Beam	F_o e Moment Diagram	Midspan Camber Due to F_o e Moments
	$F_o e$	$(\Delta_i)_{F_o} = F_o e \, L^2/8 \, E_{ci} I_g$
	$F_o e_c$	$(\Delta_i)_{F_o} = F_o e_c L^2/12 E_{ci} I_g$
	$F_o e_c$	$(\Delta_i)_{F_o} = \dfrac{F_o(e_c - e_o)L^2}{12 \, E_{ci} \, I_g} + \dfrac{F_o e_o L^2}{8 E_{ci} I_g}$
	$F_o e_c$	$(\Delta_i)_{F_o} = \dfrac{F_o(e_c + e_o)L^2}{12 \, E_{ci} \, I_g} - \dfrac{F_o e_o L^2}{8 E_{ci} I_g}$
	$F_o e_c$	$(\Delta_i)_{F_o} = 5 \, F_o \, e_c \, L^2/48 \, E_{ci} \, I_g$
	$F_o e_c$	$(\Delta_i)_{F_o} = \dfrac{5F_o(e_c - e_o)L^2}{48 \, E_{ci} \, I_g} + \dfrac{F_o e_o L^2}{8 E_{ci} I_g}$
	$F_o e_c$	$(\Delta_i)_{F_o} = \dfrac{5F_o(e_c + e_o)L^2}{48 \, E_{ci} \, I_g} - \dfrac{F_o e_o L^2}{8 E_{ci} I_g}$
	$F_o e_c$	$(\Delta_i)_{F_o} = \dfrac{F_o \, e_c}{E_{ci} I_g}\left(\dfrac{L^2}{8} - \dfrac{a^2}{6}\right)$
	$F_o e_c$	$(\Delta_i)_{F_o} = \dfrac{F_o(e_c - e_o)}{E_{ci} \, I_g}\left(\dfrac{L^2}{8} - \dfrac{a^2}{6}\right) + \dfrac{F_o e_o L^2}{8 E_{ci} I_g}$
	$F_o e_c$	$(\Delta_i)_{F_o} = \dfrac{F_o(e_c + e_o)}{E_{ci} \, I_g}\left(\dfrac{L^2}{8} - \dfrac{a^2}{6}\right) - \dfrac{F_o e_o L^2}{8 E_{ci} I_g}$

Strain Gradient and the Stress-Strain Relationship of Concrete in Compression

S. K. GHOSH, Department of Civil Engineering, University of Pittsburgh; and
V. K. HANDA,* Department of Civil Engineering, College of Petroleum and Minerals, Dhahran, Saudi Arabia

The effects of strain gradient on the stress-strain relationship of concrete in compression, when such effects are not influenced by the presence of a differential strain rate for different fibers of a section, are studied. An experimental procedure is developed that permits maintenance of a constant strain gradient under uniform strain rates, making it possible to separate strain rate and strain gradient effects. Concrete prisms are tested under 3 different strain gradients and at the same uniform rate of straining. Test results indicate that strain gradient, when it is not accompanied by strain rate effects, has very little influence on the stress-strain curves of concrete in compression.

•WHETHER IT IS APPROPRIATE to apply concrete stress-strain curves obtained from compression tests under uniform strain to a situation where a strain gradient prevails is a long-debated question to which a satisfactory answer has not as yet been found.

The problem was investigated at some length by Hognestad et al. ([1]) during the mid-1950's. They, on the basis of their research, came to the conclusion that the general characteristics of stress-strain relationships for concrete in concentric compression were applicable also to flexure. Smith ([2]) also carried out similar investigations, and his results did not seem to disagree with this conclusion. Around 1960, however, this conclusion began to be seriously challenged. Rasch ([3]) had shown earlier that the effect of strain rate on the stress-strain relationship of concrete is quite significant. Rüsch ([4]) now directed attention to the fact that, because the fibers on the compression side of a beam are subjected to different strain rates, different stress-strain curves should be invoked for different fibers. In 1965, Sturman et al. ([5]) reported an investigation into the influence of flexural strain gradients on microcracking and the stress-strain behavior of plain concrete. They found that the peak of the flexural curve was located at a strain about 50 percent higher and a stress about 20 percent larger than the peak of the curve for concentric compression. Sargin ([6]) later tested concrete specimens under both concentric and eccentric loading to observe the effect of flexural strain gradients on concrete stress-strain relationships. In his eccentric tests, he obtained a peak strain about 30 percent higher than a peak stress very nearly equal to that obtained in his concentric tests.

It should be pointed out at this stage that the compression zone of a beam section differs from a section under concentric compression in 2 important respects. First, the fibers on the compression side of a beam are subjected to different strain rates, varying from zero at the neutral axis to a maximum at the extreme fiber. Second, the less highly strained fibers on the compression side of a beam have a restraining effect

---

on the adjacent more highly strained ones. All the investigators mentioned so far, except Rüsch (4), studied the combined effects of these 2 different factors. Rüsch ascribed any differences between the stress-strain curves of concrete under concentric compression and those under flexural compression to the first of these 2 factors and neglected the second one altogether. The first and only attempt so far to study the relative significance of these 2 factors—strain rate and strain gradient—was made by Clark, Gerstle, and Tulin (7). They devised an experimental procedure that permitted maintenance of a constant strain gradient under uniform strain rates, making it possible to separate the strain rate and strain gradient effects. They found that, whereas the effect of strain rate was as predicted by Rüsch (4), the presence of a strain gradient as such had no significant effect on the stress-strain curves. These findings cannot, however, be accepted without some further verification, in view of the following reasons (8):

1. In the construction of their stress-strain curves, Clark et al. followed an approach similar to the one used previously by Rüsch (4) and Rüsch et al. (9). The method consisted of drawing a parabolic stress diagram limited by the 2 edge strains corresponding to each level of loading. This resulted in overlapping segments of parabolas that were then fitted into a continuous stress-strain envelope. This procedure may give good results for small strain gradients where the 2 edge strains are close to each other. However, where large strain gradients are involved, because each of the segments mentioned covers quite a large portion of the stress-strain diagram, the choice of an arbitrary parabola for segments may lead to erroneous results.

2. The authors obtained unusually high maximum stress and peak strain values in concentric as well as eccentric tests on plain concrete specimens.

3. The authors tried to explain the discrepancy between their results and those reported by Sturman et al. (5) by attributing it to the presence of a differential strain rate for different fibers in the latter case. But a close look at Figure 5 of Rüsch's paper (4) reveals that strain rate effects alone cannot possibly produce a 20 percent increase in maximum stress and a 50 percent increase in peak strain simultaneously. It should be noted, however, that there is not much of a conflict between the authors' findings and those of Sargin (6). A 30 percent increase in peak strain, unaccompanied by any increase in maximum stress, can be caused by strain rate effects alone.

The object of the present investigation was to supplement the findings of Clark et al. through a further series of tests. The effects of strain gradient on concrete stress-strain relationships, when they are not accompanied by strain rate effects, were studied.

OUTLINE OF TESTS

A total of 13 specimens was tested in 3 different sets. The specimens were necked concrete prisms measuring 22 in. in length and 5 by 5 in. in cross section in the test region. No longitudinal reinforcement was used in any of the specimens. All of them, however, were laterally reinforced. The transverse reinforcement consisted of No. 2 ties at a longitudinal center-to-center spacing of 3 in. At each end of the specimens, 3 ties were placed at a spacing of $1\frac{1}{2}$ in. in order to reduce the effect of stress concentration at the ends. The No. 2 bars were round and plain and had an average yield stress of 44 ksi. The center-to-center dimensions of the ties were $3\frac{3}{4}$ by $3\frac{3}{4}$ in.

Four of the 13 specimens were tested under concentric and the remaining 9 under eccentric loading. Of the 9 eccentrically loaded specimens, 4 were tested under a strain gradient of 0.0004 radian/in. and 5 under a strain gradient of 0.0006 radian/in. The primary variable in this investigation was strain gradient. The concrete used had, on an average, a cylinder strength of 5,100 psi. All the specimens were cast with their longitudinal axes in a vertical position. The age of the specimens at the time of testing varied from 26 to 29 days.

TEST SETUP AND TEST PROCEDURE

For eccentric loading tests, an experimental procedure was employed that provided for the individual control of bending and axial loads, permitting maintenance of a

constant strain gradient under uniform strain rates and making it possible to separate strain rate and strain gradient effects. The same experimental procedure was employed for concentric loading tests also to ensure the maintenance of a zero strain gradient across the test cross section at all stages of loading. Thus, each specimen was tested under the action of a major load applied directly to the specimen and a minor load applied through 2 steel brackets fixed to the enlarged ends of the specimen. The test setup is shown in Figure 1. The minor load was applied at a distance of $32\frac{1}{2}$ in. from the centerline of the specimen and the major load at an eccentricity of $\frac{3}{8}$ in. in the same direction. The minor load was applied to the brackets by means of a small hydraulic jack of 10-ton capacity. A 20,000-lb load cell was used to measure this load. A closed-loop materials test system, consisting of a 500,000-lb capacity load frame, was utilized for applying the major load. The load frame contained a servoram actuator that imposed a force on the specimen and that was made to move at a constant rate throughout each test. The load applied by the actuator was transferred to the concrete specimen through 2 parallel knife-edge supports. The load was measured by a 250,000-lb load cell incorporated in the load frame.

Longitudinal strains were measured along 5-in gage lengths on 2 opposite faces of each specimen. Lateral deflections undergone by eccentrically loaded specimens at
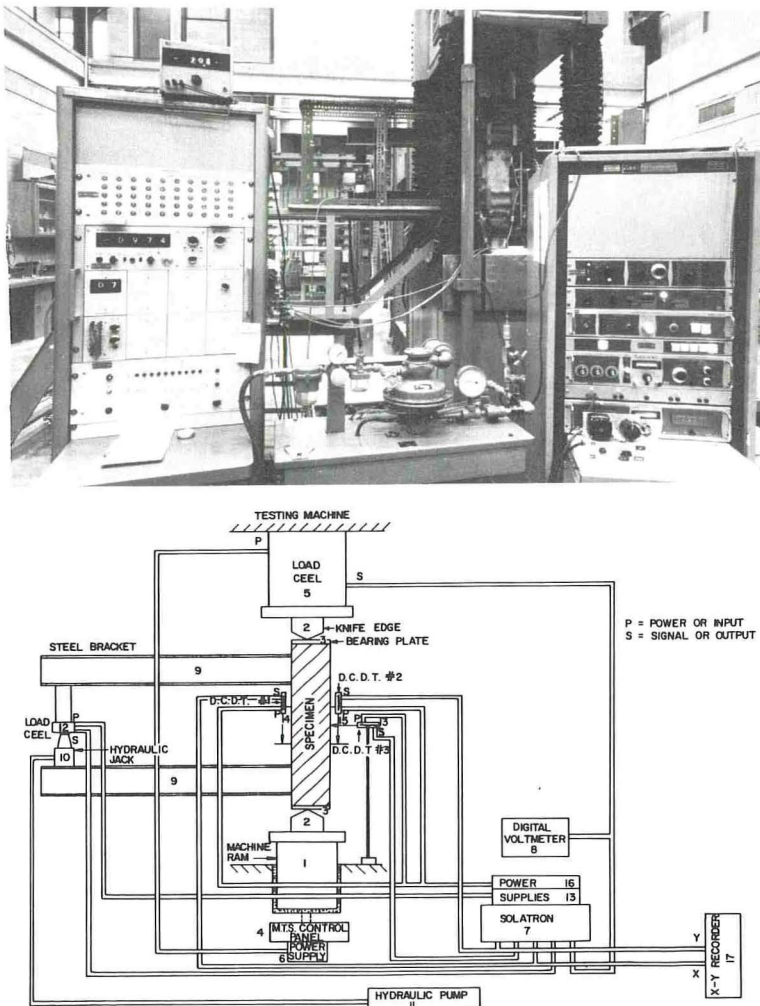

Figure 1. Test setup.

various stages of loading were also measured at the midheight of each specimen. Sanborn Model 7 DCDT-250 displacement transducers were used to measure both the strains and the deflection.

At the beginning of each test, the 2 DCDT's on 2 opposite faces of the specimen were connected to the X and Y axes of an X-Y recorder. A ramp function generator that was used to regulate the movement of the machine ram was then switched on. The machine ram thus began to move at a predetermined constant rate of 0.66 in./hr. As the specimen was strained, the pen of the X-Y recorder began to move. When the test is concentric, the pen should move along a 45-deg line. The movement of the pen was closely watched throughout each test. As soon as it started deviating from the 45-deg line, in a concentric test, it was brought back by increasing or decreasing the minor load. In an eccentric test the secondary load was regulated so that the pen, instead of moving along a 45-deg line, initially moved along a line parallel to the axis to which the strain gage on the most strained face of the specimen was connected. After the pen had moved horizontally by a certain distance, i.e., after the difference between the strains on 2 opposite faces of the specimen had reached a certain desired value, the pen was made to move along a 45-deg line as before, so that the strain difference be-

Figure 2. Strain and stress distribution in the test region of an eccentrically loaded specimen.

tween the 2 opposite faces remained constant at all subsequent stages of loading.

The signals from the 2 load cells, measuring the major and minor loads, and the 3 DCDT's, measuring longitudinal strains and deflection, were fed into a Solatron data logger that displayed these voltages in digital form. The displayed signals were read at regular intervals throughout each test.

ANALYSIS OF TEST RESULTS

Concentrically Loaded Specimens

Strain and stress distributions are assumed to be uniform over the critical cross section of the specimen. Say, at any time, P_1 is the major load applied on the specimen and P_2 is the minor load. Then, if P_3 is the weight of each minor load carrying bracket, the resultant load on the specimen at that particular time is

$$P = P_1 - P_2 + P_3 \qquad (1)$$

If Δ is the deformation corresponding to this load measured over a gage length L_0 and A_t the cross-sectional area, then

$$\text{Stress } \sigma = P/A_t \qquad (2)$$

and

$$\text{Strain } \epsilon = \Delta/L_0 \qquad (3)$$

Eccentrically Loaded Specimens

A numerical method is employed in this analysis. It is more general than the one used by Hognestad et al. (1) and very similar to the one used by Sargin (6).

In an eccentric test, initially, the strain at one face of each specimen is maintained at zero, while the strain on the opposite face is increased continuously till the differ-
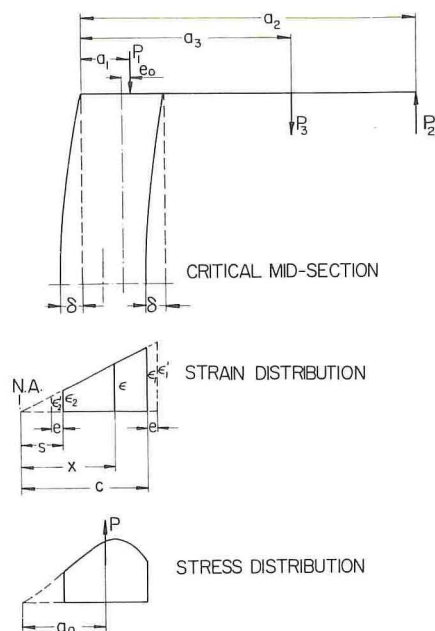
ence between these 2 strains reaches a certain value. This strain difference is maintained constant during all subsequent stages of loading. The analyses of test data are slightly different for these 2 parts of each test. Here an analysis for the second part (Part A) is presented first. A method of analysis for the initial part (Part B) can be derived as a special case of this analysis and is presented later in this section.

Part A—From force and moment equilibriums, the magnitude and point of application of the internal resultant force can be calculated directly. From Figure 2,

$$P = P_1 - P_2 + P_3 \tag{1}$$

and

$$a_0 = [P_1(a_1 + \delta + s) - P_2(a_2 + \delta + s) + P_3(a_3 + \delta + s)]/P$$

where

a_1, a_2, and a_3 = distances of points of application of P_1, P_2, and P_3 respectively from the least strained fiber of critical cross section, neglecting deflection;
  s = distance of neutral axis from least strained fiber;
  δ = lateral deflection of the specimen; and
  a_0 = distance of point of application of P from neutral axis.

Assuming a linear strain distribution, strain compatibility of the section can be written as

$$\frac{\epsilon_2'}{s - e} = \frac{\epsilon_2}{s} = \frac{\epsilon}{y} = \frac{\epsilon_1}{c} = \frac{\epsilon_1'}{c + e} \tag{5}$$

where

ϵ_1 and ϵ_2 = strains in most and least strained fibers respectively;
ϵ_1' and ϵ_2' = strains measured by transducers attached to most and least strained faces respectively;
  c = distance of neutral axis from most strained fiber;
  ϵ = strain in any fiber;
  y = distance of this fiber from neutral axis; and
  e = distance from center of deformation transducer to specimen surface.

Equation 5 makes it possible for ϵ_1 and ϵ_2 to be expressed in terms of the measured strains ϵ_1' and ϵ_2'.

If all fibers are assumed to follow one and the stress-strain curve

$$\sigma = f(\epsilon)$$

then force and moment equilibriums in the section can be written as

$$\int_s^c f(\epsilon)\,b\,dy = P = f_0 bc \tag{6}$$

$$\int_s^c f(\epsilon)\,by\,dy = Pa_0 = m_0 bc^2 \tag{7}$$

where

$f_0 = P/bc$ and $m_0 = Pa_0/bc^2$, and
  b = width of cross section.

Using Eq. 5, Eqs. 6 and 7 can be rewritten for a rectangular section as

$$\int_{\epsilon_2}^{\epsilon_1} f(\epsilon)\,d\epsilon = f_0 \epsilon_1 \tag{8}$$

$$\int_{\epsilon_2}^{\epsilon_1} f(\epsilon)\,\epsilon d\epsilon = m_0 \epsilon_1^2 \tag{9}$$

Differentiating Eqs. 8 and 9 with respect to ϵ_1, solving the resulting equations simultaneously, and substituting finite differences for differentials, the following stress-strain relationships are obtained:

$$f(\epsilon_1) = \frac{\epsilon_1}{\epsilon_1 - \epsilon_2}\left[2m_0 - f_0\,\frac{\epsilon_2}{\epsilon_1} + \epsilon_1\left(\frac{\Delta m_0}{\Delta\epsilon_1} - \frac{\Delta f_0}{\Delta\epsilon_1}\frac{\epsilon_2}{\epsilon_1}\right)\right] \tag{10}$$

$$f(\epsilon_2) = \frac{\epsilon_1 \Delta\epsilon_1}{\epsilon_1 - \epsilon_2 \Delta\epsilon_2}\left[2m_0 - f_0 + \epsilon_1\left(\frac{\Delta m_0}{\Delta\epsilon_1} - \frac{\Delta f_0}{\Delta\epsilon_1}\right)\right] \tag{11}$$

Part B—ϵ_2 is expressed, in this case, in terms of ϵ_1 using Eq. 5, and both s (s = e) and c (c = s + d, where d = depth of cross section) are constants. Eqs. 10 and 11 get reduced to

$$f(\epsilon_1) = \frac{c}{c - s}\left[2m_0 - f_0\,\frac{s}{c} + \epsilon_1\left(\frac{\Delta m_0}{\Delta\epsilon_1} - \frac{\Delta f_0}{\Delta\epsilon_1}\frac{s}{c}\right)\right] \tag{10a}$$

$$f(\epsilon_2) = \frac{c^2}{s(c - s)}\left[2m_0 - f_0 + \epsilon_1\left(\frac{\Delta m_0}{\Delta\epsilon_1} - \frac{\Delta f_0}{\Delta\epsilon_1}\right)\right] \tag{11a}$$

GENERAL STRESS-STRAIN RELATIONSHIP FOR CONCRETE IN COMPRESSION

Experimental stress-strain diagrams defined at some discrete points are obtained from an analysis of test data by the method just explained. In each of these diagrams, experimental scatter manifests itself in the form of deviations from the general trend. In order to find out what the general trend in each case is, it is necessary to postulate a general form for the stress-strain relationship of concrete in compression. Test results can then be used to find empirical coefficients of this stress-strain relationship for a best correlation. Of all the available formulations of the stress-strain relationship of concrete in compression, the one proposed by Sargin (6) is by far the most general. For the purpose of the present study, it is postulated that the general form of the stress-strain relationship of concrete in compression can be represented by the following equation proposed by Sargin:

$$\sigma = k_3 f_c'\,\frac{Ax + (D - 1)x^2}{1 + (A - 2)x + Dx^2} \tag{12}$$

where

A = $E_c \epsilon_0 / k_3 f_c'$;
x = ϵ / ϵ_0;
f_c' = cylinder strength of concrete;
E_c = initial modulus of elasticity;
k_3 = ratio of maximum stress to cylinder strength;
ϵ_0 = strain corresponding to maximum stress; and
D = parameter that mainly affects the slope of the descending branch of a stress-strain curve.

The principal factors affecting concrete behavior can be introduced into the stress-strain relationship through these 5 parameters (f_c', E_c, k_3, E_0, and D). In the present study, a nonlinear regression analysis is employed to find the parameters of Eq. 12

for a best correlation with test results obtained for each specimen. The details of the regression analysis are given elsewhere ($\underline{10}$).

TEST RESULTS

Concentrically Loaded Specimens

Analytical stress-strain curves of the form given by Eq. 12 were fitted to experimental data obtained for each specimen. The values of the parameters of these curves for best correlation with experimental data are given in Table 1. The experimental and analytical stress-strain diagrams are shown in Figure 3.

Eccentrically Loaded Specimens

A complete stress-strain diagram for the most strained fiber of each specimen was obtained by fitting a curve of the form given by Eq. 12 to the experimental points given by Eqs. 10 and 10a). It was observed both by Sargin ($\underline{6}$) and by the authors that Eq. 11a gave very erratic stress values. These values were ignored, and it was assumed that the initial portion of the stress-strain curve for the most strained fiber of a specimen was valid for the least strained fiber also. A complete stress-strain diagram for the least strained fiber of each specimen was thus obtained by fitting a curve of the form given by Eq. 12 to experimental points given by Eqs. 10a and 11. The initial portion of each stress-strain diagram obtained in this way was subject to both strain rate and strain gradient effects. This did not, however, affect the purpose of the present study because the subsequent portion (which included the peak) of each diagram was free from strain rate effects, and, in drawing conclusions, only the k_3 and ϵ_0 values of the different curves were compared. The analytical and experimental stress-strain diagrams for the most and least strained fibers of each specimen of series E_1 are shown

TABLE 1
EXPERIMENTALLY OBTAINED STRESS-STRAIN CURVE PARAMETERS

Specimen	f'_c (psi)	E_c (psi)		k_3		ϵ_0 (percent)		D	
		I^a	II^b	I	II	I	II	I	II
C-1	4,260	$45,484\sqrt{f'_c}$		0.775		0.4452		0.9699	
C-2	4,110	$43,571\sqrt{f'_c}$		0.691		0.3237		0.9881	
C-3	4,110	$48,635\sqrt{f'_c}$		0.676		0.4052		0.6414	
C-4	5,700	$38,158\sqrt{f'_c}$		0.725		0.3354		1.3540	
Avg.	4,545	$43,962\sqrt{f'_c}$		0.717		0.3774		0.9884	
E_1-1	5,700	$50,182\sqrt{f'_c}$	$48,149\sqrt{f'_c}$	0.751	0.761	0.3351	0.3446	0.2185	0.2510
E_1-2	5,400	$65,382\sqrt{f'_c}$	$58,014\sqrt{f'_c}$	0.761	0.774	0.3590	0.3809	0.8257	0.8030
E_1-3	5,400	$51,945\sqrt{f'_c}$	$50,189\sqrt{f'_c}$	0.790	0.795	0.2743	0.2934	0.4834	0.4242
E_1-4	5,150	$52,841\sqrt{f'_c}$	$52,841\sqrt{f'_c}$	0.802	0.829	0.2557	0.2590	1.6092	1.6134
Avg.	5,413	$53,693\sqrt{f'_c}$		0.783		0.3128		—	
E_2-1	5,150	$48,579\sqrt{f'_c}$	$45,085\sqrt{f'_c}$	0.773	0.797	0.3592	0.3748	0.9275	0.9143
E_2-2	5,550	$31,579\sqrt{f'_c}$	$34,771\sqrt{f'_c}$	0.682	0.647	0.2619	0.2935	0.9547	0.7937
E_2-3	5,550	$52,497\sqrt{f'_c}$	$52,356\sqrt{f'_c}$	0.649	0.598	0.2957	0.3635	0.8578	0.4783
E_2-4	5,200	$49,018\sqrt{f'_c}$	$47,019\sqrt{f'_c}$	0.742	0.765	0.3457	0.3545	0.8384	0.8393
E_2-5	5,200	$46,301\sqrt{f'_c}$	$49,168\sqrt{f'_c}$	0.765	0.780	0.3370	0.3262	0.7584	0.8000
Avg.	5,330	$45,637\sqrt{f'_c}$		0.720		0.3312		0.8162	

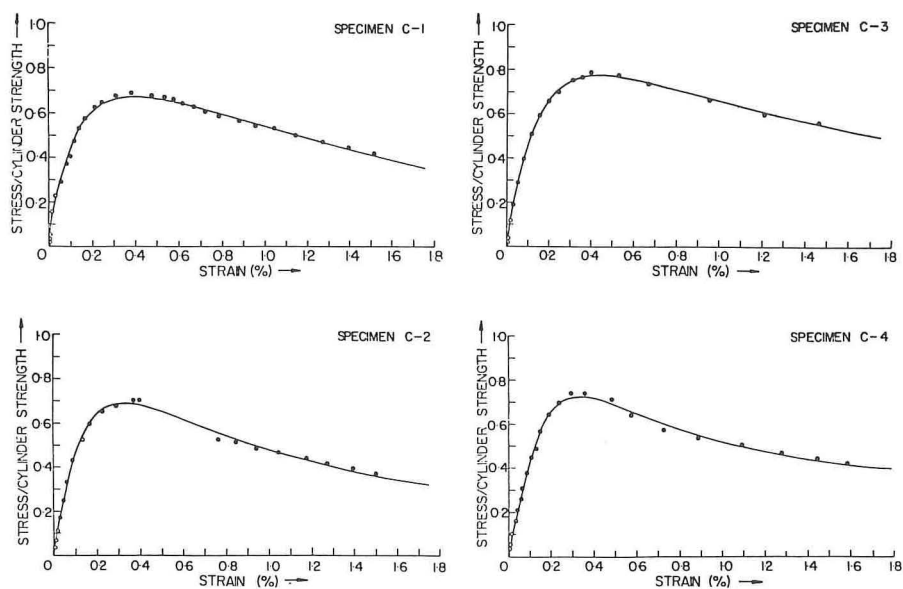^{a}Most strained fibers. ^{b}Least strained fibers.

Figure 3. Analytical and experimental stress-strain diagrams for the specimens of Series C.
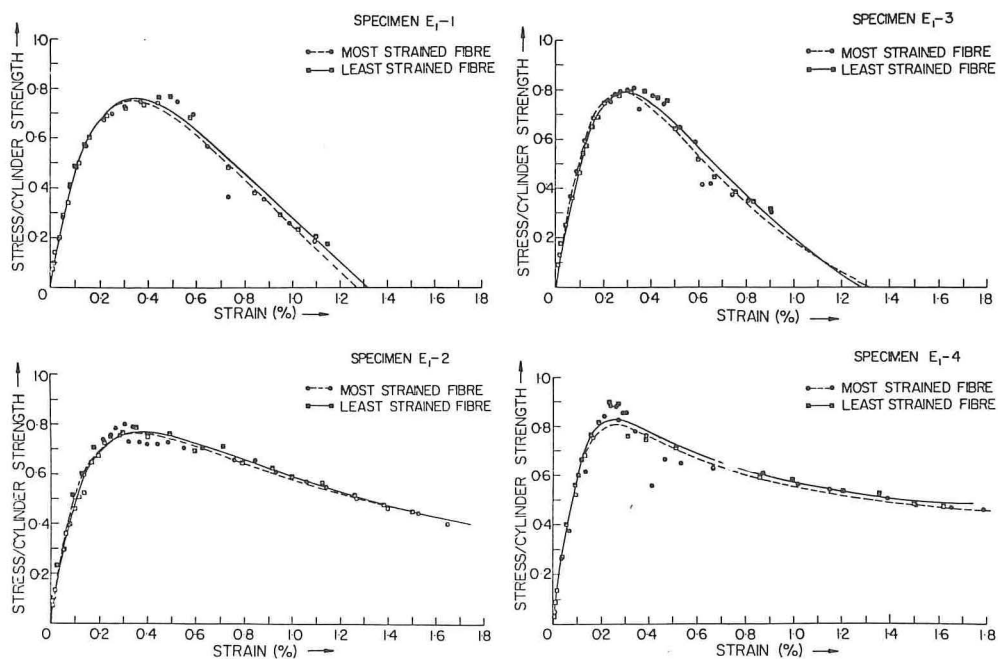
Figure 4. Analytical and experimental stress-strain diagrams for the specimens of Series E₁.
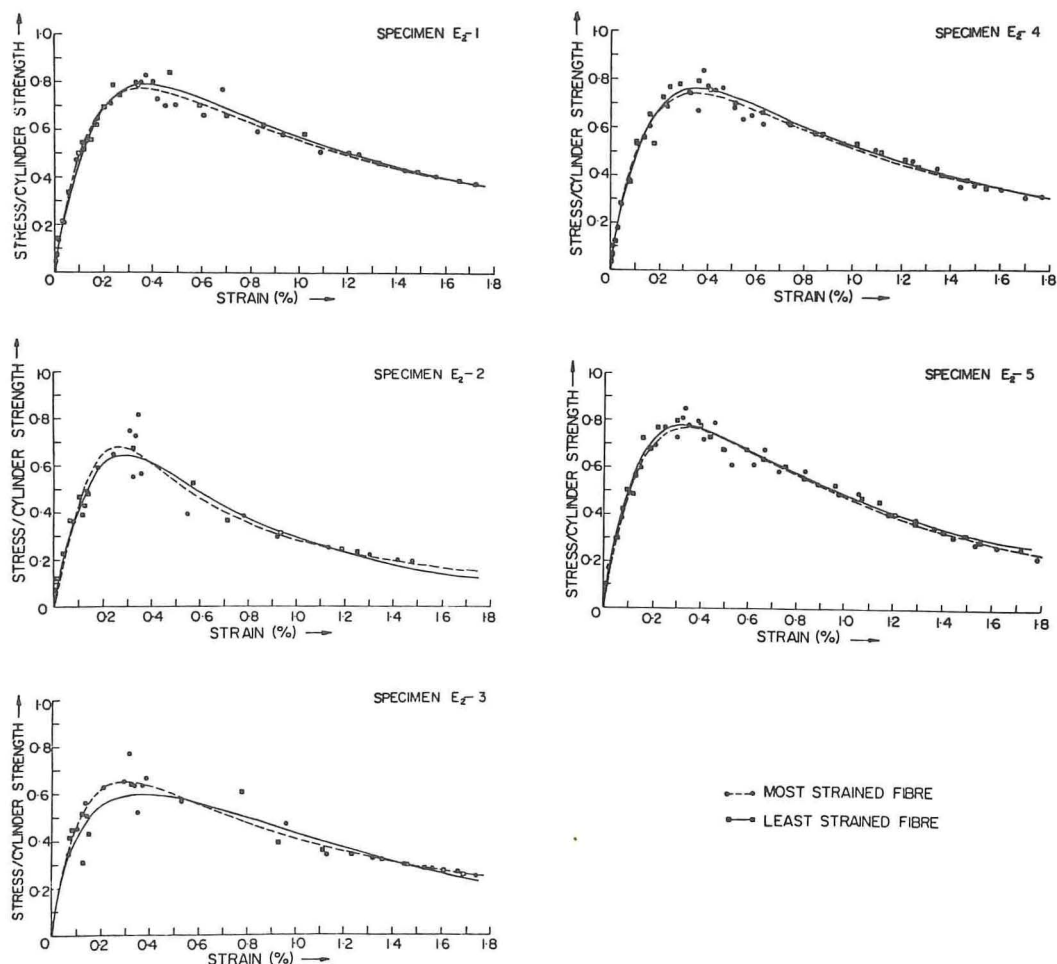
Figure 5. Analytical and experimental stress-strain diagrams for the specimens of Series E_2.

in Figure 4 and those for the specimens of series E_2 are shown in Figure 5. The different parameters associated with each stress-strain diagram are given in Table 1.

DISCUSSION OF TEST RESULTS

The average values of k_3 and ϵ_0 obtained in test series C, E_1, and E_2 are as follows:

Item	Series C	Series E_1	Series E_2
Average concrete strength (psi)	4,545	5,413	5,330
Strain gradient (rad/in.)	0	0.0004	0.0006
k_3	0.717	0.783	0.720
ϵ_0 (percent)	0.3774	0.3128	0.3312

It can be seen that no general trend in the effects of strain gradient on the k_3 and ϵ_0 parameters can be established. This very lack of trend, however, suggests that the effects of strain gradient on the k_3 and ϵ_0 parameters, when they are separated from strain rate effects, are not very pronounced. If there are, in fact, any such effects, they are so insignificant that they could not even be observed in the present case because

of (a) a slight variation in the concrete strengths of the different specimens, (b) the fact that lateral reinforcement may have slightly different effects on bound concrete under concentric and eccentric loading, and (c) normal experimental scatter. The present study, therefore, leads to a conclusion similar to the one reached earlier by Clark et al. (7). It also shows that Rüsch's assumption to the effect that any difference between the stress-strain curves of concrete under concentric and flexural compression can be ascribed to the presence of a differential rate of straining for different fibers in the latter case (4) was substantially correct.

Any conclusion regarding the effect of strain gradient on the descending branches of stress-strain curves is not attempted here, in view of the large scatter in the D-values obtained in test series E_1.

CONCLUSION

On the basis of the results reported and the discussion given, it can be concluded that strain gradient, when it is not accompanied by strain rate effects, has very little or no influence on the stress-strain curves of concrete up to their peak points.

ACKNOWLEDGMENTS

REFERENCES

1. Hognestad, E., Hanson, N.W., and McHenry, D. Concrete Stress Distribution in Ultimate Strength Design. ACI Jour., Proc. Vol. 52, No. 4, Dec. 1955, pp. 455-479.
2. Smith, R. G. The Determination of Compressive Stress-Strain Properties of Concrete in Flexure. Magazine of Concrete Research, Vol. 12, No. 36, Nov. 1960, pp. 165-170.
3. Rasch, C. Stress-Strain Diagrams of Concrete Obtained by Constant Rates of Strain. Symposium on the Influence of Time on the Strength and Deformation of Concrete, Munich, RILEM, Paris, 1958.
4. Rüsch, H. Researches Toward a General Flexural Theory for Structural Concrete. ACI Jour., Proc. Vol. 57, No. 1, July 1960, pp. 1-28.
5. Sturman, G. M., Shah, S. P., and Winter, G. Effect of Flexural Strain Gradients on Microcracking and Stress-Strain Behavior of Concrete. ACI Jour., Proc. Vol. 62, No. 7, July 1965, pp. 805-822.
6. Sargin, M. Stress-Strain Relationship for Concrete and the Analysis of Structural Concrete Sections. Univ. of Waterloo, Ontario, Canada, PhD thesis, March 1968, p. 334.
7. Clark, L. E., Gerstle, K. H., and Tulin, L. G. Effect of Strain Gradient on the Stress-Strain Curve of Mortar and Concrete. ACI Jour., Proc. Vol. 64, No. 9, Sept. 1967, pp. 580-586.
8. Sargin, M., and Handa, V. K. Discussion of paper Effect of Strain Gardient on the Stress-Strain Curve of Mortar and Concrete (Clark, L. E., Gerstle, K. H., and Tulin, L. G.), ACI Jour., Proc. Vol. 65, No. 3, March 1968, pp. 232-233.
9. Rüsch, H., Grasser, E., and Rao, P. S. Principes de Calcul du Béton Armé Sous des Etats de Contraintes Monaxiaux. Comité Européen du Béton, Luxembourg, Bull. d'Information 36, June 1962, pp. 1-112.
10. Ghosh, S. K. A Study into the Effectiveness of Cover and the Effects of Strain Gradient on Concrete Stress-Strain Relationships. Univ. of Waterloo, Ontario, Canada, MASc thesis, April 1969, p. 204

The Effect of Holes on Tensile Deformations in Plain Concrete

IGNATIUS D. C. IMBERT, University of the West Indies

Recent research has shown that concrete can exhibit considerable inelastic deformation in tension. This is particularly evident in flexural and uniaxial tensile tests in stiff machines and in tests where strain gradients are present. This paper describes experimental work on the effect of centrally located holes on tensile deformation in thin concrete plates. Tests were conducted in a special uniaxial-tension machine, and strain measurements along the horizontal axes of the plates showed that extensive inelastic deformation occurred in the vicinity of the hole edges. Strains somewhat further away remained "elastic" for most of the loading range, being quite small in specimens with diamond holes. The presence of holes had apparently little effect on tensile strength. Specimen behavior is explained in terms of the energy-release concept of fracture mechanics, it being concluded that inelastic deformation is the result of progressive and extensive microcracking. Such microcracking, in which crack lengths remain relatively short, apparently occurs when the critical strain-energy release rate is retarded, and it seems certain that the strain gradients created by the presence of holes have this retarding effect. These gradients clearly localize cracking in the vicinity of the hole edges and inhibit it considerably elsewhere. With regard to tensile strength, it may be concluded that, as inelastic deformation near hole edges reaches a certain stage, stress redistribution and eventual uniformity take place.

●THE TENDENCY IN RECENT YEARS to exploit an increasingly higher proportion of the ultimate strength of concrete in the design of structures has made research into its basic nature and behavior essential. As a result of such research, it is now fully recognized that strength, deformation, and crack development and propagation are closely interrelated. It has also been discovered that the mechanism of fracture is similar under most types of loading and that crack propagation, which leads to failure, is directly related to internal tension. This discovery together with the fact that tensile strength and deformation are of particular importance in connection with shear strength, flexure, torsion, and design of prestressed concrete and liquid-retaining structures, pavements, and airfields has pointed to the necessity for thorough studies of the behavior of concrete in tension.

It is the purpose of this paper to make a brief review of research on the deformational behavior of concrete in tension and to extend the field of knowledge by presenting results and discussion of experimental work by the writer. This work consisted principally of tests in uniaxial tension of long concrete plates containing centrally located holes. Microcracking and the energy concepts of fracture mechanics are discussed where appropriate.

PREVIOUS RESEARCH ON TENSILE DEFORMATION IN CONCRETE

A number of researchers have investigated tensile deformation in concrete in both uniaxial tension and flexure (1 through 18). They have reported "cracking" strains

ranging from 40 to 180 $\mu\epsilon$, but the bulk of the research indicates that the range of 90 to 120 $\mu\epsilon$ covers most concretes. Cracking strain is defined here as the strain at which there is significant departure from linearity in the load-strain curve and is known as the "extensibility" of concrete. It may also be considered as the elastic limit of the material.

Evans (3) and Todd (5) both considered that cracking strain had a value of about 100 $\mu\epsilon$ but, whereas Todd claimed that ultimate strain did not much exceed this value, Evans found that it sometimes exceeded 200 $\mu\epsilon$. Flexural tests on plain concrete beams by Blackman, Smith, and Young (7) gave values of 250 $\mu\epsilon$ for ultimate strain, and similar tests by Evans and Kong (14) and Welch (16) some years later produced values of nearly 500 $\mu\epsilon$.

A significant feature of the work of Blackman, Smith, and Young, who conducted tests not only in pure flexure but also in uniaxial and eccentric tension, was the discovery that the presence of a strain gradient affected the magnitude of ultimate strain. This strain varied from 140 $\mu\epsilon$ in uniaxial tension (zero strain gradient) to a maximum of 250 $\mu\epsilon$ in pure flexure. They also discovered that concrete had its lowest tensile strength in uniaxial tension and that the variation of ultimate strain with strain gradient agreed with the difference between uniaxial tensile strength and the modulus of rupture. Their findings were confirmed by Kaplan (11), who also discovered that, as the percentage of coarse aggregate increased, both cracking and ultimate strains decreased. Cracking strain in uniaxial tension, for example, decreased to a value as low as 40 $\mu\epsilon$.

The results reported so far were obtained from the usual short-term tests. Ohno and Shibata (9) have shown, however, that the magnitude of ultimate strain is also a function of rate and duration of loading. In tests conducted at relatively slow rates of loading over periods of several days, they recorded ultimate strains of over 500 $\mu\epsilon$ in uniaxial tension. That such strains could occur in concrete in uniaxial tension was a significant discovery, especially when one realizes that the tests were conducted in a relatively "soft" machine incapable of providing much restraint to the specimens.

The effect of restraint on the behavior of concrete has received particular attention in recent years, and it has come to be recognized that the magnitude of tensile strain is a function of the degree of restraint in the tensile zone. Keeton (19) has shown that tensile strains of nearly 2,100 $\mu\epsilon$ can occur internally in cylinders under concentric compression. Zielinski and Rowe (20) have found that large tensile strains can also occur in similarly loaded prisms and cubes and, as their maximum measurement of 1,170 $\mu\epsilon$ was the average over a gage length of 50.8 mm (2 in.), it is likely that the maximum tensile strain was much larger than this. From these results, it may be concluded that concrete can undergo large tensile strains under certain loading conditions. These conditions undoubtedly create some form of restraint that inhibits or retards failure. Such restraint occurs not only in the usual compressive tests but also in compressive, flexural, and tensile tests conducted in stiff machines.

By using a machine sufficiently stiff to produce the required restraint, Sturman, Shah, and Winter (15) were able to measure tensile strains in flexure as large as 1,780 $\mu\epsilon$. Because their specimens were removed from the machine before failure so that they could be specially examined for microcracking, this strain magnitude was clearly less than that of ultimate strain. Their tests also indicated that the presence of a strain gradient considerably increased the capacity of the concrete to deform, the deformation depending on the magnitude of the gradient. It seemed clear, therefore, that restraint was produced not only by the stiffness of the machine but also by the strain gradient.

Hughes and Chapman (17) were among the first researchers to test concrete in uniaxial tension in an adequately stiff machine. The stiffness of the machine made it possible for them to control the rate of strain, and they were able to record "peaked" load-strain curves. At the peak load, they measured strains of about 100 $\mu\epsilon$ and then, as the load decreased, continued to measure strains that reached as high as 1,840 $\mu\epsilon$ before failure. Similar tests by Evans and Marathe (18) produced values of ultimate strain as high as 2,800 $\mu\epsilon$.

This capacity of the material to deform under certain conditions of restraint possibly explains why it has a higher tensile strength in ordinary flexure than in ordinary

uniaxial tension. In flexure, the extreme "fibers" are initially the most highly stressed and strained, and restraint appears to be provided by the less highly strained adjacent ones. Such restraint apparently makes it possible for relatively large deformation to take place in the extreme fibers as loading increases. Kaplan's bending tests on notched beams (21) indicate that this is what happens and that the deformation is similar to the plastic type in metals. If this happens, there must come a stage in the deformation when the load-carrying capacity of the extreme fibers begins to decrease. The higher stresses are transferred to the adjacent fibers that now begin to deform more extensively, and the process continues, with external load increasing, until the zone of extensive deformation penetrates deep enough for failure to take place. An explanation of this deformational behavior in terms of microcracking and the concepts of fracture mechanics has been given by the writer (22).

TESTS ON SPECIMENS WITH HOLES

Types of Holes

The deformational behavior of concrete in tension that was revealed by tests in which restraint was produced by stiff machines and/or flexural strain gradients prompted the writer to investigate the effect of strain gradients on specimens loaded in uniaxial tension. Such strain gradients can be created by the presence of holes, and it was decided that tests would have most satisfactory results if the holes were centrally located in relatively thin concrete plates. These tests were part of a program of research on the effects of holes in concrete (23).

The holes were of various shapes and sizes, but the results shown diagrammatically here are for circular and diamond shapes of one particular size only. These results are considered sufficient to demonstrate the general behavior of the concrete. A complete report of results for all the shapes and sizes can be found elsewhere (23).

Specimens and Method of Test

The specimens were made from a specially "scaled-down" concrete mix that had a maximum aggregate size of 4.76 mm ($^3/_{16}$ in.). This was found to be the smallest size required for producing a true concrete and ensuring at the same time that gage lengths were sufficiently short for measurement to be as nearly at a "point" as possible. Such measurement was essential in view of the fact that strain in the vicinity of a hole was expected to change rapidly from point to point. Tests of 28 days on cubes and uniaxial tension specimens without holes gave strengths of 48.3 N/mm^2 (7,000 lbf/in.^{2}) in compression and 3.7 N/mm^2 (540 lbf/in.^{2}) in tension.

The specimens were 1,200 mm long by 200 mm wide by 35 mm thick and were tested in a uniaxial tension machine designed by the writer (23). The tensile force was applied through a self-centering, "lazy-tongs" device that gripped the specimens laterally. The clear length of the specimens between the upper and the lower grips was 620 mm. This length ensured that a condition of pure tension was produced at the central, minimum cross section where strain measurements were made. The gripping device was an improved and larger version of one designed by O'Clery and Byrne (24) at Dublin University nearly 10 years ago. The upper grips were connected through a pinned link to a double-flanged, universal coupling of the type used on drive shafts in agricultural machinery and thence to a rod attached to a hydraulically operated center-pull jack. The jack was located at the center of the top plate of the machine. The lower grips were connected to the base plate through a pinned link and universal coupling identical to the ones at the top. Preliminary experiments on specimens without holes indicated that the machine could provide a reliable uniaxial tension test.

Strain was measured by means of polyester-backed, electrical resistance strain gages, 10 mm long by 1.5 mm wide. These gages were placed along the horizontal axis of one face of the specimens, 5 on each side of the hole, and connected to the 10-point switching unit of a strain indicator. They were located on the specimens for which results are given here such that their centerlines were at distances from the hole edges of 2, 10, 20, 40, and 58 mm respectively. The transparency of the gage

backing and the clearly marked centerlines made accurate location relatively simple. The first 2 gages on each side of the hole were grouped relatively close together because of the rapid variation of strain expected along those sections of the horizontal axis near to the hole edges. The specimens were loaded in steps of 0.91 kN (205 lbf), and strain readings were taken at each step until failure.

Test Results

Diagrams of vertical strain distribution along the horizontal axis of typical specimens are shown in Figures 1 and 2. The distribution is shown for each load step until failure, and the points representing measured strains are joined by linear interpolation. Although the strain variation between gage locations was not likely to be linear, this method of interpolation is considered the best one for drawing the diagrams. In any case, the patterns of strain distribution are clearly illustrated by this method.

A study of the diagrams reveals some interesting features of strain behavior. These are briefly described as follows:

1. Strain distribution was such that the existence of strain gradients was clearly evident. These gradients started to increase quite early in the loading range, the strains in the vicinity of the hole edges becoming increasingly larger than those at locations farther away. This behavior began at strain levels well below the cracking strain or elastic limit. The gradients became quite steep as failure approached, particularly in the specimens with the diamond holes.

2. As loading increased, the rate of strain increase in the vicinity of the hole edges became more rapid, particularly after the elastic limit had been passed. The increase in the final load stage was very rapid indeed. Most of the strains at
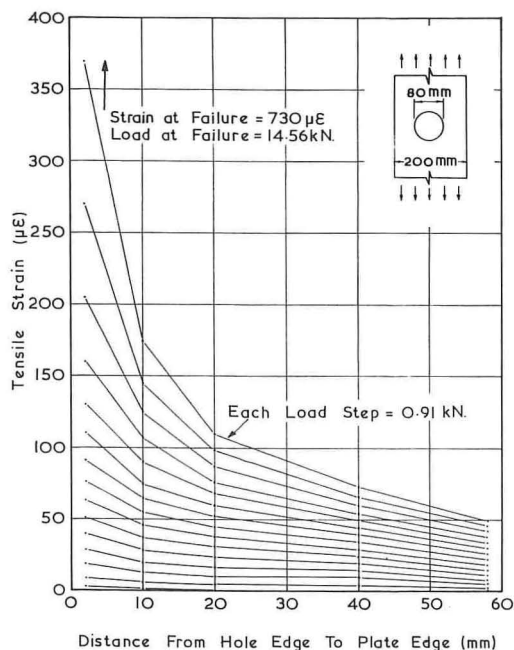

Figure 1. Vertical strain distribution along horizontal axis of specimen with central circular hole.
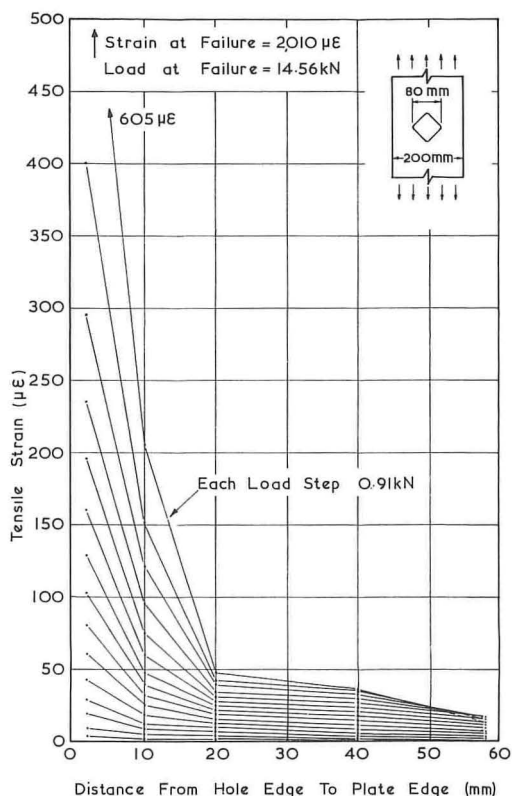

Figure 2. Vertical strain distribution along horizontal axis of specimen with central diamond hole (corner radius = 2.9 mm).

locations farther away increased at reasonably uniform rates and rarely exceeded the range of cracking strains. They were also rather smaller in the specimens with diamond holes than in those with circular ones.

3. The strains at the hole edges reached quite high values in the specimens with diamond holes, the maximum strain exceeding 2,000 $\mu\epsilon$ in 2 specimens. In a substantial proportion of the specimens with diamond holes and a somewhat smaller proportion of those with circular holes, the maximum strain at the hole edges reached values well over 1,000 $\mu\epsilon$. The strains near the specimen edges, on the other hand, were quite small and, as failure approached, showed little or no increase. In some specimens, there was even a strain decrease near failure. This strain relaxation was also evident in some of the specimens with circular holes.

Although results shown in the diagrams are for one size of hole only, it has already been explained that there were various sizes of holes for each shape. The variation of size had a marked effect on strain distribution. In the specimens with the largest size of hole, the strains at locations away from the hole edges became distinctly smaller and smaller as the specimen edges were approached. As the holes became smaller, however, the relative differences among the strains at these locations became correspondingly smaller and, in some cases, the strains at the specimen edges were equal to, or a little larger than, those at locations farther inside. The variation of size had no effect on the magnitude of ultimate strain at the hole edges. In particular, the maximum strains in most of the specimens with diamond holes were very large whatever the size of the hole.

A significant and important result of the research program was the discovery that relatively large holes and the elastic stress concentration associated with them had no appreciable effect on ultimate tensile strength of concrete. The only effect on the specimens was to reduce their central cross section and thus reduce the magnitude of ultimate load. That this behavior was almost certainly related to the deformational characteristics of concrete and its cracking mechanism is discussed in a later section of the paper.

FRACTURE MECHANICS AND MICROCRACKING

An understanding of the behavior exhibited in the tests can best be understood by a consideration of the energy concept of fracture mechanics and its relation to microcracking and crack propagation in concrete. It is appropriate, therefore, that an outline and brief discussion of research in this field be presented before proper analysis of the test results can be made.

In 1920, Griffith (25) suggested that the tensile fracture strength of brittle materials was greatly affected by the presence of small cracks and other discontinuities that existed before, or were formed after, load was applied. He claimed that these flaws acted as tensile stress concentrators and proposed a strength theory based on the energy-release concept. According to his theory, a flaw would extend by cracking when the stress concentration at its tip exceeded a certain value, thus causing the creation of a new crack surface and the transformation of strain energy to surface energy. He suggested that the crack would extend rapidly when the rate of release of strain energy was at least equal to the rate of increase of surface energy due to the formation of new surface area.

The Griffith condition for crack initiation and extension is given by the equation

$$\frac{2\Pi c \sigma^2}{E} = 4T \tag{1}$$

in which 2c is the length of the crack, σ is the tensile field stress remote from the crack, T is the specific surface energy, and E is the modulus of elasticity.

This approach has been extended by Irwin (26) and Orowan (27) who took into account the irrecoverable work done in materials in which plastic flow occurs. They suggested that the surface energy term in Eq. 1 should be augmented by the work of plastic deformation. The view is now held that, if the augmented surface energy term is replaced by the total energy absorbed in crack initiation and extension, the modified

Griffith theory may be applied to concrete. Irwin has designated the rate of release of strain energy as G and has further designated it as G_C when it reaches the critical value required for unstable crack extension and eventual fracture. Kaplan (21) and Romualdi and Batson (28) have attempted to make quantitative determinations of $\overline{G_C}$ for concrete but, as Popovics (29) points out, the elusive values of E and T make this an extremely difficult and uncertain exercise. Nevertheless, it seems clear that G_C is a fundamental property of concrete.

In uniaxial tension tests conducted in the usual "soft" machines, fracture occurs fairly soon after the load-strain curve deviates from linearity. An explanation for this has been given by Glucklich (30), who says that, up to a certain stress, the behavior of the concrete is strictly elastic and the stress-strain curve is a straight line. At that stress, the most severe crack existing prior to load begins to extend slowly, and the specimen cross section capable of sustaining load decreases. The stress now begins to increase at a faster rate, the crack extends farther, and the stress-strain curve begins to deviate from linearity. The strain-energy release rate, $2\Pi c\sigma^2/E$, increases even faster and is soon equal to the maximum rate of energy absorbed by the crack surface, with resultant unstable crack extension and fracture.

The abrupt termination of the stress-strain curve after a relatively small deviation from linearity indicates either that there is little inelastic deformation in ordinary uniaxial tension or that the rapidity of the strain-energy release rate prevents observation of such deformation. Flexural tests of plain concrete beams in ordinary machines have shown, however, that concrete can exhibit appreciable inelastic deformation in tension, the magnitude of ultimate strain being many times greater than that of cracking strain, as mentioned earlier. The capacity of concrete to deform in this way is even more clearly demonstrated by the stiff-machine tests in uniaxial tension and flexure that are reported earlier in the paper. It seems certain that the inelastic deformation is due to a process of progressive microcracking (31, 32, 38) in which the critical rate or release of strain energy, G_C, is retarded. This relationship and the near certainty that the microcracking process is intimately related to the restraint imparted by the loading system and/or strain distribution bring us to a consideration of microcracking.

That microcracking occurs in concrete at loads measurably below the ultimate was first suspected by Brandtzaeg (33) some 40 years ago. Ultrasonic, acoustic, microscopic, X-ray, and electrical-resistance-strain-gage techniques (4, 6, 11, 13 through 16, 18, 31, 34 through 38) have since been used to study microcracking, and it has been established that microcracking exists before any load is applied. These cracks are mainly in the form of bond cracks that form along the interface between coarse aggregate and mortar. Up to about 30 percent of ultimate load, the extension of these cracks is negligible but, above this load level, the cracks begin to increase appreciably in length, width, and number. At about 50 to 60 percent of ultimate load, mortar cracks begin to bridge between already existing bond cracks, but the process is still one of controlled crack growth and is confined to short lengths. This is the "prerupture" stage (34). At about 70 to 85 percent of ultimate load, the number and length of mortar cracks begin to increase appreciably, continuous crack patterns develop, and the load-strain curve bends significantly to the horizontal. The "critical" load has now been reached and fracture soon follows. If fracture can be retarded by some form of restraint, microcracking continues progressively, an extensive cracking pattern develops, and considerable inelastic deformation takes place. The load-strain curve also begins to descend and then flattens out.

The behavior described has been established primarily from tests in uniaxial compression and flexure, but research (17, 18, 32, 36) has indicated that similar behavior occurs in concrete in uniaxial tension. The almost identical shapes of the load-strain curves obtained from stiff-machine tests in uniaxial compression (39) and tension (17, 18) give nearly certain confirmation of this similarity of behavior.

What seems to happen in stiff-machine tests is that the strain energy is only partially released into the specimen, the rest being absorbed by the machine. Consequently, the rate of release of strain energy into the specimen is retarded, the energy released is rapidly absorbed by the numerous crack surfaces distributed throughout the material,

and crack extension is soon stabilized. Crack extension is also arrested or controlled when the need for release of strain energy is increased by bond cracks entering a tougher mortar phase or mortar encountering a zone of higher strength such as an aggregate particle or a region of advanced hydration. As load increases, cracking progresses by the growth of other cracks next in order of weakness. These are, in turn, soon arrested; the load continues to increase and others begin to grow. Eventually, the microcracking progresses to a stage where the load-carrying capacity of the concrete decreases and the load-strain curve descends. Fracture, however, does not yet take place because the extensive multiplication of microcracks still provides sufficient crack surfaces for energy absorption. At some stage, the cracking pattern becomes extensive enough for only a few areas of the concrete to be able to sustain load or for no further cracks to form. Critical stresses and crack lengths now occur, G_c can no longer be retarded, rapid crack extension occurs, and fracture takes place. If the extensive multiplication of microcracks occurs within the measuring area of a strain gage, the gage will indicate considerable deformation and this is the reason for the phenomenally large strains measured by Evans and Marathe (18).

Retardation of the strain-energy release rate also seems to occur in the presence of strain gradients. This was indicated by the flexural tests of Sturman, Shah, and Winter (15) that are mentioned earlier in the paper. From their microscopic examinations, they discovered that strain gradients retarded crack extension considerably, especially in the mortar, and caused any appreciable cracking to be localized at and near the extreme fibers. The steeper the gradient, the more noticeable was this effect. It seems clear that this behavior was responsible for the extensive inelastic deformation in tension that their specimens exhibited and that strain gradients must somehow have a restraining effect sufficient to arrest or retard critical cracking.

ANALYSIS AND DISCUSSION OF TEST RESULTS

The effect of holes on stress and strain distribution in homogeneous elastic and elastoplastic materials is well treated in the relevant literature, and the writer has already made a review of research in this field (23). Figure 3 shows the distribution of vertical strain along the horizontal axis of a relatively long plate of homogeneous, elastic material subjected to a uniform tensile stress σ_a in the vertical direction. The plate contains a centrally located circular hole, the diameter of the hole and the width of the plate being the same as those of the specimen shown in Figure 1.

The maximum strain, ϵ_m, occurs at the hole edge such that

$$\frac{\epsilon_m}{\epsilon_a} = 3.74 \qquad (2)$$

where ϵ_a is the elastic strain proportional to σ_a, the applied stress. The ratio ϵ_m/ϵ_a is known as the strain concentration factor. The corresponding stress concentration factor is σ_m/σ_a.

The strain distribution curve shows that a strain gradient exists from the very commencement of application of σ_a. The writer is not aware of any published work on strain distribution in plates of finite width containing diamond holes. Isida (40) has, however, determined that the maximum vertical strain at the hole edge along the horizontal axis of elastic plates containing diamond holes of the size and corner curvature shown in Figure 2 is such that

Figure 3. Vertical strain distribution along horizontal axis of elastic plate with central circular hole.

$$\frac{\epsilon_m}{\epsilon_a} = 10.1 \tag{3}$$

This value and the strain distribution diagrams obtained from research on plates with circular and V-shaped notches indicate that the elastic strain gradient in plates containing centrally located diamond holes is steeper than in those containing circular ones.

When the elastic limit is reached at the points of maximum strain on the hole edges in elastoplastic materials such as ductile metals, plastic zones form around these points and large strains occur there. As the load increases, more plastic zones develop in the vicinity of these points and considerable increase in strain takes place. The process continues until failure, the strains at the critical points becoming several times greater than those elsewhere. Experimental results (41) show that the strain gradient along the horizontal axis can become very steep near the hole edges as failure approaches. Stress computations from these results and the values of ultimate load indicate that, as the strain gradient increases with plastic deformation, the stress gradient decreases and effectively vanishes near failure. Stress redistribution and eventual uniformity of stress must, therefore, take place.

The strain behavior of the writer's concrete specimens was similar in many respects to that of elastoplastic materials just described, and it seems clear that the existence of strain gradients from the commencement of loading led eventually to the development and localization of inelastic deformation at and near the hole edges. From the earlier discussion, this deformation must almost certainly have been due to progressive microcracking and the retardation of the strain-energy release rate associated with it. The strain behavior must also have been responsible for the fact that the magnitudes reached by ultimate loads showed that the presence of holes had no effect on tensile strength. It may be concluded that, as microcracking became extensive near the hole edges, the load-carrying capacity of the concrete there decreased, and the stresses were redistributed to other regions farther away until uniformity of stress distribution occurred. Stress concentration effects due to the presence of holes, consequently, vanished, and the material displayed tensile strength as if there were no holes.

A significant feature of strain behavior was the fact that the strain gradients started to increase early in the loading range and at strain levels well below the cracking strain or elastic limit. As such increases could only take place in homogeneous materials after the onset of inelastic deformation at the hole edges, it is clear that they were made possible by the heterogeneous nature of concrete and its resultant capacity for microcracking under load. Such microcracking must clearly have occurred early in the most highly stressed regions near the hole edges. The early gradient increases were particularly marked in the specimens with diamond holes, and this behavior can be attributed to the fact that the relatively high elastic stress concentration factors and steep elastic strain gradients were conducive to early microcracking near the hole edges.

As microcracking progressed at and near the hole edges, the rate of strain increase there became more rapid. The rate continued thus until the development of inelastic deformation when it became considerably more rapid. The maximum stress, which exceeded 2,000 $\mu\epsilon$ in some specimens, were phenomenally large. Because they were measured at locations not exactly at the hole edges and the strain gradients near failure were very steep at these locations, the strains at the actual edges must have been even larger still. There were 2 other factors that made it very likely that the strains at the actual edges were significantly larger than those recorded. First, the strains were measured by gages that, although quite small, had finite area and could only measure average and not peak values. Second, the strains increased so rapidly before fracture that it was impossible to measure the actual values at fracture accurately. The writer estimates that the strain at fracture in some specimens was probably as large as 3,000 $\mu\epsilon$ at the actual hole edges.

The relatively small strains at locations some distance away from the hole edges and the particularly small ones at the edges of specimens with diamond holes led to the

inescapable conclusion that the effect of the strain gradients and their early increase must have been such as to inhibit deformation at these locations considerably. Moreover, the reasonably uniform rates of strain increase indicated that the concrete in these regions remained elastic till fracture. The material obviously underwent only a small amount of microcracking and crack extension despite the ultimately high stresses transferred by redistribution as failure approached. Another phenomenon was the strain relaxation in these regions, particularly at the specimen edges, just prior to failure in most of the specimens with diamond holes. The writer postulates that, as large, rapid deformations caused the concrete to "open out" at the hole edges, some form of "clothes-peg" action occurred. Such action would have caused a pinching effect at those locations away from the hole edges that were outside the "pin" of the clothes-peg.

The tendency of the strain distribution curves to have a relatively gentle gradient at locations some distance away from the hole edges in the specimens with the smaller holes was not surprising in view of the well-known findings of research on the effect of holes on homogeneous materials (Fig. 3). The fact that the strains at the edges of some of these specimens were a little larger than those at locations farther inside can be explained by the heterogeneous nature of concrete, some regions of the material being more susceptible to deformation than others. What was remarkable, however, was the fact that the size of the hole had no apparent effect on the magnitude of ultimate strain in the vicinity of the hole edges. Because the hole size and the magnitude of its associated elastic stress concentration factor do have some effect on the magnitude of ultimate strain in these regions in homogeneous materials, it seems evident that such behavior was due to the heterogeneous nature of concrete and its capacity for progressive microcracking. This microcracking was clearly limited to the vicinity of the hole edges and caused extensive inelastic deformation there whatever the size of the hole.

CONCLUSIONS

The research reported and discussed in this paper indicates the following:

1. Although fracture in ordinary uniaxial tension occurs fairly soon after the load-strain curve deviates from linearity, concrete can exhibit extensive, inelastic deformation in tension under certain conditions of loading and strain distribution. This behavior is most noticeable in stiff-machine tests in uniaxial tension and flexure and in tests in which specimens are subjected to strain gradients created either by flexure or by the presence of holes.

2. Extensive inelastic deformation is explicable in terms of the energy concept of fracture mechanics and the microcracking inherent in concrete. If the critical strain-energy release rate is retarded in some way, critical crack extension is arrested and progressive microcracking takes place. The occurrence of such microcracking within the area of a strain gage leads to observations of phenomenally large tensile strains.

3. In stiff-machine tests, the retardation of the critical strain-energy release rate can be explained by the fact that the strain energy is only partially released into the specimen, the rest being absorbed by the machine. It can also be explained to some extent by the increased need for released strain energy when cracks encounter zones of higher strength in the heterogeneous material. It is not clear what causes retardation of the rate in the presence of strain gradients, but microscopic and X-ray examinations have shown that cracks, especially in the mortar, are localized in the regions of largest strain and confined to short lengths.

4. Uniaxial tension tests on long, thin concrete plates show that the strain gradients created by the presence of centrally located holes have a marked effect on the deformational behavior of concrete. Inelastic strains develop and localize at and near points on hole edges where the highest stresses occur in the elastic range. These strains can become very large and reach values several times higher than limiting elastic strain. Strains at locations some distance away from the hole edges, on the other hand, are relatively small and generally remain within the elastic range up to failure. Those at the specimen edges can be very small indeed, and, clearly, the presence of strain gradients inhibits deformation in these regions considerably.

5. The strain relaxation evident at those locations outside the regions of large deformation just prior to failure in most of the specimens with diamond holes can be explained by the writer's clothes-peg theory. It seems that, as the large, rapid deformations occur near failure and cause the concrete to open out at the hole edges, some form of clothes-peg action takes place, resulting in a pinching effect at locations some distance away from the hole. The effect is more marked as the specimen edges are approached.

6. The presence of relatively large holes has apparently no effect on tensile strength of concrete specimens apart from the weakening effect of reduced cross section. This can be explained by the fact that concrete exhibits similar deformational behavior to that of elastoplastic materials containing centrally located holes, uniform stress distribution occurring before failure. The only difference is that "plasticity" in concrete is really the result of brittle microbehavior.

ACKNOWLEDGMENT

REFERENCES

1. Hatt, W. D. Extensibility of Concrete. ACI Jour., Proc. Vol. 22, 1926, pp. 364-385.
2. Carlson, L. W. Attempts to Measure the Cracking Tendency of Concrete. ACI Jour., Proc. Vol. 11, No. 6, June 1940, pp. 533-540.
3. Evans, R. H. Extensibility and Modulus of Rupture of Concrete. The Structural Engineer, Vol. 23, No. 12, Dec. 1946, pp. 636-659.
4. Blakey, F. A., and Beresford, F. D. Tensile Strains in Concrete. Australian Division of Building Research, Part I, Rept. C2.2-1, 1953, and Part II, Rept. C2.2-2, 1955.
5. Todd, J. D. The Determination of Tensile Stress-Strain Curves for Concrete. Institution of Civil Engineers, Proc. Vol. 4, No. 2, Part I, March 1955, pp. 201-211.
6. Blakey, F. A. Some Considerations of the Cracking or Fracture of Concrete. Civil Engineering and Public Works Review, Vol. 52, No. 615, Sept. 1957, pp. 1000-1003.
7. Blackman, J. S., Smith, G. M., and Young, L. E. Stress Distribution Affects Ultimate Tensile Strength. ACI Jour., Proc. Vol. 30, No. 6, Dec. 1958, pp. 679-684.
8. Trott, J. J., and Fox, E. N. Comparison of the Behaviour of Concrete Beams Under Static and Dynamic Loading. Magazine of Concrete Research, Vol. 11, No. 31, March 1959, pp. 15-24.
9. Ohno, K., and Shibata, T. On the Extensibility of Fresh Concrete Under Slowly Increasing Tensile Load. RILEM, Paris, Bull. 4, Oct. 1959, pp. 24-31.
10. Trott, J. J. A Simple Technique for Recording Load-Strain Curves for Concrete Beams in Flexure. Magazine of Concrete Research, Vol. 14, No. 42, Nov. 1962, pp. 155-158.
11. Kaplan, M. F. Strains and Stresses of Concrete at Initiation of Cracking and Near Failure. ACI Jour., Proc. Vol. 60, No. 7, July 1963, pp. 853-880.
12. Ward, M. A. The Testing of Concrete Materials by Precisely Controlled Uniaxial Tension. Univ. of London, PhD thesis, March 1964, p. 312.
13. Oladapo, I. O. Cracking and Failure in Plain Concrete Beams. Magazine of Concrete Research, Vol. 16, No. 47, June 1964, pp. 103-110.
14. Evans, R. H., and Kong, F. K. The Extensibility and Microcracking of the In-Situ Concrete in Composite Prestressed Concrete Beams. The Structural Engineer, Vol. 42, No. 6, June 1964, pp. 181-189.
15. Sturman, G. M., Shah, S. P., and Winter, G. Effect of Flexural Strain Gradients on Microcracking and Stress-Strain Behavior of Concrete. ACI Jour., Proc. Vol. 62, No. 7, July 1965, pp. 805-822.

64

16. Welch, G. B. Tensile Strains in Unreinforced Concrete Beams. Magazine of Concrete Research, Vol. 17, No. 54, March 1966, pp. 9-18.
17. Hughes, B. P., and Chapman, G. P. The Complete Stress-Strain Curve for Concrete in Direct Tension. RILEM, Paris, Bull. 30, March 1966, pp. 95-97.
18. Evans, R. H., and Marathe, M. S. Microcracking and Stress-Strain Curves for Concrete in Tension. Materials and Structures—Research and Testing, Vol. 1, No. 1, Jan.-Feb. 1968, pp. 61-64.
19. Keeton, J. R. Comparison of Methods of Strain Measurement in Portland Cement Concrete Cylindrical Specimens. U.S. Naval Civil Eng. Laboratories, Port Hueneme, Calif., Tech. Rept. 056, Feb. 1962.
20. Zielinski, J., and Rowe, R. E. The Stress Distribution Associated With Groups of Anchorages in Post-Tensioned Concrete Members. Cement and Concrete Assn., Research Rept. 13, Oct. 1962.
21. Kaplan, M. F. Crack Propagation and the Fracture of Concrete. ACI Jour., Proc. Vol. 58, No. 5, Nov. 1961, pp. 591-610.
22. Imbert, I. D. C. Some Aspects of the Behaviour of Plain Concrete in Compression and Tension. West Indian Jour. Engineering, Vol. 2, No. 1, April 1969, pp. 62-86.
23. Imbert, I. D. C. The Effect of Centrally Located Holes on Concrete Plates Tested in Uniaxial Tension. Univ. of Dublin, PhD thesis, Sept. 1968, p. 252.
24. O'Clery, D. P., and Byrne, J. G. Testing Concrete and Mortar in Tension. Engineering, Vol. 189, March 1960, pp. 384-385.
25. Griffith, A. A. The Phenomena of Rupture and Flow in Solids. Philosophical Transactions, Royal Soc. of London, A 221, 1920, pp. 163-198.
26. Irwin, G. R. Fracture Dynamics. In Fracturing of Metals, American Soc. for Metals, Cleveland, 1948, pp. 147-166.
27. Orowan, E. Fundamentals of Brittle Behavior in Metals. Symposium on Fatigue and Fracture of Metals, M.I.T., Cambridge, June 1950, pp. 138-147.
28. Romualdi, J. P., and Batson, G. B. Mechanics of Crack Arrest in Concrete. Jour. Engineering Mechanics Div., Proc. ASCE, Vol. 89, No. EM3, Proc. Paper 3558, June 1963, pp. 147-168.
29. Popovics, S. Fracture Mechanism in Concrete: How Much Do We Know? Jour. Engineering Mechanics Div., Proc. ASCE, Vol. 95, No. EM3, Proc. Paper 6604, June 1969, pp. 531-544.
30. Glucklich, J. Fracture of Plain Concrete. Jour. Engineering Mechanics Div., Proc. ASCE, Vol. 89, No. EM6, Proc. Paper 3715, Dec. 1963, pp. 127-138.
31. Shah, S. P., and Slate, F. O. Internal Microcracking, Mortar-Aggregate Bond and the Stress-Strain Curve of Concrete. Internat. Conference on the Structure of Concrete, Imperial College, London, Preprint Paper B3, 1965.
32. Kaplan, M. The Application of Fracture Mechanics to Concrete. Internat. Symposium on the Structure of Concrete, Imperial College, London, Preprint Paper D1, 1965.
33. Richart, F. E., Brandtzaeg, A., and Brown, C. A Study of the Failure of Concrete Under Combined Compressive Stresses. Univ. of Illinois, Eng. Exp. Station, Urbana, Bull. 185, April 1929.
34. L'Hermite, R. G. What Do We Know About the Plastic Deformation and Creep of Concrete? RILEM, Paris, Bull. 1, March 1959, pp. 21-51.
35. Rüsch, H. Physical Problems in the Testing of Concrete. Cement and Concrete Assn., London, Library Translation Cj. 86, 1960.
36. Jones, R. The Development of Microcracks in Concrete. RILEM, Paris, Bull. 9, Dec. 1960, pp. 110-114.
37. Robinson, G. S. The Influence of Microcracking and State of Stress on the Elastic Behaviour and Discontinuity of Concrete. Internat. Symposium on the Theory of Arch Dams, Southampton Univ., Pergamon Press, 1965, pp. 713-721.
38. Shah, S. P., and Winter, G. Inelastic Behavior and Fracture of Concrete. ACI Jour., Proc. Vol. 63, No. 9, Sept. 1966, pp. 925-930.
39. Barnard, P. R. Researches Into the Complete Stress-Strain Curve for Concrete. Magazine of Concrete Research, Vol. 16, No. 49, Dec. 1964, pp. 203-210.

40. Isida, M. On the Tension of an Infinite Strip Containing a Square Hole With Rounded Corners. Japanese Soc. of Mechanical Engineers, Bull. 3, No. 10, 1960, pp. 254-259.

41. Durelli, A. J., and Sciammarella, C. A. Elastoplastic Stress and Strain Distribution in a Finite Plate With a Circular Hole Subjected to Unidimensional Load. Jour. Applied Mechanics, Proc. ASCE, Vol. E30, No. 1, March 1963, pp. 115-121.

Deformation of Concrete and Its Constituent Materials in Uniaxial Tension

C. D. JOHNSTON, University of Calgary

Stress-strain curves for concrete loaded in uniaxial tension are shown for a wide variety of mixes. The data illustrate the influence of water-cement ratio and maximum size, grading, and type of aggregate on the form of the stress-strain curve. In addition, all mixes are found to conform to a dimensionless stress-strain curve plotted in terms of tensile strength and failure strain. Stress-strain curves for cement paste and rock are also shown, and values for the bond strength of various paste-rock combinations are included. Experimental values of the initial tangent modulus of different concretes are compared with analytical values obtained by using equations proposed in the literature, and fairly good agreement is observed.

● THE STRESS-STRAIN BEHAVIOR of concrete loaded in uniaxial compression has been the subject of a great deal of research and is now considered to be fairly well understood. Although many researchers believe that the behavior in uniaxial tension is very similar, the data supporting or repudiating this view are very limited. This paper gives tensile stress-strain curves obtained for a wide variety of concrete mixes and attempts to isolate the influence of various mix parameters on the form of the curve. Tensile stress-strain curves for cement paste and different rocks from which the aggregate was crushed are shown, and paste-rock bond strengths are also included. In conclusion, an attempt is made to explain concrete behavior in uniaxial tension in terms of the tensile properties of the constituents, using some of the different models referred to in the literature to explain its behavior in compression.

TESTS

Testing Technique

Uniaxial tension tests were performed at a loading rate of 25 psi/min on 6 in. square (aggregate maximum size $1\frac{1}{2}$ in.) or 4 in. square (aggregate maximum size $\frac{3}{4}$ or $\frac{3}{8}$ in.) prisms. Four-in. square prisms were used for cement paste, rock, and paste-rock bond tests. Load was applied through tension grips in which the specimen was held solely by friction. Strains were optically recorded by a pair of 8-in. roller extensometers. The test method has been analysed and discussed in detail in a previous paper (1), where coefficients of variation ranging from 4 to 6 percent depending on aggregate maximum size are quoted for concrete. All data subsequently discussed refer to Type 1 cement concretes or pastes cured in water for 28 days and tested in a saturated condition.

Mixes

The mixes used in the test program fall into 2 main groups referred to as Series 1 and 2. Series 1 comprised 36 basalt aggregate mixes in 3 groups of 12 having effective

---

water-cement ratios of 0.35, 0.45, and 0.55. Twelve different aggregate gradings, 4 each for aggregate maximum sizes of $1\frac{1}{2}$, $\frac{3}{4}$, and $\frac{3}{8}$ in., are examined, and the percentage of material finer than a No. 4 sieve is indicated where appropriate. The gradings employed are those given in Road Note 4 (2) and Research Report 4 (3). Series 2 comprised 36 mixes employing 5 crushed rock aggregates and an irregular gravel. Effective water-cement ratios were as in Series 1, and 3 gradings, representing each aggregate maximum size, were selected from the range covered in Series 1.

INFLUENCE OF MIX PARAMETERS

Aggregate Maximum Size and Grading

Figures 1, 2, and 3 show the tensile stress-strain curves obtained from the Series 1 mixes. It is evident that both the tensile strength and the failure strain increase as the aggregate maximum size decreases, and that, for a constant aggregate size, both increase as the sand (material finer than a No. 4 sieve) content increases. The variation of both parameters with aggregate maximum size and grading has been related in a previous paper (4) to the mean particle diameter for the grading and will not be discussed further. As the present paper is mainly concerned with values of elastic moduli, the important feature of Figures 1, 2, and 3 is the essentially constant value of the initial tangent modulus at any particular water-cement ratio. Only in the 2 finest $\frac{3}{8}$-in. gradings is a slight decrease evident. This is attributable to the relatively higher paste content of these mixes compared with the other ten in each figure. These results imply that the tangent modulus is independent of aggregate size and grading. However, it is likely to be affected to a small extent by changes in the proportion of fine to coarse aggregate, because these 2 materials do not generally have the same elastic modulus.

Water-Cement Ratio

Figures 1, 2, and 3 show that both the tensile strength and the failure strain decrease as the water-cement ratio increases, and appropriate relationships have been developed

Figure 1. Tensile stress-strain curves for basalt aggregate concretes (Series 1 mixes) of water-cement ratio 0.35.

68

Figure 2. Tensile stress-strain curves for basalt aggregate concretes (Series 1 mixes)
of water-cement ratio 0.45.

in the earlier paper (4). As far as the tangent modulus is concerned, a slight decrease
is evident as the water-cement ratio increases. However, it is incorrect to try to re-
late this change to water-cement ratio alone, as both the elastic modulus of the paste
and its volumetric proportion in the mix alter when the water-cement ratio changes.

Aggregate Type

Figures 4, 5, and 6 show relevant tensile stress-strain curves obtained from the
Series 2 mixes. Once again, relationships involving tensile strength and failure strain
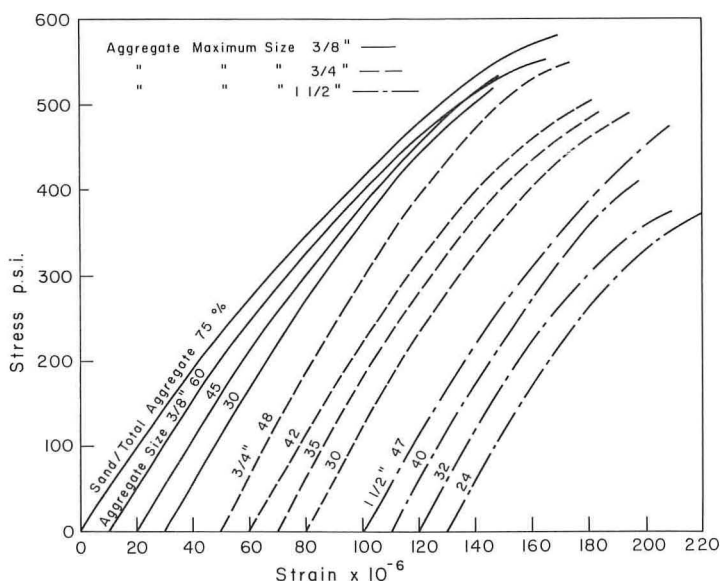

Figure 3. Tensile stress-strain curves for basalt aggregate concretes (Series 1 mixes)
of water-cement ratio 0.55.

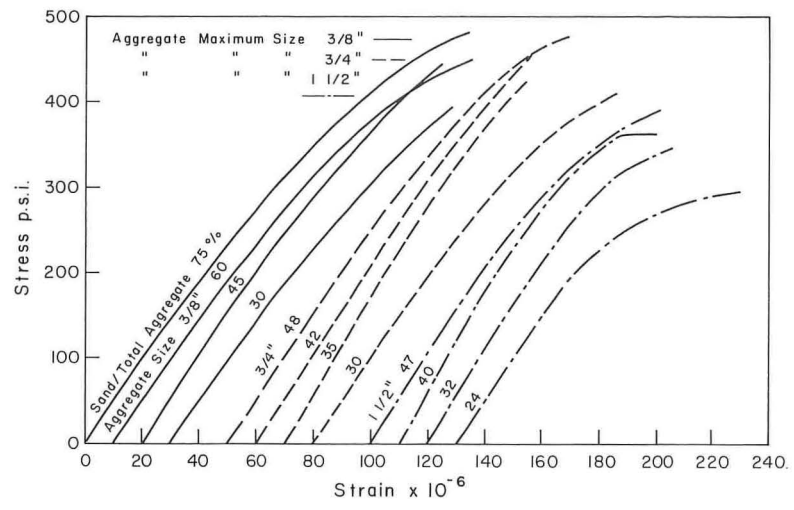Figure 4. Tensile stress-strain curves for different aggregate concretes (Series 2 mixes) of water-cement ratio 0.35.

are dealt with in the earlier paper (4), and it is sufficient to note that, while the tensile strength increases, the failure strain decreases as the elastic modulus of the aggregate increases. Figures 4, 5, and 6 also show a marked change in the initial tangent modulus of concrete as the elastic modulus of the aggregate alters, while its value is once again seen to be essentially independent of aggregate size and grading for any given aggregate. The relationship is more clearly shown in Figure 7 where points for concretes
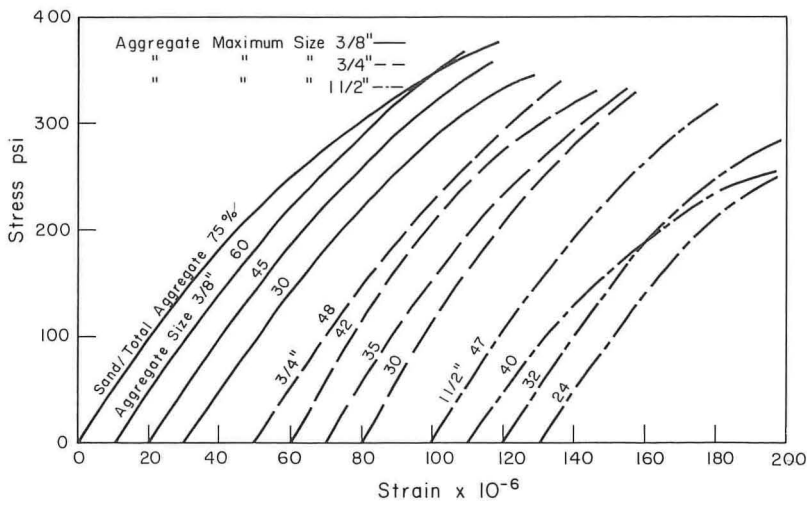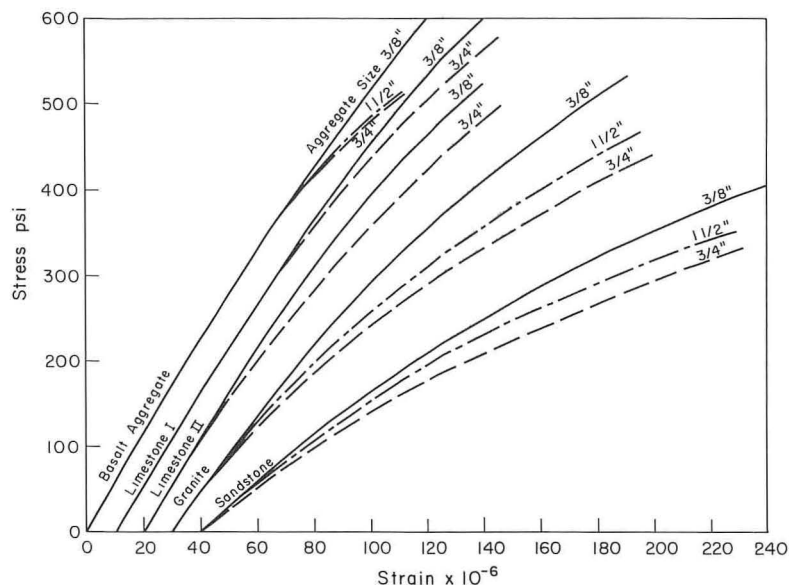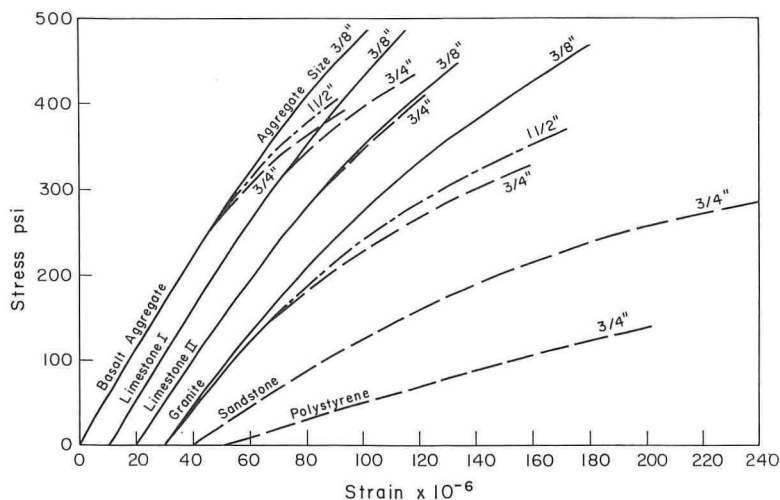

Figure 5. Tensile stress-strain curves for different aggregate concretes (Series 2 mixes) of water-cement ratio 0.45.
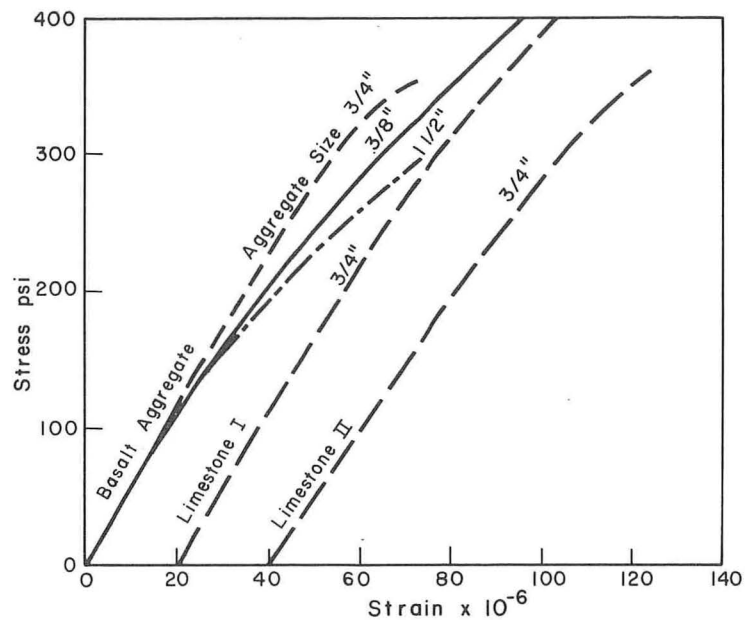
Figure 6. Tensile stress-strain curves for different aggregate concretes (Series 2 mixes) of water-cement ratio 0.55.
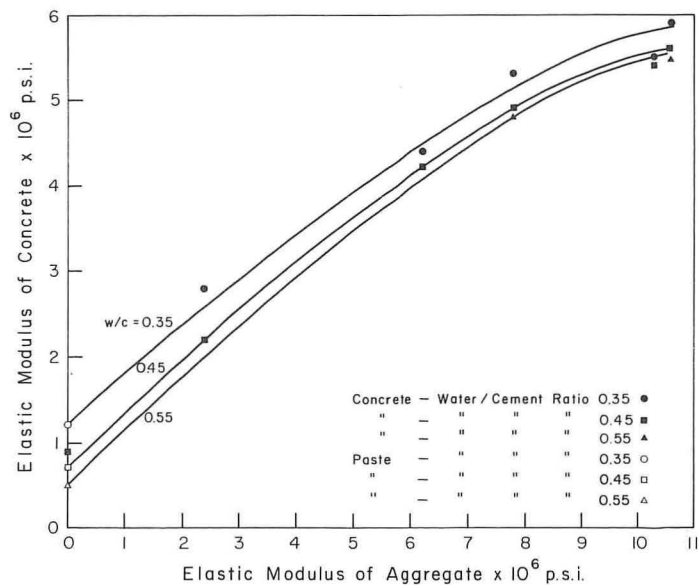

Figure 7. Elastic modulus of an aggregate and the initial tangent modulus of its concretes.

TABLE 1
MATERIAL PROPERTIES OF CONCRETE

Water-Cement Ratio	Paste Content (percent)	Aggregate	Elastic Modulus (10^{-6} psi)		
			Concrete	Aggregate	Paste
0.35	42	Basalt	5.9	10.6	2.84
		Limestone I	5.5	10.3	2.84
		Limestone II	5.3	7.8	2.84
		Granite	4.4	6.2	2.84
		Sandstone	2.8	2.4	2.84
		Voids	1.2	0.0	2.84
0.45	33	Basalt	5.6	10.6	2.05
		Limestone I	5.4	10.3	2.05
		Limestone II	4.9	7.8	2.05
		Granite	4.2	6.2	2.05
		Sandstone	2.2	2.4	2.05
		Voids	0.7	0.0	2.05
		Polystyrene	0.9	?	2.05
0.55	29	Basalt	5.4	10.6	1.63
		Limestone I	5.5	10.3	1.63
		Limestone II	4.8	7.8	1.63
		Voids	0.5	0.0	1.63

containing aggregate of zero elastic modulus are also included. These are calculated by using appropriate values of the elastic modulus of cement paste and the volumetric proportion of paste in the mix given in Table 1. It is interesting to note the close agreement between the 0.45 water-cement ratio paste and a similar concrete made with polystyrene aggregate of very low elastic modulus, whose properties became available by chance from a separate undergraduate project.

DIMENSIONLESS STRESS-STRAIN FUNCTION FOR TENSION

In view of the dimensionless nature of the stress-strain curve for compression observed by Gilkey (5), the preceding stress-strain curves for tension are analysed in a similar manner. The reference parameters are the maximum stress achieved and the corresponding strain. This is the maximum strain achievable, except when special stiff testing apparatus is used to detect the descending portion of the stress-strain curve. As an example, the percentage strain corresponding to 50 percent maximum stress is considered. The results for the Series 1 mixes, in which the variables are water-cement ratio and aggregate grading, are given in Table 2, and those for the Series 2 mixes, in which the variable is aggregate type, are given in Table 3. It is apparent from Tables 2 and 3 that there is no definite change in the tabulated value with mix parameters and that the values are sufficiently similar to be regarded as constant. The similarity of the mean value and standard deviation obtained in each table support this view, and the dimensionless curve shown in Figure 8 is accordingly obtained. This curve makes it possible for the 28-day stress-strain curve for any concrete containing

TABLE 2
STRAIN (PERCENTAGE OF FAILURE STRAIN) AT A STRESS OF 50 PERCENT OF THE TENSILE STRENGTH, SERIES 1 MIXES

Water-Cement Ratio	Basalt Aggregate in All Mixes											
	$1\frac{1}{2}$-in. Aggregate Grading				$\frac{3}{4}$-in. Aggregate Grading				$\frac{3}{8}$-in. Aggregate Grading			
	No. 1	No. 2	No. 3	No. 4	No. 1	No. 2	No. 3	No. 4	No. 1	No. 2	No. 3	No. 4
0.35	36.1	36.1	45.4	38.9	38.8	35.5	38.3	38.0	39.8	42.6	36.9	37.9
0.45	36.8	41.0	41.5	36.7	40.6	44.0	46.0	38.8	42.2	42.3	38.1	41.6
0.55	43.2	35.8	33.7	40.0	44.8	39.5	34.7	41.4	39.0	41.2	40.9	35.9

Note: Mean value 39.4 percent; standard deviation ±3.0.

TABLE 3

STRAIN (PERCENTAGE OF FAILURE STRAIN) AT A STRESS OF 50 PERCENT OF THE
TENSILE STRENGTH, SERIES 2 MIXES

Aggregate Type	Water-Cement Ratio for 1½-in. Aggregate Grading No. 2			Water-Cement Ratio for ¾-in. Aggregate Grading No. 1			Water-Cement Ratio for ⅜-in. Aggregate Grading No. 2		
	0.35	0.45	0.55	0.35	0.45	0.55	0.35	0.45	0.55
Basalt	42.9	41.4	36.4	41.8	36.8	40.4	45.0	45.5	43.9
Granite	39.4	35.5		38.5	36.0		39.7	40.5	
Gravel	34.7	31.8		37.8	36.2		39.3	38.9	
Sandstone	40.0			40.3	38.4		36.5		
Limestone I				41.2	37.2	44.5	41.5	44.3	
Limestone II				42.1	42.7	43.7	39.8	42.0	

Note: Mean value 39.9 percent; standard deviation ±3.2.

Type 1 cement to be derived once the tensile strength and the failure strain are known. These parameters can be predicted by using the relationships developed by Johnston (4).

PROPERTIES OF THE CONSTITUENT MATERIALS

Stress-Strain Behavior of Cement-Paste and Aggregate

Stress-strain curves for the 5 rock types and for cement pastes having water-cement ratios equal to those of the concretes of Series 1 and 2 are shown in Figure 9. The data shown in Figure 9 indicate that most rocks and cement pastes, unlike concrete, have linear stress-strain curves. Some difficulty was experienced in testing the white limestone (limestone II) because of the presence of numerous, almost invisible, geological joints and fossils commonly found in this type of rock, so it is doubtful whether the full extent of the curve for this material is shown. With the exception of the curve for limestone II, the data indicate that aggregate tensile strength is greater than that of the strongest corresponding concrete. Therefore, it is to be expected that concrete failure in tension involves negligible aggregate fracture, a fact observed throughout the wide variety of mixes tested.

In contrast to the fairly consistent behavior of concrete, that is coefficients of variation in strength of 4 to 6 percent, the behavior of cement paste was extremely variable. Although the slope of the various stress-strain curves obtained was essentially constant at a particular water-cement ratio, the tensile strength varied considerably, coefficients of variation being about 3 times those for concrete. This suggests that the relatively less variable strength of concrete is attributable to the presence of aggregate particles acting as crack arrestors in the paste, which on its own behaves as a brittle material with very variable strength governed by the presence of randomly oriented flaws.

Paste-Rock Bond Strength

The first series of bond tests was performed on 4-in. square cross sections of cement paste and sawed rock joined in the orientation shown in Figure 10a. The uni-
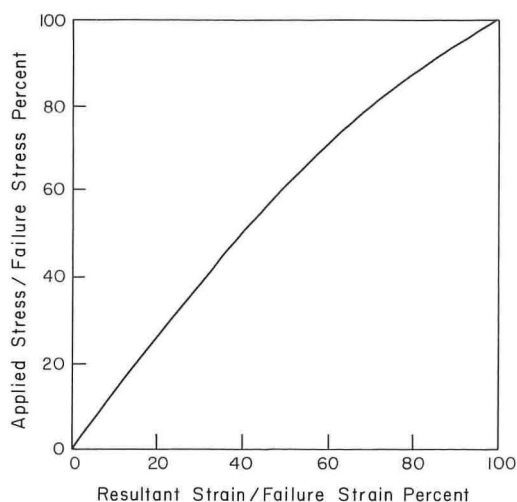

Figure 8. Dimensionless stress-strain function for concrete in uniaxial tension.
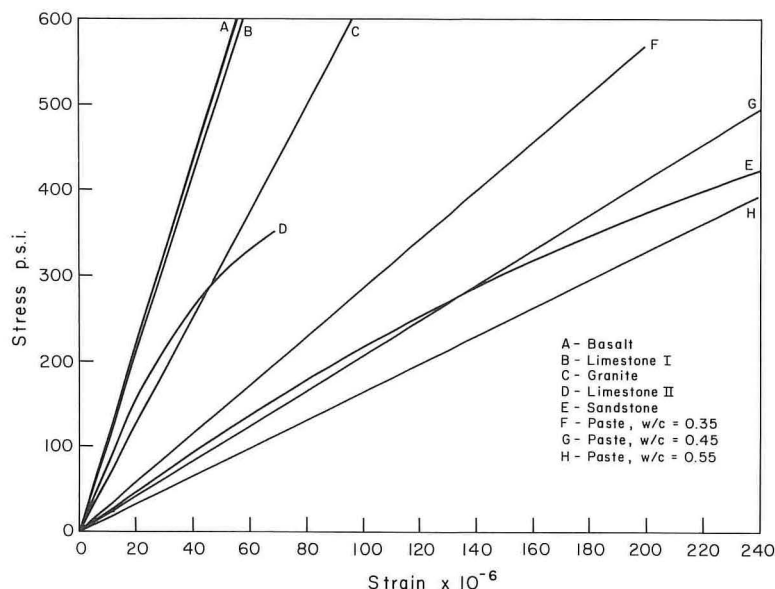
Figure 9. Tensile stress-strain curves for various rocks and cement pastes.

axial tensile bond strengths of various paste-rock combinations are given in Table 4. Results are the mean obtained from 4 tests and, in common with other similar investigations (6, 7), exhibit high coefficients of variation. However, they establish the order of tensile bond strength, although no quantitative relationship to rock type or water-cement ratio is evident in this limited number of results. Alexander (6), from more extensive data, has indicated that bond strength decreases with increasing water-cement ratio and decreasing silica content. However, the strengths given in Table 4 are several orders of magnitude lower than those of Alexander (6). One possible contributory factor is the well-known difference between strengths obtained from midpoint flexural loading and those obtained from uniaxial tensile loading. Moreover, Hsu and Slate (7) have obtained values of the same order as the writer, so it appears that bond strength is very dependent on the method of determination.

The second series of tests was performed by using a 0.45 water-cement ratio paste joined to sawed basalt in all the
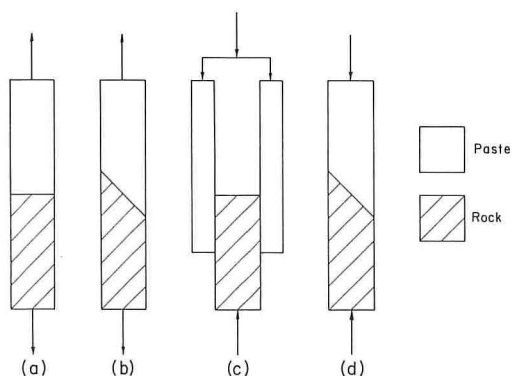
Figure 10. Orientations used for testing the paste-rock bond strength.

TABLE 4

PASTE-ROCK BOND STRENGTHS IN UNIAXIAL TENSION

Rock Type	Bond Strength (psi)			
	W-C Ratio 0.35	W-C Ratio 0.45	W-C Ratio 0.55	Mean
Basalt	212	195	199	202
Limestone I (dolomitic)	234	130	190	185
Limestone II (white)	64	78	71	71
Granite	107	173	233	171
Sandstone	109	112	146	122

various configurations shown in Figure 10, and results are given in Table 5. It is apparent that the paste-rock bond strength is very dependent on orientation, increasing from a minimum in pure tension to a maximum in pure compression when the strength of the weaker material rather than bond becomes the criterion. In addition, Alexander (6) has shown that bond strength depends on the orientation of the interface relative to the direction of casting, and he gives values of 108 and 46 percent for top and bottom surfaces respectively, relative to side or vertical surfaces as 100 percent. These variations are attributable to various degrees of bleeding of water from the cement paste and its accumulation at the interface.

TABLE 5

BOND STRENGTHS FOR VARIOUS LOADING ORIENTATIONS

Loading Orientation	Bond Strength (psi)
Uniaxial tension	186
Equal tension and shear at 45 deg	139
Pure shear	251
Equal compression and shear at 45 deg	924
Uniaxial compression	5,500[a]

[a]Cement paste strength.

ANALYTICAL MODELS

Some of the most significant work in this field has been presented by Hansen (8) in a paper that summarizes the variety of mathematical expressions for the elastic modulus of concrete derived by him and many other workers. The following are 2 simple equations suggested in Hansen's paper for a 2-phase material consisting of elastic particles, subscripted 2, dispersed in a matrix, subscripted 1.

Based on equal strains in each phase,

$$E = V_1 E_1 + V_2 E_2 \qquad (1)$$

and based on equal stresses in each phase,

$$E = \frac{1}{\dfrac{V_1}{E_1} + \dfrac{V_2}{E_2}} \qquad (2)$$

In addition, a complex equation for spherical particles evenly distributed in a continuous matrix, obtained by Hashin, has been simplified by assuming that Poisson's ratio for all phases is 0.2. This yields the following result:

$$E = \left[\frac{(1 - V_2) E_1 + (1 + V_2) E_2}{(1 + V_2) E_1 + (1 - V_2) E_2} \right] E_1 \qquad (3)$$

Equation 1 is the upper bound value for the elastic modulus of a 2-phase material, which Hansen suggests is applicable for $E_1 > E_2$. Equation 2 is the lower bound value, which he suggests is applicable for $E_1 < E_2$, provided that there is no bond between particles and matrix. Equation 3 is an intermediate value, which he suggests is applicable for $E_1 > E_2$ and also for $E_1 < E_2$, provided that there is maximum bond between particles and matrix.

Average values for concrete, obtained for the Series 1 mixes shown in Figures 1, 2, and 3 are compared with values from Eqs. 2 and 3 given in Table 6, as the condition $E_1 < E_2$ applies. It is apparent that Eq. 3 gives good agreement, particularly at the higher water-cement ratios. In view of this a similar comparison is given for

TABLE 6

EXPERIMENTAL AND CALCULATED ELASTIC MODULI FOR SERIES 1 MIXES

Water-Cement Ratio	Experimental	Eq. 2	Eq. 3
0.35	6.1	4.92	5.71
0.45	5.4	4.22	5.38
0.55	5.1	4.05	5.14

Note: Amounts are in 10^{-6} psi.

TABLE 7

EXPERIMENTAL AND CALCULATED ELASTIC MODULI
FOR SERIES 2 MIXES

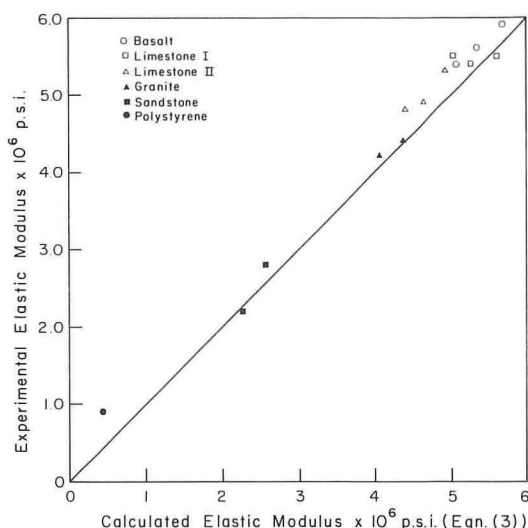| Water-Cement Ratio	Experimental	Eq. 1	Eq. 2	Eq. 3	Eq. 3 Amended
0.35	5.9	7.31	4.90	5.68	5.71
	5.5	7.14	4.88	5.61	5.66
	5.3	5.70	4.48	4.93	5.21
	4.4	4.78	4.13	4.38	4.91
	2.8	2.59	2.57	2.58	3.54
		1.20	0.0	0.76	
0.45	5.6	7.67	4.37	5.34	5.36
	5.4	7.48	4.33	5.26	5.31
	4.9	5.83	3.98	4.62	4.90
	4.2	4.55	3.66	4.08	4.58
	2.2	2.28	2.27	2.27	3.24
	0.9P	0.70	0.0	0.42	
0.55	5.4	7.92	4.02	5.08	5.10
	5.5	7.71	3.98	5.02	5.07
	4.8	5.96	3.66	4.40	4.67
		0.49	0.0	0.29	

Note: Amounts are in 10^{-6} psi.

Figure 11. Comparison of experimental and calculated
elastic moduli.

the wider variety of mixes of Series 2 in Table 7 and Figure 11. Once again, Eq. 3 gives good agreement while tending to slightly underestimate the experimental values. Although Eq. 1 may apply for $E_1 > E_2$ (see polystyrene concrete), it substantially overestimates the experimental values for $E_1 < E_2$. Eq. 2 is inaccurate for $E_1 < E_2$, yields the trivial answer of zero when E_2 is zero, and gives reasonable values only if $E_1 \simeq E_2$, when both Eqs. 1 and 3 also give similar values. In short, it might be concluded that Eq. 3 represents normal-weight concrete and Eq. 1 represents lightweight concrete. However, one unknown factor in these analyses is the elastic modulus of the fine aggregate. Up to now E_2 has been assumed to be equal to the elastic modulus of the coarse aggregate, but it is, of course, the resultant of the volumetric proportioning of the moduli of the fine and coarse aggregates. By using a value of 11.0×10^6 psi given by Hansen (8) for pure quartz sand similar to that used in this investigation, amended values for Eq. 3 have been calculated, and it is evident that they introduce a marked discrepancy when the modulus of the coarse aggregate is noticeably less than that of the fine aggregate. Therefore, in spite of the good agreement with the original values obtained by using Eq. 3, it must be asked whether the aggregate particles behave in such a way that only the modulus of the large particles is of paramount importance, or whether the modulus of the sand is considerably smaller than assumed. Unfortunately, no further data are available to answer this question.

CONCLUSIONS

1. The initial tangent modulus of the stress-strain curve in uniaxial tension is essentially independent of aggregate maximum size and grading, somewhat dependent on water-cement ratio, and very dependent on the elastic modulus of the aggregate. The tensile strength and the failure strain are related to all 3 mix parameters as shown by Johnston (4).

2. The tensile stress-strain curves for any 28-day concrete containing Type 1 cement can be included in a single curve plotted by using dimensionless coordinates, as shown in Figure 8.

3. Cement paste and rock, unlike concrete, have linear stress-strain curves in tension. Cement paste is particularly brittle and variable in its behavior, and it is concluded that the relatively less variable behavior of concrete is attributable to the

crack-arresting action of the aggregate particles. Paste-aggregate bond strengths in both tension and shear are considerably less than concrete strengths, so the progressive curvature of the stress-strain curve occurs as bond is broken down. Unlike compression, when aggregate particles may still transmit stress in the absence of bond, the stress in the aggregate must fall gradually to zero under uniaxial tension, and it is to be expected that the concrete just before failure will behave as if it contained aggregate of zero elastic modulus.

4. The initial tangent modulus of normal-weight concrete seems to be accurately predicted for a wide range of aggregates by using Eq. 3 and by assuming that the modulus of elasticity of the coarse aggregate is representative of the combined fine and coarse aggregates. This finding is contrary to that of Hansen, who concludes, mainly on the basis of compression test data, that Eq. 2 is applicable to normal-weight concrete.

ACKNOWLEDGMENT

REFERENCES

1. Johnston, C. D., and Sidwell, E. H. Testing Concrete in Tension and Compression. Magazine of Concrete Research, Vol. 20, No. 65, Dec. 1968, pp. 221-228.
2. Road Research Laboratory. Design of Concrete Mixes. Her Majesty's Stationery Office, London, Road Note 4, 1955, p. 16.
3. McIntosh, J. D., and Erntroy, H. C. Design of Concrete Mixes With Aggregate of $\frac{3}{8}$ In. Maximum Size. Cement and Concrete Assn., London, Research Note 4, 1950, p. 20.
4. Johnston, C. D. Strength and Deformation of Concrete in Uniaxial Tension and Compression. Magazine of Concrete Research, Vol. 22, No. 70, March 1970, pp. 5-16.
5. Gilkey, H. J. Water/Cement Ratio Versus Strength—Another Look. ACI Jour., Proc. Vol. 57, April 1961, pp. 1287-1312.
6. Alexander, K. M., Wardlaw, J., and Gilbert, D. J. Aggregate-Cement Bond, Cement Paste Strength and the Strength of Concrete. Internat. Conf., London, Sept. 1965, Cement and Concrete Assn., London, Proc., 1968, pp. 59-81.
7. Hsu, T. C., and Slate, F. O. Tensile Bond Between Aggregate and Cement Paste. ACI Jour., Proc. Vol. 60, April 1963, pp. 465-486.
8. Hansen, T. C. Influence of Aggregate and Voids on Modulus of Elasticity of Concrete, Cement Mortar and Cement Paste. ACI Jour., Proc. Vol. 62, Feb. 1965, pp. 193-214.

Young's Modulus, Creep, and Shrinkage of Gap-Graded Concrete Versus Continuously Graded Concrete

SHU-T'IEN LI and V. RAMAKRISHNAN,
South Dakota School of Mines and Technology

This paper presents experimental results verifying the authors' previous hypothesis that gap-graded air-entrained concrete has higher Young's modulus of elasticity in compression, less shrinkage, and less creep than its continuously graded counterpart of the same maximum size of coarse aggregate and same amount of entrained air. These attributes are the direct results of less specific surface in gap grading, compared to that in continuous grading, requiring less water-cement ratio, less cement, less water, less matrix, and higher aggregate-matrix ratio. The inapplicability of existing equations for gap-graded concrete is shown, and new mathematical relationships are derived for modulus of elasticity and creep for both gap-graded and continuously graded concretes. The equations are further compared with other existing results for gap-graded concrete.

•A KNOWLEDGE of the deformations of concrete is important for the design of any structure with reinforced or prestressed concrete. The strains that cause deformations in concrete may be classified as elastic strains, plastic strains, creep strains, shrinkage strains, and thermal strains. In the design of concrete structures, particularly those for highways, all of these deformations are to be considered. In this paper 3 of them, elastic, creep, and shrinkage strains for gap-graded concrete, are discussed.

OBJECTIVES AND SCOPE

Li had proposed the hypothesis in his previous papers ($\underline{1}$, $\underline{2}$) that gap-graded concrete would have higher modulus of elasticity in compression, less shrinkage, and less creep than its continuously graded counterpart of the same maximum size of coarse aggregate and same amount of entrained air. All other things being equal, the specific surface per unit volume for gap-graded concrete is much less than that for continuously graded concrete, and gap grading eliminates loose juxtaposition and particle interference that are inherent in continuous grading. Because of these facts there are many advantages in using gap-graded concrete. The reduction of smaller sizes in coarse aggregate, and often in fine aggregate as well, leads to better workability and much less cement. In comparison with continuously graded concrete, gap-graded concrete thus requires less water, less water-cement ratio, less matrix, and hence higher aggregate-matrix ratio.

To verify Li's hypothesis, an extensive research program sponsored by the South Dakota Department of Highways and the U.S. Bureau of Public Roads has been carried out to study all aspects of gap-graded concrete as compared to those of continuously graded concrete. Summarized here are the findings of the experimental results in regard to the basic mechanical property, modulus of elasticity, and the physical properties, creep and shrinkage, for both gap-graded and continuously graded concretes having the

same amount of entrained air and mixes with similar workability to the extent that they require similar attention and compaction.

MATERIALS AND TEST PROGRAM

Sand from Oral, South Dakota, with an absorption of 2.04 percent and a specific gravity of 2.63, crushed limestone with an absorption of 0.58 percent and a saturated surface-dry specific gravity of 2.73, Type 1 portland cement, and "Protex" air-entraining agent were used throughout the investigation.

Aggregates of gap-graded concrete consisted of a narrow-size range of coarse aggregate and a narrow-size range of fine aggregate in which undesirable intermediate sizes and extreme fines were removed. The optimum mixes for the comparison of gap-graded and continuously graded concretes were developed through pilot experiments so that they would have practically the same workability with respect to placement and finishing. Thus, the improvement in the physical and mechanical properties and other merits of gap-graded concrete enumerated in this paper are the achievable advantages from a practical point of view. Strengths of mix designs selected for this investigation were 3,000, 4,500, 6,000, and 7,500 psi to correspond to those commonly used in structural concrete. In all cases the actual strengths obtained were within a variation of ± 5 percent of the design strengths.

The mixes used were stiff. They were designed to give 0- to $\frac{1}{2}$-in. slump for 7,500- and 6,000-psi concretes and 0- to $\frac{3}{4}$-in. slump for 4,500- and 3,000-psi concretes. The consistency of each mix was measured by means of a "Vebe" consistometer. The time in seconds required to consolidate the slump cone into a cylindrical mass $9\frac{3}{8}$ in. in diameter constituted a measure of the consistency of the mix. The cylinder specimens were consolidated by internal vibration according to ASTM C 31-62T. The prisms used for shrinkage tests were consolidated on a small vibrating table. For plastic unit weights, the concrete was compacted by rodding. All the specimens except those for creep were cured in lime-saturated water for 28 days. All test procedures were according to ASTM.

The elastic modulus was determined by an axially mounted strain frame fastened to concrete cylinders for the compressive-strength test. The modulus of elasticity is the "chord modulus" defined by ASTM C 469-65.

Creep tests were conducted on three 6- by 12-in. cylinders taken from each of the relevant mixes. These specimens were stored in moist sacks at a temperature of 73.4 F until the age of 7 days. They were next kept in the humidity-controlled room in an ambient temperature of 73.4 F and relative humidity of 50 percent until the age of 28 days. Then they were subjected to a sustained load of 30,000 lb (1,063 psi). The sustained load was checked at frequent intervals by a calibrated pressure gage and adjusted by hydraulic jacks. Creep measurements were taken by a mechanical strain gage over a 10-in. gage length.

TABLE 1

GRADINGS OF COARSE AND FINE AGGREGATES

Sieve	Maximum Size of Percentage Passing Gap Grading			Maximum Size of Percentage Passing Continuous Grading		
	1 in.[a]	$\frac{3}{4}$ in.	$\frac{1}{2}$ in.	1 in.	$\frac{3}{4}$ in.	$\frac{1}{2}$ in.
1 in.	100.0 (100)			100		
$\frac{3}{4}$ in.	36.5 (40)	100.0		78	100.0	
$\frac{1}{2}$ in.	36.5 (40)	36.5	100.0	56	72.5	100.0
$\frac{3}{8}$ in.	36.5 (40)	36.5	36.5	42	45.0	71.5
No. 4	36.5 (40)	36.5	36.5	28	30.0	30.0
No. 8	36.5 (40)	36.5	36.5	21	23.0	20.0
No. 16	0 (12)	0	36.5	15	16.0	15.0
No. 30	(0)		0	8	9.0	10.0
No. 50				0	0	0

[a]Numbers in the parentheses indicate grading used for the 4,500-psi concrete. To get a good finish, these gradings were arrived at by trial mixes.

TABLE 2

DETAILS OF MIX PROPORTIONS

Mix No.	Maximum Size (in.)	Water-Cement Ratio	Aggregate-Cement Ratio	Cement Content (lb/cu yd)	Slump (in.)	Vebe Time (sec)	Vibration Time (sec)	Plastic Unit Weight (pcf)
Gap-Graded Concrete								
G182	$\frac{1}{2}$	0.32	3.7	819	$\frac{1}{8}$	14	17	142
G180		0.40	5.0	644	$\frac{1}{16}$	9	9	144
G183		0.52	6.2	527	$\frac{5}{8}$	8	8	144
G179	$\frac{3}{4}$	0.32	4.2	752	0	15	17	145
G178		0.45	6.0	562	$\frac{1}{4}$	6	7	147
G181		0.52	6.9	492	$\frac{1}{4}$	8	14	147
G189	1	0.33	4.5	714	0	16	25	145
G190		0.40	6.5	527	$\frac{1}{8}$	13	12	142
G191		0.48	7.0	486	$\frac{1}{8}$	6	5	145
Continuously Graded Concrete								
C104	$\frac{1}{2}$	0.32	2.7	1013	$\frac{1}{4}$	11	7	144
C105		0.38	3.4	852	$\frac{7}{16}$	7	5	152
C106		0.50	4.9	638	$\frac{5}{8}$	3	4	149
C109	$\frac{3}{4}$	0.32	3.1	923	$\frac{1}{4}$	13	20	144
C101		0.40	4.0	757	$\frac{1}{2}$	5	5	151
C102		0.48	5.9	551	$\frac{3}{8}$	5	5	151
C107	1	0.32	3.5	862	$\frac{5}{16}$	10	17	153
C 98		0.37	4.9	665	$\frac{1}{16}$	14	10	150
C100		0.46	5.8	576	$\frac{9}{16}$	7	4	150

Measurements of drying shrinkage were made on prisms 3 in. square and 11.5 in. long. All of the shrinkage specimens, after 28 days of curing, were stored in a temperature- and humidity-controlled room at a temperature of 73.4 F and relative humidity of 50 percent. Shrinkage strains were recorded according to the schedule stipulated by ASTM.

The concrete mixes used in this program are given in Tables 1 and 2.

TEST RESULTS OF MODULUS OF ELASTICITY, CREEP, AND SHRINKAGE

Modulus of Elasticity

Measured modulus-of-elasticity values for all the 18 mixes are given in Table 3. The relation between modulus of elasticity in compression and cylinder compression strength is shown separately for gap-graded and continuously graded concretes in Figure 1. The modulus of elasticity for gap-graded concrete is consistently higher throughout all strengths than that for continuously graded concrete.

The comparison of moduli of elasticity for gap-graded and for continuously graded concrete is shown in Figure 2 on the basis of equal cement content, equal workability, and equal ease of placement. The curves are plotted separately for each maximum size of coarse aggregate because the optimum cement content is dependent on such size. The data shown in this figure clearly bear out the hypothesis (1, 2) that the mod-
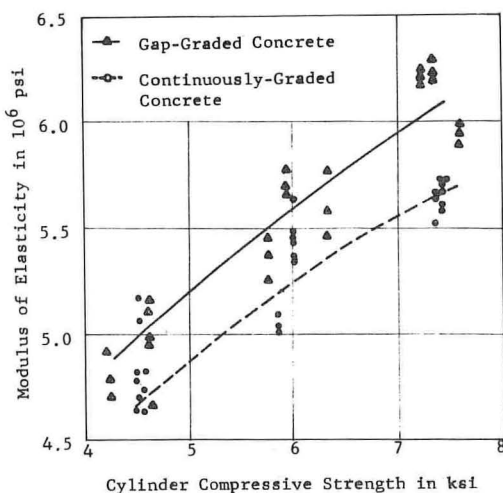

Figure 1. Comparison of relationship between cylinder comperssive strength and modulus of elasticity for gap-graded and continuously graded concretes.

TABLE 3

TEST RESULTS OF MODULUS OF ELASTICITY

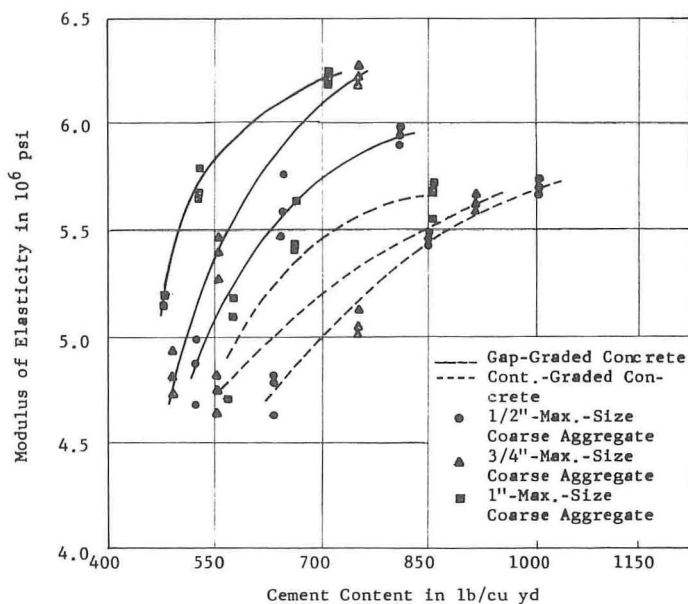| Gap-Graded Concrete				Continuously Graded Concrete			
Mix No.	Compressive Strength[a] (psi)	Density (pcf)	Modulus of Elasticity (10^6 psi)	Mix No.	Compressive Strength[a] (psi)	Density (pcf)	Modulus of Elasticity (10^6 psi)
G182	7,606	153.0	5.93	C104	7,412	151.5	5.72
		153.0	5.88			152.0	5.72
		153.5	5.98			151.0	5.72
G180	6,325	153.0	5.46	C105	6,007	151.0	5.43
		153.0	5.58			151.0	5.45
		155.0	5.76			150.0	5.47
G183	4,638	150.0	4.98	C106	4,510	150.0	4.78
		149.0	4.66			150.0	4.62
		149.0	4.94			149.0	4.81
G179	7,338	154.0	6.29	C109	7,402	152.5	5.68
		155.0	6.20			152.5	5.61
		155.5	6.20			153.5	5.60
G178	5,769	152.0	5.25	C101	5,875	151.5	5.10
		154.0	5.38			152.0	5.01
		152.0	5.45			151.5	5.02
G181	4,276	153.5	4.92	C102	4,594	152.5	4.82
		153.0	4.71			152.5	4.63
		152.5	4.80			153.0	4.72
G189	7,208	155.5	6.17	C107	7,376	154.0	5.67
		156.0	6.21			154.0	5.67
		156.0	6.22			154.5	5.54
G190	5,980	155.0	5.65	C 98	6,025	154.5	5.37
		156.0	5.65			154.0	5.37
		155.0	5.77			154.0	5.67
G191	4,660	153.0	5.10	C100	4,567	154.0	5.08
		154.0	5.14			154.0	5.17
						154.5	4.69

[a]Average of 4 cylinders.

Figure 2. Comparison of relationship between cement content and modulus of elasticity for gap-graded and continuously graded concretes.
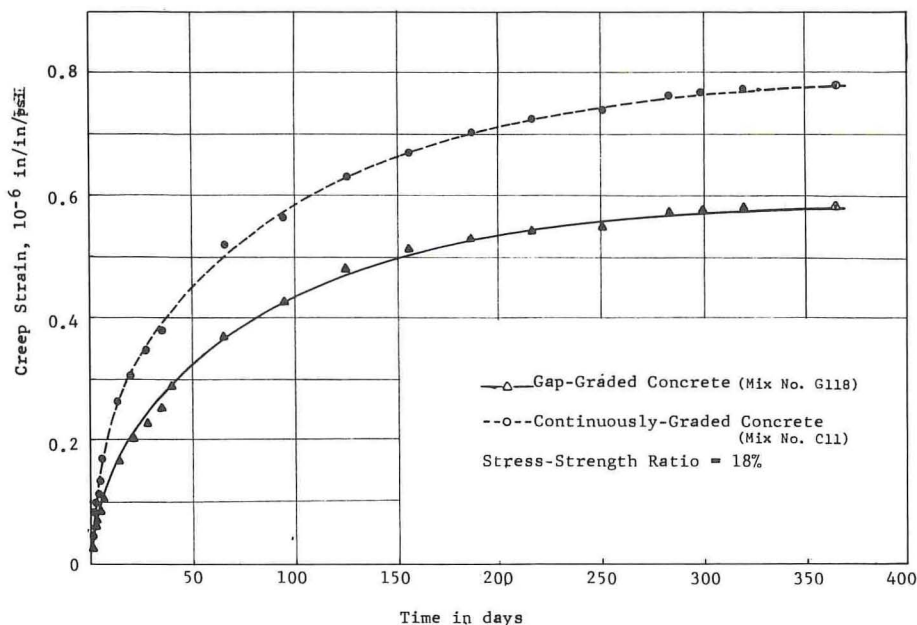
Figure 3. Comparison of creep strains for gap-graded and continuously graded concretes for 6,000-psi nominal strength.

ulus of gap-graded concrete is higher than that of continuously graded for all maximum-size aggregates. Both Figures 1 and 2 indicate that the same strength and elastic modulus could be obtained with a considerable amount of saving in cement by adopting gap grading instead of the conventional grading.

Creep

Creep strains measured at a constant stress of 1,063 psi are shown in Figure 3 for a period of 320 days for both gap-graded and continuously graded concretes. The creep strains are the average of 6 values measured on 2 diametrically opposite faces of each of the 3 cylinders. It was noted that there was very little variation among the 6 readings, indicating that the load was applied without eccentricity. The mix details and test results are given in Table 4.

Figure 3 shows that the gap-graded concrete of equal strength creeps less than the continuously graded concrete at all ages. At an age of 320 days, the continuously graded concrete has creeped 35 percent more than the corresponding gap-graded concrete. The creep was observed at a stress-strength ratio of 18 percent, referred to the strength at the time of application of the load. This slightly lower stress-strength ratio was adopted

TABLE 4

TEST RESULTS OF CREEP STRAINS

Mix No.	Maximum Size (in.)	Water-Cement Ratio	Aggregate-Cement Ratio	Slump (in.)	Vebe Time (sec)	Vibration Time (sec)	28-Day Strength (psi)	Modulus of Elasticity (psi)	Elastic Strain for 1,063 psi Stress
G118	$3/4$	0.45	6.0	$1/2$	5	7	5,840	4.84×10^6	220×10^{-6}
C011	$3/4$	0.40	3.85	$1/2$	7	5	5,980	4.25×10^6	250×10^{-6}

because of the limitations of the loading device. It is expected that, for a higher stress-strength ratio, the creep strains will be considerably higher and the difference between the creeps of gap-graded concrete and continuously graded concrete will be considerably higher. Litvin and Pfeifer (3) used a higher stress-strength ratio, and they found a higher difference in creep between gap-graded and continuously graded concrete.

When the specimens were subjected to a load of 30,000 lb at the end of 28 days, the unit elastic strains measured at a stress of 1,063 psi were 220×10^{-6} and 250×10^{-6} in./in. respectively for gap-graded and continuously graded concretes. Hence the corresponding secant moduli of elasticity are respectively 4.84×10^{6} and 4.25×10^{6} psi, showing 14 percent higher for gap-graded concrete, even though the actual cylinder strength for this concrete was 140 psi less than that for continuously graded concrete.

Shrinkage

Shrinkages of gap-graded and continuously graded concretes have been compared for mixes with 1-, $^{3}/_{4}$-, and $^{1}/_{2}$-in. maximum-size coarse aggregates and for 3 different nom-
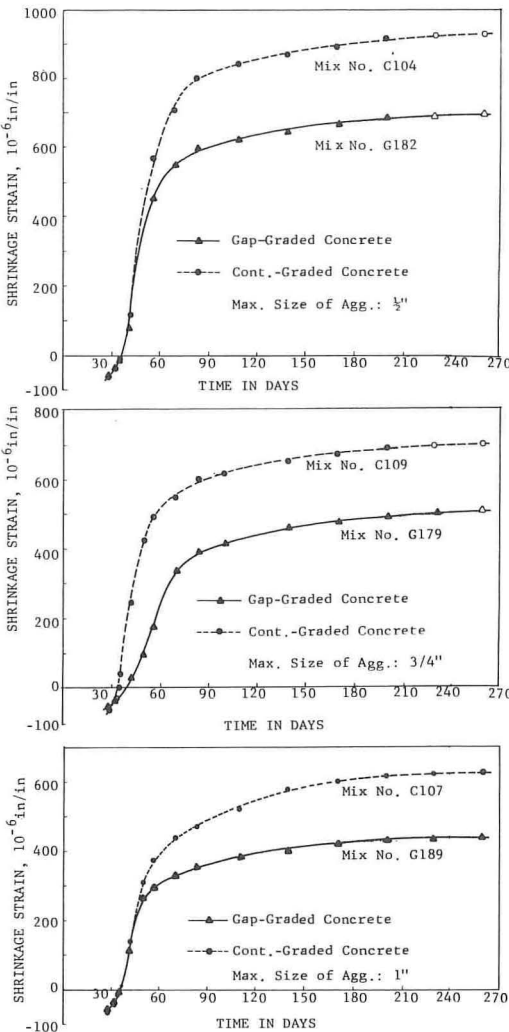
Figure 4. Comparison of shrinkages for gap-graded and continuously graded concretes of 7,500-psi strength.
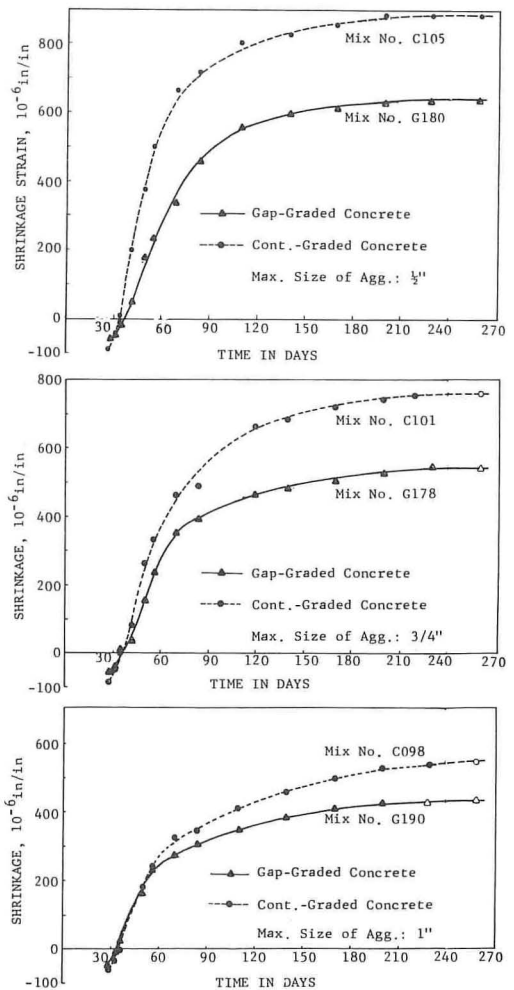
Figure 5. Comparison of shrinkages for gap-graded and continuously graded concretes of 6,000-psi strength.

inal strengths of 7,500, 6,000, and 4,500 psi. The details of gradings and mixes are given in Tables 1 and 2, and test results are given in Table 3. Three specimens were cast for each mix, and each point plotted represents the average of 3 values. It was noted consistently that the readings in all 3 specimens were nearly the same in all 16 mixes tested. The batches were made in pairs, one gap-graded and one continuous, so as to reduce possible systematic errors.

The measured shrinkage strains and the duration observed are shown in Figures 4, 5, and 6. The concretes compared had the same maximum size of coarse aggregate, same cylinder compressive strength, and the same workability and ease of placement, but the gap-graded concrete had less water content, less cement content, and higher aggregate-cement ratio.

Figures 4, 5, and 6 show that, for all maximum sizes of aggregates and for all strengths, the shrinkage of gap-graded concrete is considerably less than that of continuously graded concrete. This again confirms the hypothesis previously proposed. At 100 days, the shrinkage of continuously graded concrete with $3/4$-in. maximum-size aggregate and 7,500-psi nominal strength was 48 percent higher than that of the corresponding gap-graded concrete.

A comparative study of Figures 4, 5, and 6 further indicates that (a) the shrinkage is smaller when larger size aggregates are used, (b) shrinkage increases as the strength of concrete increases, (c) shrinkage reduces as the aggregate-cement ratio is increased, (d) shrinkage increases as the water-cement ratio is increased, and (e) shrinkage increases as the cement content increases. This phenomenon is true for both gap-graded and continuously graded concretes.
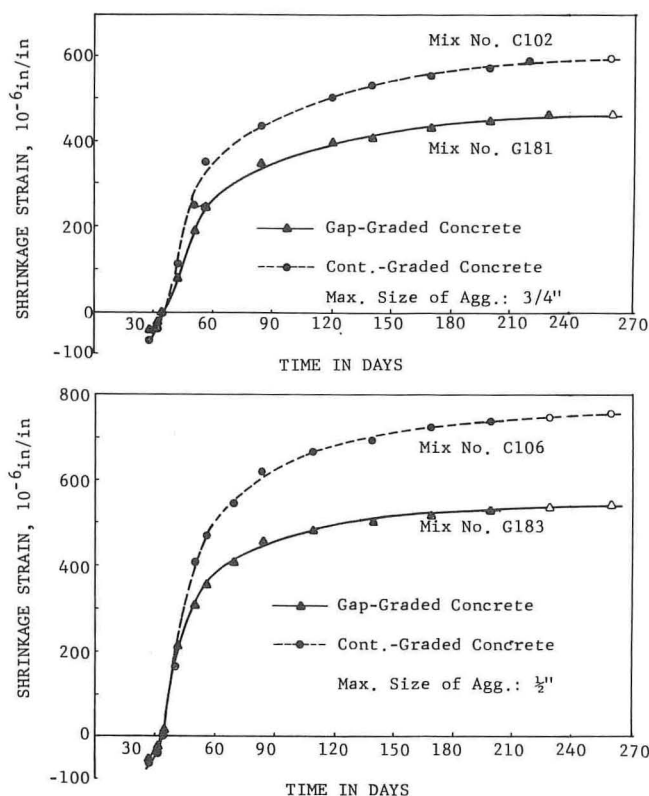

Figure 6. Comparison of shrinkages for gap-graded and continuously graded concretes of 4,500-psi strength.

PROPOSED EQUATIONS FOR YOUNG'S MODULUS AND CREEP

Young's Modulus

Modulus of elasticity for concrete is a basic property, and its accurate determination is important. Many factors such as strength of concrete, age of concrete, grading of aggregates, properties of aggregates, type of concrete (lightweight or normal weight), rate of loading, water-cement ratio, type and size of specimen and its density, and moisture content at the time of testing influence the results.

Several empirical formulas have been suggested previously for use in design calculations, mostly expressed as a function of ultimate compressive strength only; but the relationships proposed by various investigators do not show any acceptable agreement, especially when they are applied to concretes of different densities such as structural lightweight concrete. An empirical formula was proposed by Pauw (4) expressing the modulus of elasticity of concrete, E_c, as a function of density, w, and ultimate compressive strength, f_c', as

$$E_c = 33w^{3/2}\sqrt{f_c'}$$

This formula has been adopted by the ACI Code 318-63. The results of the present investigation are compared with Pauw's equation and shown in Figure 7 in which the test results for gap-graded concrete obtained by Litvin and Pfeifer (3) are also shown. The figure reveals clearly that Pauw's equation does not correctly predict the modulus-of-elasticity values for gap-graded concretes tested in this investigation and at PCA Laboratory by Litvin and Pfeifer. It is to be noted that the results of this investigation and those of Litvin and Pfeifer show the same pattern.

Further this investigation has proved that gap-graded concrete is generally slightly denser and has higher strength than its continuously graded counterpart of the same maximum-size coarse aggregate. Even when compared on an equal strength basis, it has also shown that gap-graded concrete is likewise denser than continuously graded
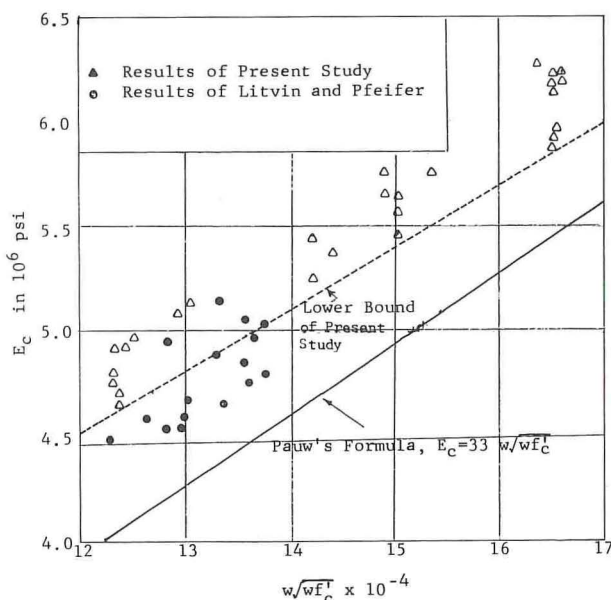

Figure 7. Comparison of modulus of elasticity of gap-graded concrete with Pauw's formula for continuously graded concrete.

concrete. Therefore it is not logical to expect a single equation to predict the moduli of elasticity of both concretes. Hence 2 separate equations, one for gap-graded and another for continuously graded, are proposed. Even though a wide range of density has not been covered in this investigation, a plot of the density versus modulus of elasticity, shown in Figure 8, indicates clearly that the density of concrete is an influencing parameter in the determination of moduli of elasticity for both concretes. Therefore, it could be expected that modulus of elasticity of concrete could vary as a colinear function of density and compressive strength. To make it perfectly general, and to account for the difference between cylinder and cube strength, let

$$E_c = \alpha \left(\frac{wA}{1728h} \right) + \beta f'_c + \gamma \tag{1}$$

where

$$
\begin{aligned}
E_c &= \text{Young's modulus in psi (chord modulus as defined in ASTM C 469-65);} \\
\alpha \text{ and } \beta &= \text{dimensionless coefficients;} \\
\gamma &= \text{an unknown constant in psi;} \\
w &= \text{unit weight of concrete in pcf;} \\
A &= \text{area of cross section of specimen in sq in.;} \\
h &= \text{height of the specimen in in.; and} \\
f'_c &= \text{compressive strength in psi.}
\end{aligned}
$$

This equation is dimensionally consistent and automatically takes into account the difference in cylinder and cube specimens, while α, β, and γ would be different for the 2 types of specimens.

Let

$$\frac{A}{1728h} = \frac{36\pi}{4(1728)12} = \alpha_1$$

for 6- by 12-in. cylinders. Then the colinear relation among Young's modulus, density, and strength with cylinder tests becomes

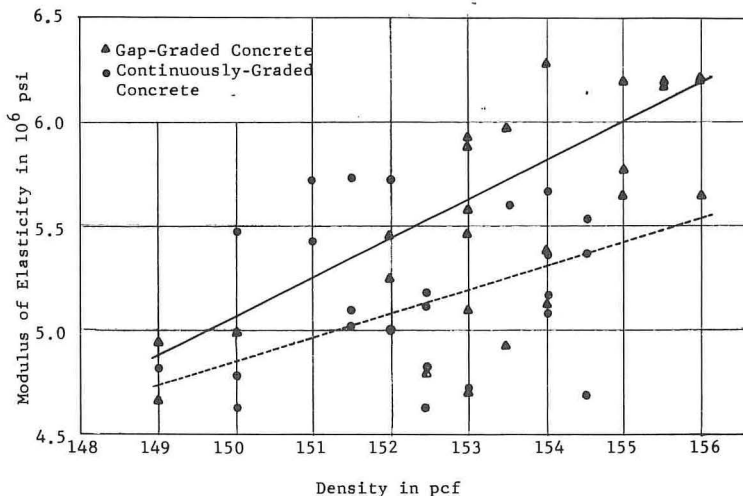$$E_c = \alpha_1 w + \beta f'_c + \gamma \tag{2}$$

Figure 8. Comparison of relationship between density and modulus of elasticity for gap-graded and continuously graded concretes.

By using the test results of E_c, w, and f'_c, 2 curves, one E_c versus f'_c and another E_c versus w, were plotted as shown in Figures 1 and 8 respectively for both gap-graded and continuously graded concretes. By choosing 3 points, the corresponding E_c, w, and f'_c values are read directly from the figures. Substituting these values 3 times into Eq. 2, we can solve for these unknowns. Different values were obtained for gap-graded and continuously graded concretes. The separate equations obtained are as follows:

For gap-graded concrete,

$$E_{cg} = 0.109 \times 10^6 w + 185\, f'_c - 12.14 \times 10^6 \tag{3}$$

For continuously graded concrete,

$$E_c = 0.0670 \times 10^6 w + 185\, f'_c - 6.223 \times 10^6 \tag{4}$$

where

E_{cg} = Young's modulus for gap-graded concrete in psi;
E_c = Young's modulus for continuously graded concrete in psi;
w = density of 6- by 12-in. cylinder specimen in pcf; and
f'_c = compressive strength of 6- by 12-in. cylinder in psi.

It is recognized that the maximum size of coarse aggregate may influence the values α, β, and γ, but the results available do not justify to derive separate equations for different sizes of aggregates. The proposed equations are applicable for a range of f'_c from 4,000 to 8,000 psi, which are the limits of the tests.

TABLE 5

COMPARISON OF CALCULATED AND TEST RESULTS FOR GAP-GRADED CONCRETE

	Li and Ramakrishnan					Litvin and Pfeifer				
Mix No.	Unit Weight (pcf)	Compressive Strength (psi)	Modulus of Elasticity (10^6 psi) Test	Calculated	Ratio of Test to Calculated	Mix No.	Unit Weight (pcf)	Compressive Strength (psi)	Modulus of Elasticity (10^6 psi) Test	Calculated	Ratio of Test to Calculated
G182	153.0	7,606	5.93	5.97	0.99	Elgin gravel concrete	145.2	3,880	3.91	4.43	0.88
	153.0	7,606	5.88	5.97	0.98		145.2	5,600	4.42	4.74	0.93
	153.5	7,606	5.98	6.02	0.99		145.9	6,160	4.75	4.90	0.97
G180	153.0	6,325	5.46	5.73	0.96		148.1	5,870	4.61	5.09	0.91
	153.0	6,325	5.58	5.73	0.97		147.2	6,020	4.71	5.07	0.93
	155.0	6,325	5.76	5.93	0.97		146.5	6,170	4.70	5.00	0.94
G183	150.0	4,638	4.98	5.07	0.98		144.3	5,140	4.41	4.56	0.97
	149.0	4,638	4.66	4.97	0.94		144.4	5,700	4.47	4.66	0.96
	149.0	4,638	4.94	4.97	0.99		144.2	6,050	4.37	4.73	0.92
G179	154.0	7,338	6.29	6.02	1.04	Elmhurst limestone concrete	148.9	5,340	4.85	5.05	0.96
	155.0	7,338	6.20	6.12	1.01		146.0	5,170	4.59	4.75	0.97
	155.5	7,338	6.20	6.17	1.00		145.1	5,420	4.52	4.67	0.97
G178	152.0	5,769	5.25	5.53	0.95		146.3	5,450	4.69	4.87	0.96
	154.0	5,769	5.38	5.73	0.94		148.1	5,690	4.85	5.06	0.96
	152.0	5,769	5.45	5.53	0.99		147.4	5,870	4.99	5.04	0.99
G181	153.5	4,276	4.92	5.35	0.92		146.5	5,170	4.97	4.81	1.03
	153.0	4,276	4.71	5.30	0.89		145.4	5,840	5.17	4.84	1.07
	152.5	4,276	4.80	5.25	0.92		144.4	6,360	5.06	4.80	1.05
G189	155.5	7,208	6.17	6.12	1.01						
	156.0	7,208	6.21	6.17	1.01						
	156.0	7,208	6.22	6.17	1.01						
G190	155.0	5,980	5.65	5.87	0.96						
	156.0	5,980	5.65	5.97	0.95						
	155.0	5,980	5.77	5.87	0.98						
G191	153.0	4,660	5.10	5.42	0.94						
	154.0	4,660	5.14	5.54	0.93						

Note: Coefficient of variation = 4.10 percent; standard deviation = 0.04; and mean of ratio of test to calculated = 0.97.

Equation 3 for gap-graded concrete has been compared with the test results of this investigation (Table 5) and of Litvin and Pfeifer (3) and shows excellent agreement. The mean of the ratios of test value to calculated value is 0.97, the coefficient of variation is 4.10 percent, and the standard deviation is 0.04.

Creep

With the method of least squares, the following 2 equations, one for gap-graded concrete and another for continuously graded concrete, were obtained for the 2 curves shown in Figure 3.

$$C_g = \frac{t}{78 + 1.5\,t} \text{ for } t \geq 40 \tag{5}$$

$$C_g = \frac{t}{36 + 2.91\,t} \text{ for } t \leq 40 \tag{5a}$$

$$C = \frac{t}{59 + 1.117t} \text{ for } t \geq 40 \tag{6}$$

$$C = \frac{t}{23 + 2\,t} \text{ for } t \leq 40 \tag{6a}$$

where

C_g = creep in./in./psi, for gap-graded concrete;
C = creep in./in./psi, for continuously graded concrete; and
t = time under sustained load in days.

These equations are applicable for a stress-strength ratio of 18 percent. Nasser and Neville (5) have reported that the creep in concrete is proportional to the stress-strength ratio. By assuming that these concretes conform to the proportionality between creep and stress-strength ratio, the creep at other loads could be estimated from these equations.

CONCLUSIONS

Young's modulus, creep, and shrinkage are basic to the analysis and design of reinforced and prestressed concrete structures. Such data are not fully available at present for gap-graded concrete. The results presented here, though not exhaustive, will be quite useful to design engineers.

The general conclusions that can be drawn within the premise of this investigation are as follows:

1. Gap-graded concrete has higher modulus of elasticity than its equivalent continuously graded concrete. Because modulus of elasticity is inversely related to deformations and deflections of a structure, higher modulus would mean higher structural stiffness and hence lesser elastic deformations and deflections under applied loads. Also, the higher the modulus, the lesser will be the loss in the initial prestressing force in pretensioned concrete members.

2. For grade-separation structures, higher modulus of elasticity will permit shallower stringers and less gradient for overpasses.

3. Under identical conditions, gap-graded concrete has less creep and shrinkage than the corresponding continuously graded concrete. This has special advantages in structural concrete under prestress. In a prestressed concrete member, creep and shrinkage act together to reduce the initial prestressing force. Any decrease in creep and shrinkage strains would decrease the loss of prestress. Because creep and shrinkage strains alone usually cause about 70 percent of the total losses in prestress, any reduction in this would be a significant advantage.

4. In any indeterminate structure, small displacements of one member, whether they be due to creep or shrinkage, may give rise to additional stresses and moments in other members. Although, in concrete structures subjected to thermal gradients, creep and shrinkage will reduce stresses due to thermal rise, they will cumulate the

effects due to thermal fall. Such detrimental effects of creep and shrinkage will be much reduced when gap-graded concrete is used.

5. Based on test data, equations have been derived for the determination of modulus of elasticity and creep strains for structural concrete in compression. The suggested equations for gap-graded concrete have also shown excellent agreement with the results previously obtained by Litvin and Pfeifer at PCA Laboratory.

6. With regard to shrinkage, gap-graded concrete behaves in a manner similar to that of continuously graded concrete: Shrinkage increases as the strength of concrete or the water-cement ratio or the cement content is increased; and shrinkage decreases when larger size aggregates are used or when the aggregate-cement ratio is increased.

7. The present test data have clearly shown the advantages of gap-graded concrete over continuously graded concrete. For the same cement content and equal workability, gap-graded concrete has higher compressive strength than continuously graded concrete. This would mean lower cement requirements. The test results show a possible savings in cement of about 30 percent. This investigation has further shown that gap-graded concrete is denser than the continuously graded counterpart of the same maximum-size coarse aggregate.

These conclusions confirm the authors' previously published hypothesis. The authors recommend wider adoption of gap grading in concrete aggregates not only for the advantages mentioned here but also for a better adaptation to any naturally occurring aggregates that do not contain all the needed sizes and quantities for optimum continuous grading.

REFERENCES

1. Li, Shu-t'ien. Proposed Synthesis of Gap-Graded Shrinkage-Compensating Concrete. ACI Jour., Proc. Vol. 64, No. 10, Oct. 1967, pp. 654-661.
2. Li, Shu-t'ien. Non-Shrinking Gap-Graded Concrete—Its Synthetic Technology. In Materials Technology—An Inter-American Approach, ASME, New York, May 1968, pp. 206-214.
3. Litvin, A., and Pfeifer, D. W. Gap-Graded Mixes for Cast-in-Place Exposed Aggregate Concrete. ACI Jour., Proc. Vol. 62, No. 5, May 1965, pp. 521-537.
4. Pauw, A. Static Modulus of Elasticity of Concrete as Affected by Density. ACI Jour., Proc. Vol. 57, No. 12, Dec. 1960, pp. 679-687.
5. Nasser, K., and Neville, A. M. Creep of Old Concrete at Normal and Elevated Temperatures. ACI Jour., Proc. Vol. 64, No. 2, Feb. 1967, pp. 97-104.

The Inelastic Deformation of Concrete

NARAYAN SWAMY, Department of Civil and Structural Engineering,
University of Sheffield

A knowledge of the complete stress-strain curve of concrete is essential for ultimate strength design. Conventional stress-controlled tests give little information on deformation beyond the maximum load. Tests are reported on concrete cylinders and prisms at constant rate of straining using a servomechanism connected to the hydraulic system and automatically recording the load deformation. The effect of specimen size, aggregate type, age, strength, and cyclic loading on the deformational behavior of concrete is studied. The strain at maximum load tends to increase with concrete strength and with age. The ultimate strain at collapse is many times that at maximum load and is independent of strength and height-width ratio of specimen. At equal deformations beyond the maximum load, low-strength concrete and specimens of smaller height-width ratio possess greater load resistance. Age and strength also influence the shape of the stress-strain curve. The elastic modulus based on total strain is about 55 to 80 percent of that obtained from strains in the central part. The presence of the falling branch suggests different cracking and failure mechanisms in the ascending and descending parts, and the significance of internal friction at decreasing loads. The ability to sustain decreasing loads at increasing deformation relieves stress concentrations and ensures plastic flow without violent failure.

•THE STRESS-STRAIN RELATION of a material forms the basis of all design of structural members. With a material such as concrete, which is subjected to time-dependent deformation due to environmental conditions in addition to that due to superimposed load, a knowledge of the complete stress-strain behavior including the post-yield deformation is necessary for an adequate appreciation of the ultimate strength design of concrete members, for the prevention of cracks, and for the design for movements in concrete structures. Although the principles of ultimate strength design of reinforced and prestressed concrete members are well-established, it is still far from clear as to the exact nature of the relationship of the stress-strain characteristics of concrete in concentric compression and in flexural compression.

Very high ultimate strains are generally required if a structural member is to develop its full moment of resistance and exhibit ductile characteristics of failure, and these strains cannot normally be measured when a compression specimen is tested at a constant rate of loading. In a conventional stress-controlled test, the test specimen fails suddenly at a peak strain of about 2,000 microstrains (10^{-6} mm/mm) and gives the impression that concrete behaves like a brittle material with little or no inelastic deformation prior to fracture. The behavior of concrete in flexural compression, on the other hand, shows considerable inelasticity, and ultimate strains in excess of 4,000 microstrains have often been observed in the compression fibers of flexural failure.

This apparent brittle behavior of concrete is due to the flexibility of the hydraulic system and the lack of rigidity of the testing machine, rather than to an inherent property of the material. The possibility of increasing deformation with decreasing loads beyond the maximum was recognized more than 30 years ago ([1], [2]), but it was Whitney ([3]),

---

who first reported the complete stress-strain curves in compression and showed that concrete possesses a post-peak deformation that is represented by the falling portion of the stress-strain curve. By applying deformation at a constant rate, strains up to 8,000 microstrains were reported. Because of the increasing deformation with falling loads, the rate of straining has a significant effect on the shape of the stress-strain curve (4, 5, 6). The lack of stiffness of the testing machine is much more significant when testing high-strength concrete, and even with a very stiff machine sudden failures could occur with high-strength concrete (7, 8).

Conventional testing machines with control of load rate can be transformed into control of strain rate by using the machine to deform an elastic member, the deformation of which can be utilized to control the deformation of the test specimen. Such techniques have been successfully used for compression tests (9, 10, 11, 12) and, more recently, for axial tension tests (13), modulus of rupture tests (14), and splitting tests (15). On the other hand, the elastic characteristics of the test frame can be modified by the use of a hydraulic compensator (16). Machines capable of applying a constant rate of deformation have also been developed (17, 18). All these tests show that the specimens remain reasonably intact even when loaded to strains many times that of the stress-controlled test.

CONSTANT STRAIN DEVICE

The major difficulty in obtaining the post-yield deformation arises from the fact that the stiffness of the concrete specimen is of the same order as that of a conventional hydraulic testing machine. In a conventional stress-strain test, the stiffness or the spring rate K_s of the specimen is initially positive, becomes zero at the peak load, and then becomes negative; whereas, the stiffness of the machine K_m remains constant and is represented by a straight line. Over the falling branch of the stress-strain curve the stiffness of the specimen becomes negative, and, if this value is greater than the stiffness of the machine, a region of instability occurs soon after the maximum load that precipitates either a sudden failure or a crack through to a new position of equilibrium (Fig. 1). In using an elastic frame as a load-carrying device during the post-yield deformation stage, the total applied load increases with increase in the total deformation, and the overall stiffness of the system remains always positive.

In the tests reported here this incompatibility of the stiffness characteristics of the specimen and the testing machine has been overcome by the use of a servomechanism and 3 displacement transducers mounted between the platens of the testing machine.
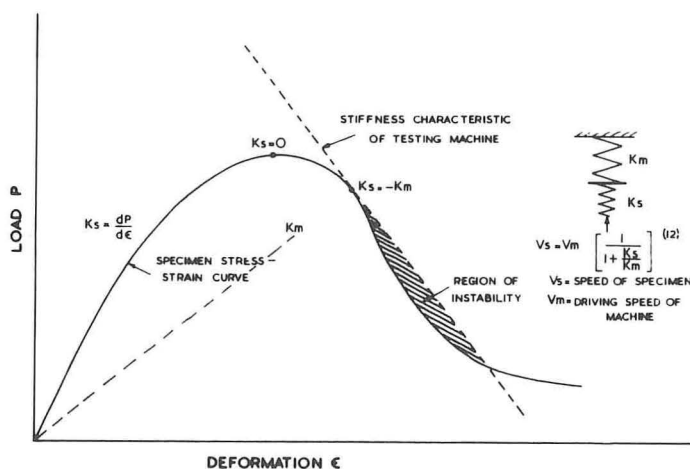

Figure 1. Instability condition due to stiffness characteristics of test specimen and testing machine.

The unit is designed for use with any hydraulically controlled testing machine and, by direct connection to the pressure line, regulates the applied load to the specimen by the operation of an electromagnetic valve. Any desired strain rate of loading can be achieved by comparing the measured strain with that required, which is done automatically using a servoamplifier, the output of which controls the electromagnetic valve. By control of the hydraulic system, the machine is made sufficiently stiff to reduce the loading at the instant of instability to maintain a constant rate of straining, so that the complete load-deformation curve of the specimen can be obtained. The load and deformation regulating console, together with the servomechanism and the hydraulic regulating valve, is shown in Figure 2.
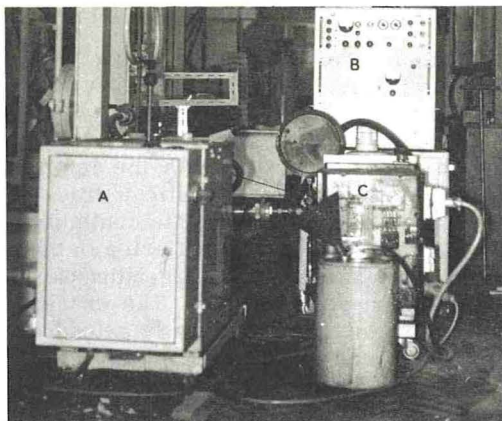

Figure 2. Load-deformation regulating console and servosystem for constant rate of straining (A, pump unit; B, strain control console; and C, hydraulic paver supply and servosystem).

DESCRIPTION OF TESTS

The tests reported here were carried out on prisms and cylinders of various sizes. Ordinary portland cement obtained from one delivery was used throughout the tests. Four different types of aggregates, consisting of crushed gravel and crushed rocks of granite, basalt, and limestone, were used. Two different gradings of coarse aggregate were used: a single size of 10 mm and a continuous grading of 5 to 19 mm. The same fine aggregate was used for all the tests and consisted of a washed pit sand with an average fineness modulus of 3.1.

Different mix proportions were generally used. The crushed gravel (5 to 19 mm) and the crushed basalt and crushed limestone tests were all carried out with nominal 1:2:4 mix proportions. The size and grading of the aggregate, the size of the specimen, and the mix proportions are shown in the figures.

All the specimens were cast under the same conditions and were internally vibrated. The specimens were kept in molds for 3 days, were then kept under water for 7 days, and were subsequently stored in a room of constant temperature and humidity. The tests were carried out in a 2,000-kN Amsler hydraulic testing machine with the hydraulic load regulator attached to the pressure system. The displacement of the platens was controlled by 3 differential-transformer type transducers, and, along with the load, was directly fed to an X-Y plotter. In addition, the end-to-end displacement of the specimen was also measured by means of 3 dial gages reading to about 10×10^{-3} mm.

All the tests were carried out at a constant strain rate of 2,000 to 2,500 microstrains per minute. At least 3 specimens of any batch were tested at any given age. Because of the variations of concrete in the specimens, small fluctuations in the loading rate and differences in the stress-strain characteristics were inevitable. All but Figure 4 show as near reproductions as possible of the curves recorded through the X-Y plotter. The dial gage readings measuring end-to-end displacements of the specimen generally agreed within 3 percent, and tests with larger differences were discarded. It is emphasized that the strains reported represent the overall average strains measured end-to-end of the specimen. In a few tests, strains over the central part of the specimen were also measured by electric resistance gages on opposite sides. From the large amount of information obtained from the tests, only typically representative data are presented here.

92

DISCUSSION OF TEST RESULTS

The first cracks observed in the tests were invariably vertical and occurred near the midheight of the specimen. They generally became visible only at loads near the maximum load. As the deformation proceeded, more vertical cracks could be seen forming, and this continued process of cracking was reflected in the lack of smoothness of the descending part of the stress-strain curve. The cracks prior to final collapse generally extended from end-to-end of specimen. The strain at maximum load varied between 2,000 and 4,000 microstrains, and the ultimate strain prior to collapse reached up to 1.5 to 2.0 percent. The strain when the specimen ceased to carry any further load

Figure 3. Appearance of concrete prisms, cylinders, and cubes after straining to 1.0 to 1.5 percent at a constant rate.

was about 6 to 8 times the strain at maximum load. In spite of the very large strains, the prisms and cylinders remained intact, but cubes showed considerable disintegration (Fig. 3).
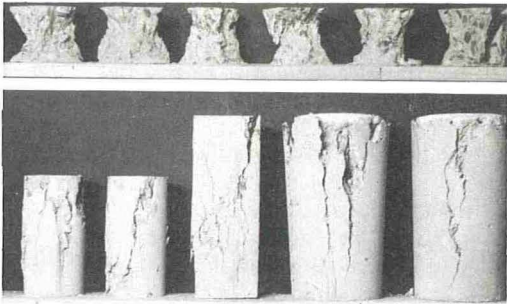
CYLINDER AND PRISM TESTS

Figure 4 shows the stress-strain relationships for 150- by 300-mm cylinders of 3 different mixes and made of crushed granite of 10-mm size. The figure is typical of the effect of strength on the stress-strain characteristics of the material. Although the curves for high- and low-strength concretes are similar in shape, there are 3 differences among them worth noting: (a) The strain at maximum load tends to be greater for the stronger concrete; (b) the low-strength concrete shows a much flatter region at the peak load than the high-strength concrete; and (c) at equal deformations the low-strength concrete shows greater load resistance in the falling branch of the curve. The ultimate strains at collapse of the test specimens, however, are not very different for the 3 strengths.

The slopes of both the rising and falling branches of the curves increase with the maximum stress of the specimen. High strength concretes thus tend to become more unstable immediately after the peak load is reached, and this lack of stability increases with increased rate of straining (4, 5).
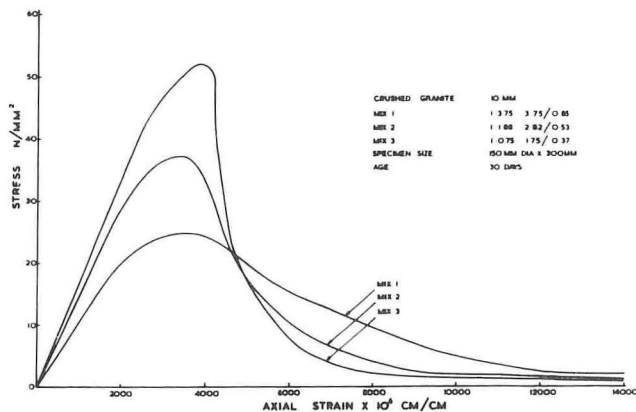

Figure 4. Stress-strain curves for 150- by 300-mm cylinders of crushed granite aggregate.

TABLE 1

RESULTS OF CYLINDER TESTS AT CONSTANT STRAIN

Mix	Initial Tangent Modulus $(N/mm^2 \times 10^4)$	At Proportional Limit		At Maximum Stress		Cube Strength[a] fu (N/mm^2)	Cylinder Strength[a] f_c' (N/mm^2)	$\frac{\sigma_m}{fu}$	$\frac{\sigma_m}{f_c'}$
		Stress (N/mm^2)	Strain $(cm/cm \times 10^{-6})$	Stress σ_m (N/mm^2)	Strain $(cm/cm \times 10^{-6})$				
1	0.95	19.8	1,800	24.6	3,500	26.3	24.2	0.935	1.020
2	1.42	27.6	1,950	37.3	3,500	44.1	37.5	0.845	0.995
3	1.71	39.3	2,300	52.4	3,850	61.4	52.0	0.854	1.010

[a]Average of 3 tests.

The main characteristics of the curves shown in Figure 4, together with the associated cube and cylinder strengths, are given in Table 1. The initial tangent moduli shown are based on the end-to-end deformation of the specimen and are seen to be much less than the normal values obtained when strains are measured over the central part of the specimen. The strain distribution in compressively loaded concrete specimens depends not only on the location of the gage length but also on the type of gage used (19). With mechanical gages, surface strains are known to differ by as much as 30 percent from strains measured between embedded inserts; with resistance gages, the measured strain depends on the relation between the gage length and the maximum aggregate size (20). Strains measured with gage lengths of 6 to 8 times the size of aggregate can show variations up to 50 percent over those measured with gage lengths of the same size as the largest aggregate. The overall deformation of a specimen measured between the platens is always greater than that measured over the central portion (19), so that elastic moduli based on end-to-end strain measurements are bound to be significantly lower. There is, in addition, an unknown degree of end restraint that would alter the observed strain values.

In general, the initial tangent modulus measured in these tests for a range of concrete strengths varied from about 55 to 80 percent of the corresponding value, based on strain measurements in the central region of the specimen both at constant strain rate and at constant stress rate of loading. It is, of course, questionable whether elastic moduli measured over the central part in prisms and cylinders are applicable to stress computation in structural members in service, because of the monolithic nature of their construction and the inevitable end restraints produced. This variability of elastic moduli, depending on the size and location of gage, partly explains the large discrepancies in the stresses in reinforced concrete beams computed by the elastic theory.

The stress and strain values at proportional limit given in Table 1 refer to the end of the linear range of the stress-strain curve. It was generally found that the maximum stress of prisms nearly coincided with cylinder crushing strength, and similar results have also been obtained for necked specimens (21).

The results of tests on crushed gravel prisms are shown in Figures 5 and 6; Figure 5 refers to 100 mm cubes, and Figure 6 refers to 200- and 300-mm high prisms of the same cross section. In general, specimens of different height showed more or less the same order of strain capacity prior to collapse, although individual specimens showed wide variations (Fig. 6). At equal deformations, the load capacity during the falling portion of the stress-strain curve depends on the height-width ratio of the specimen and decreases with increasing height of the specimen.

The stress-strain curve for a prism in which additional strain gage measurements were taken in the center of the specimen is shown in Figure 6. Although these strains were recorded in a matter of seconds, there was stress relaxation during this period that increased at higher loads and during the post-peak deformation. This stress relaxation at constant rate of straining points to 2 factors. First, in restrained structural members this confirms a redistribution of stresses and a rapid reduction of peak stresses as the maximum load is approached: The rate of plastic flow is then greater the higher the stress. Second, by analogy, some creep strains are bound to be included in the observed strains in a stress-controlled test, even of short-time duration.
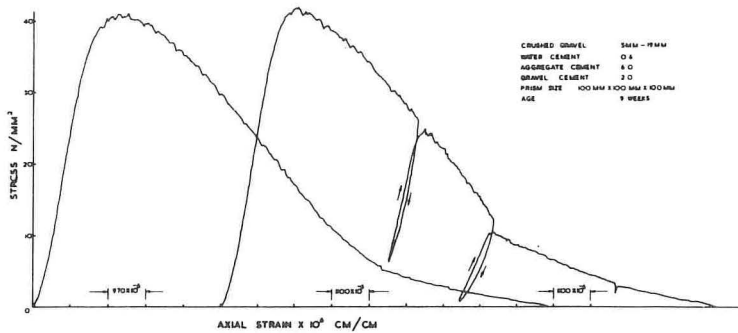
Figure 5. Stress-strain curves for 100-mm cubes of crushed gravel aggregate.
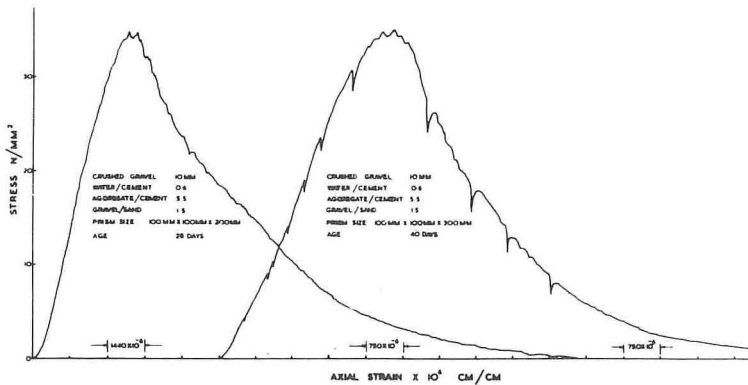

Figure 6. Stress-strain curves of 200- and 300-mm high prisms of crushed gravel aggregate.

The nonlinearity found in constant stress tests is therefore due partly to internal micro-cracking and partly to time-dependent strains. There is evidence, however, that if the effects of time and creep deformation are taken into account, then the stress-strain relationship at moderate stresses for normal concrete is reasonably linear (22, 23). The creep deformation is very rapid for lean concrete (22).

The effect of age on the stress-strain characteristics of prisms made of crushed basalt aggregate is shown in Figure 7. The 1-day and 3-day tests were carried out immediately after demolding, and the 7-day test on the water-cured surface-dry spec-imen. These curves show that the strain at maximum load increases between 1 and 3 days and between 7 and 28 days. As the age and strength increase there is a distinct hump at the peak load. The curves show generally the same characteristics as those shown in Figures 5 and 6.

The rate of straining has also a significant influence on the strength and elastic properties of concrete. Not only do strength and elastic modulus increase with increase in rate of straining, but also the observed strain capacity at the maximum load is known to be substantially greater than the corresponding value in the static tests (6, 24, 25).
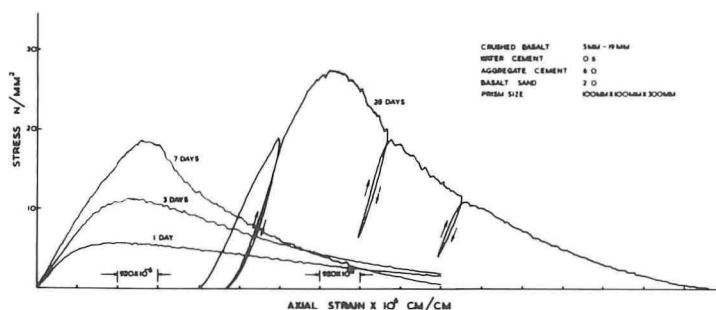
Figure 7. Influence of age on the stress-strain characterisitics of concrete
prisms of crushed basalt aggregate.

INTERNAL MICROCRACKING AND FAILURE MECHANISM

The fact that all curves shown in Figures 4 through 7 possess 2 distinct regions in their stress-strain characteristics suggests that there may well be 2 distinct mechanisms of cracking and load capacity in the ascending and descending parts of the stress-strain curve. When loaded at a constant stress rate and failure occurs in the region of the maximum load, it has been shown that preexisting and new bond cracks develop during the early part of the loading and that mortar cracks develop at about 70 to 90 percent of the failure load (11). The increase in deformation is then no longer proportional to the increase in load, and the internal cracking and the time-dependent strains cause a progressive deviation of the stress-strain relation from linearity.

In the constant strain test, the ascending part of the curve is linear up to about 70 to 80 percent of the maximum stress and is largely due to the cohesive strength of the material. The descending part, on the other hand, is far from smooth and consists of a series of minute irregular movements. Every time a microcrack forms there is a fractional relaxation of load, followed immediately by stress stabilization, further cracking, and so on. During the post-peak deformation, friction thus plays a predominant part in the load-carrying capacity of the specimen. There is probably increased breakdown of the adhesion between the matrix and the aggregate, and as the internal microcracking proceeds the internal friction becomes more significant. With further internal cracking, the material resembles more and more a granular mass and depends primarily on frictional effects to sustain the decreasing load. Low-strength concretes show the significant effects of internal friction much more than high-strength concrete (Fig. 4).

The descending part of the stress-strain curve represents, in effect, the behavior of the cracked concrete, and, although the specimen is fractured as a material, it can still withstand decreasing loads, though with increasing deformation. This ability to sustain increasing deformation without ceasing to carry the load is an important characteristic of the cracked concrete and contributes to the relief of stress concentrations in structural members, such as around openings (17, 26). In the complete stress-strain curves shown in Figures 4 through 7, the ascending part may be considered to be the characteristic properties of the material, while the falling branch represents the characteristic properties of the structural system of which the cracked specimen forms a part.

EFFECT OF REPEATED UNLOADING AND RELOADING

One of the significant characteristics of the falling branch of the stress-strain curve is that a sudden or violent failure cannot occur in a cracked specimen on the descending portion of the curve. It possesses a definite load-carrying capacity, although this decreases with increasing deformation. The stability of the cracked specimen during the post-peak deformation stage was studied by subjecting a number of specimens to
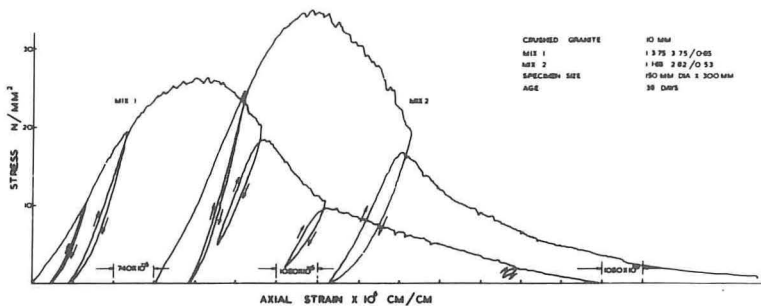
Figure 8. Deformational behavior of crushed granite cylinders under cyclic
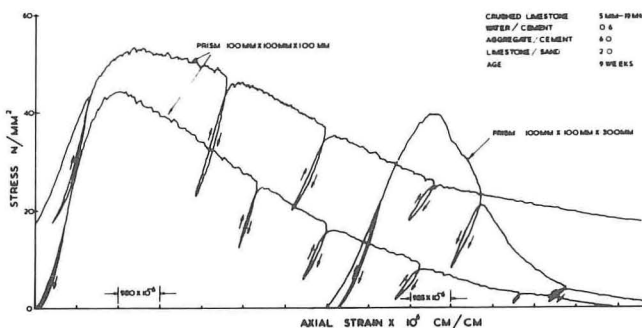loading.

Figure 9. Effect of repeated unloading and reloading on stress-strain
characteristics of crushed limestone prisms.

gradually decreasing and increasing load cycles. Typical results are shown in Figures
8 and 9, and some comparative results are shown in Figures 5 and 7. Figure 8 shows
the tests on crushed granite cylinders, and Figure 9 shows the results of tests on cubes
and prisms of crushed limestone.

All figures show that a cracked specimen subjected to load cycling in the descend-
ing part of its stress-strain curve resumes its characteristic deformational behavior
at the end of each load cycle. Further, these curves show that, even after considerable
cracking beyond the maximum load, the specimens exhibit a certain amount of elastic
behavior; they not only possess stability but also are capable of sustaining very large
strains without losing their load capacity. The loops formed by the load cycles, which
represent the energy loss during each cycle, are generally narrow. Their slope is, in
effect, a measure of the elasticity of the cracked concrete specimen and can be con-
sidered to represent the elastic modulus of the cracked specimen. This modulus is
seen to decrease with decreasing resistance of the fractured specimen. In a way, this
decrease in modulus is analogous to the decrease in the modulus of resistance under
sustained loading (27). With each cycle, the negative slope of the stress-strain curve
also decreases, thus ensuring that the cracked specimen becomes less and less liable
to sudden failure.

The load cycles during the ascending part of the stress-strain curve show that con-
crete is basically an inelastic material and that creep strains occur even under short-
term loading, although its 2 basic constituents—the coarse aggregate and the mortar

matrix—are largely elastic. There are permanent residual strains on unloading, even at low load levels. On reloading, however, the slope is nearly constant; and on repeated reloading, the straight-line sections are again nearly parallel. Upon reloading the specimen generally follows its previous deformational behavior. The energy dissipated during the ascending part is generally less than that in the descending part of the curve, and this again confirms the significance of frictional damping in its contribution to load capacity after the member has cracked. The width of the hysteresis loop generally depends on the range of stress and increases with it. The ability to absorb strain energy again depends on the rate of straining and on the strength and strain capacity at the maximum load (24).

FRICTIONAL DAMPING

The jagged nature of the descending part of the stress-strain curve and the area of the loop formed by the loading-unloading cycles also indicate a measure of the damping properties of concrete. Damping arises mainly from the inelasticity of the material and is a measure of its capacity to absorb and dissipate energy through internal friction. These tests show that frictional damping can be an important characteristic of concrete. At low loads, energy dissipation occurs through inelastic deformation; at higher loads, damping mainly occurs through energy dissipation into surface energy through crack propagation and rupture of cohesive and frictional bonds within the system. This is further assisted by local yielding and progressive inelastic deformation around the internal discontinuities and the propagating cracks. Friction damping thus occurs mainly at the interfacial boundaries between the matrix and aggregate inclusions and becomes the main load-bearing mechanism in the descending part of the stress-strain curve. It can therefore be very significant in cracked structural members and in members subjected to dynamic loading and can contribute to substantial reductions of the maximum strains within a structure. The amount of energy absorbed appears to depend on the rate of straining (24), although tests on steel specimens show damping capacity to be independent of the rate of loading.

CONCLUSIONS

1. The ultimate strain in uniaxial compression is 6 to 8 times the strain at maximum load and is generally independent of concrete strength and the height-width ratio of the specimen.
2. The strain at maximum load varies between 2,000 and 4,000 microstrains and tends to increase with concrete strength and age.
3. A cracked specimen on the falling branch of the stress-strain curve has considerable load capacity although this decreases with increasing deformation. This ability to sustain large strains without ceasing to carry load ensures relief of peak stresses and the absence of sudden and violent failure.
4. At equal deformations beyond the maximum load, low-strength concrete and specimens of small height-width ratio possess greater load resistance.
5. The internal friction due to the continued process of discrete cracking at the interfacial boundaries between the matrix and aggregate inclusions plays a significant role in the load-carrying capacity of the cracked specimen.
6. The initial tangent modulus at constant strain based on end-to-end strain of the specimen is about 55 to 80 percent of the normal value obtained from strains measured in the central section of the specimen.
7. The cracked concrete subjected to repeated cyclic loading on the falling branch exhibits a certain amount of elastic behavior. The energy loss during each cycle is generally low, and the repeated unloading and reloading does not significantly affect the load capacity of the specimen.
8. Permanent residual strains remain on unloading even at low stress levels.

REFERENCES

1. Emperger, F. V. Der Beiwert n. Beton und Eisen, Vol. 35, No. 19, Oct. 1936, pp. 324-332.

2. Saliger, R. Bruchzustand und Sicherheit im Eisenbetonbalken. Beton und Eisen, Vol. 35, Nos. 19 and 20, Oct. 1936, pp. 317-320 and 339-346.

3. Whitney, C. S. Plastic Theory of Reinforced Concrete Design. Proc. ASCE, Vol. 66, Dec. 1940, pp. 1749-1780.

4. Rasch, C. Stress-Strain Diagrams of Concrete Obtained by Constant Rates of Strain. Symposium on Influence of Time on the Strength and Deformation of Concrete, Munich, RILEM, Paris, Nov. 1958, p. 24.

5. Rasch, C. Spannungsverteilung in der Biegedruckzone unter höchster konstanter Biegedruckkraft. Materialprüfungsamt für das Bauwesen der Technischen Hochschule, München, 1961, p. 18.

6. Rasch, C. Spannungs-Dehnungs-Linien des Betons und Spannungsverteilung in der Biegedruckzone bei konstanter Dehngeschwindigkeit. Deutscher Asschuss für Stahlbeton, Wilhelm Ernst und Sohn, Berlin, Vol. 154, 1962, 72 pp.

7. Whitney, C. S. Discussion of The Plasticity Ratio of Concrete and its Effect on the Ultimate Strength of Beams. ACI Jour., Proc. Vol. 39, Nov. 1943, pp. 584-2 to 584-6.

8. Cowan, H. J. Inelastic Deformation of Reinforced Concrete in Relation to Ultimate Strength. Engineering, Vol. 174, No. 4518, Aug. 29, 1952, pp. 276-278.

9. Ramaley, D., and McHenry, D. Stress-Strain Curves for Concrete Strained Beyond the Ultimate Load. Bureau of Reclamation, U. S. Department of the Interior, Laboratory Rept. SP-12, March 1947, p. 10.

10. Brock, G. Concrete: Complete Stress/Strain Curves. Engineering, Vol. 193, No. 5011, May 4, 1962, pp. 606-608.

11. Hsu, T. T. C., Slate, F. O., Sturman, G. M., and Winter, G. Microcracking of Plain Concrete and the Shape of the Stress-Strain Curve. ACI Jour., Proc. Vol. 60, Feb. 1963, pp. 209-224.

12. Solmitz, H. A. Machines for Static and Sustained Loading. Internat. Symposium on the Evolution of Mechanical Equipment for Testing Building Materials, Stuttgart, March 1968, RILEM, Paris, General Rept., Topic 1, Vol. 2, No. 11, Sept.-Oct., 1969, pp. 347-361.

13. Hughes, B. P., and Chapman, G. P. The Complete Stress-Strain Curve for Concrete in Direct Tension. RILEM, Paris, Bull. 30, March 1966, pp. 95-97.

14. Davies, J. D., and Nath, P. Complete Load-Deformation Curves for Plain Concrete Beams. Building Science, Vol. 2, No. 3, Nov. 1967, pp. 215-221.

15. Davies, J. D. A Modified Splitting Test for Concrete Specimens. Magazine of Concrete Research, Vol. 20, No. 64, Sept. 1968, pp. 183-186.

16. Hinde, P. B. Testing Machine Stiffness Problem. The Engineer, Vol. 217, No. 5657, June 26, 1964, pp. 1124-1127.

17. Rüsch, H. Researches Toward a General Flexural Theory for Structural Concrete. ACI Jour., Proc. Vol. 67, July 1960, pp. 1-28.

18. Turner, P. W., and Barnard, P. R. Stiff Constant Rate Testing Machine. The Engineer, Vol. 214, No. 5557, July 27, 1962, pp. 146-148.

19. Keeton, J. R. Strain Distribution in Compressively Loaded Concrete Specimens. Proc. ASTM, Vol. 61, 1961, pp. 1197-1219.

20. Cooke, R. W., and Seddon, A. E. The Laboratory Use of Bonded-Wire Electrical-Resistance Strain Gauges on Concrete at the Building Research Station. Magazine of Concrete Research, Vol. 8, No. 22, March 1956, pp. 31-38.

21. Barnard, P. R. Researches Into the Complete Stress-Strain Curve for Concrete. Magazine of Concrete Research, Vol. 16, No. 49, Dec. 1964, pp. 203-210.

22. Glanville, W. H. Studies in Reinforced Concrete: III The Creep or Flow of Concrete Under Load. Department of Scientific and Industrial Research, London, Building Research Tech. Paper 12, 1939, p. 39.

23. Jones, P. G., and Richart, F. E. The Effect of Testing Speed on Strength and Elastic Properties of Concrete. Proc. ASTM, Vol. 36, Part 2, 1936, pp. 380-391.

24. Watstein, D. Effect of Straining Rate on the Compressive Strength and Elastic Properties of Concrete. ACI Jour., Proc. Vol. 49, No. 8, April 1953, pp. 729-744.

25. Penzien, J., and Hansen, R. J. Static and Dynamic Elastic Behaviour of Reinforced Concrete Beams. ACI Jour., Proc. Vol. 50, No. 7, March 1954, pp. 545-567.

26. Blanks, R. F., and McHenry, D. Plastic Flow of Concrete Relieves High-Load Stress Concentrations. Civil Engineering, Vol. 19, No. 5, May 1949, pp. 40-42.

27. Washa, G. W., and Fluck, P. G. Effect of Sustained Loading on Compressive Strength and Modulus of Elasticity of Concrete. ACI Jour., Proc. Vol. 46, No. 9, May 1950, pp. 693-700.

THE NATIONAL ACADEMY OF SCIENCES is a private, honorary organization of more than 700 scientists and engineers elected on the basis of outstanding contributions to knowledge. Established by a Congressional Act of Incorporation signed by Abraham Lincoln on March 3, 1863, and supported by private and public funds, the Academy works to further science and its use for the general welfare by bringing together the most qualified individuals to deal with scientific and technological problems of broad significance.

Under the terms of its Congressional charter, the Academy is also called upon to act as an official—yet independent—adviser to the Federal Government in any matter of science and technology. This provision accounts for the close ties that have always existed between the Academy and the Government, although the Academy is not a governmental agency and its activities are not limited to those on behalf of the Government.

The NATIONAL ACADEMY OF ENGINEERING was established on December 5, 1964. On that date the Council of the National Academy of Sciences, under the authority of its Act of Incorporation, adopted Articles of Organization bringing the National Academy of Engineering into being, independent and autonomous in its organization and the election of its members, and closely coordinated with the National Academy of Sciences in its advisory activities. The two Academies join in the furtherance of science and engineering and share the responsibility of advising the Federal Government, upon request, on any subject of science or technology.

The NATIONAL RESEARCH COUNCIL was organized as an agency of the National Academy of Sciences in 1916, at the request of President Wilson, to enable the broad community of U.S. scientists and engineers to associate their efforts with the limited membership of the Academy in service to science and the nation. Its members, who receive their appointments from the President of the National Academy of Sciences, are drawn from academic, industrial, and government organizations throughout the country. The National Research Council serves both Academies in the discharge of their responsibilities.

Supported by private and public contributions, grants, and contracts, and voluntary contributions of time and effort by several thousand of the nation's leading scientists and engineers, the Academies and their Research Council thus work to serve the national interest, to foster the sound development of science and engineering, and to promote their effective application for the benefit of society.

The DIVISION OF ENGINEERING is one of the eight major Divisions into which the National Research Council is organized for the conduct of its work. Its membership includes representatives of the nation's leading technical societies as well as a number of members-at-large. Its Chairman is appointed by the Council of the Academy of Sciences upon nomination by the Council of the Academy of Engineering.

The HIGHWAY RESEARCH BOARD, an agency of the Division of Engineering, was established November 11, 1920, as a cooperative organization of the highway technologists of America operating under the auspices of the National Research Council and with the support of the several highway departments, the Bureau of Public Roads, and many other organizations interested in the development of transportation. The purpose of the Board is to advance knowledge concerning the nature and performance of transportation systems, through the stimulation of research and dissemination of information derived therefrom.

HIGHWAY RESEARCH BOARD
NATIONAL ACADEMY OF SCIENCES — NATIONAL RESEARCH COUNCIL
2101 Constitution Avenue   Washington, D. C. 20418

ADDRESS CORRECTION REQUESTED